Effective Algorithms for Real-Time Wind Turbine Condition Monitoring and Fault Detection

by

Raed Khalaf Ibrahim

A Doctoral thesis submitted in partial fulfilment
of the requirements for the degree of
Doctor of Philosophy

June 2020

Centre for Renewable Energy Systems Technology
Electronic, Electrical and Systems Engineering
Loughborough University

To my father, mother, my loving wife and my wonderful children

Declaration

I hereby declare that I am responsible for the work submitted in this thesis, that the original work is my own except as specified in acknowledgements or in footnotes, and that neither the thesis nor the original work therein has been submitted to this or any other institution for a degree.

Raed Khalaf Ibrahim

June 2020

Acknowledgements

I would like to express my sincere gratitude to my supervisor, Prof. Simon Watson, for the professional guidance, unwavering supports, stimulating suggestions, comments and assistance of my PhD study. I am deeply impressed by his patience, motivation, enthusiasm, and immense knowledge. I could not have imagined having a better supervisor and mentor for my PhD study. Also my profound gratitude goes to my second supervisor, Dr Murray Thomson, for his invaluable support.

I would also like to express my gratitude to my colleagues in Loughborough: Jannis Tautz-Weinert, Abdullahi Daniyan and Chuka Nwabunike for the interesting discussions about our shared (research) interests. I enjoyed the friendly working atmosphere and chats with other colleagues in CREST, thank you all.

I am grateful for all data and support provided by Dr Chris Crabtree, Dr Donatella Zappalá from the University of Durham and Dr Julian Feuchtwang from the University of Strathclyde.

I would also like to acknowledge the valuable collaborative research and the stimulating discussions relating to this work with Dr Sinisa Djurović from the University of Manchester.

The following research would not have been possible without generous funding from the Higher Committee for Education Development (HCED) in Iraq, this support is gratefully acknowledged.

Lastly, I wish to express my deep and most sincere appreciation and thanks to my parents, brothers and sisters for their continual and unrelenting support and for always being there for me. A special thanks to my darling wife Fayha for her support, patience and love, my lovely kids, Luqaa, Muntadhar, Mustafa and Maryam for their patience and love.

Abstract

Reliable condition monitoring (CM) can be an effective means to significantly reduce wind turbine (WT) downtime, operations and maintenance costs and plan preventative maintenance in advance. The WT generator voltage and current output, if sampled at a sufficiently high rate (kHz range), can provide a rich source of data for CM. However, the electrical output of the WT generator is frequently shown to be complex and noisy in nature due to the varying and turbulent nature of the wind. Thus, a fully satisfactory technique that is capable to provide accurate interpretation of the WT electrical output has not been achieved to date.

The objective of the research described in this thesis is to develop reliable WT CM using advanced signal processing techniques so that fast analysis of non-stationary current measurements with high diagnostic accuracy is achieved. The diagnostic accuracy and reliability of the proposed techniques have been evaluated using data from a laboratory test rig where experiments are performed under two levels of rotor electrical asymmetry faults. The experimental test rig was run under fixed and variable speed driving conditions to investigate the kind of results expected under such conditions.

An effective extended Kalman filter (EKF) based method is proposed to iteratively track the characteristic fault frequencies in WT CM signals as the WT speed varies. The EKF performance was compared with some of the leading WT CM techniques to establish its pros and cons. The reported experimental findings demonstrate clear and significant gains in both the computational efficiency and the diagnostic accuracy using the proposed technique.

In addition, a novel frequency tracking technique is proposed in this thesis to analyse the non-stationary current signals by improving the capability of a continuous wavelet

transform (CWT). Simulations and experiments have been performed to verify the proposed method for detecting early abnormalities in WT generators. The improved CWT is finally applied for developing a new real-time CM technique dedicated to detect early abnormalities in a commercial WT. The results presented highlight the advantages of the improved CWT over the conventional CWT to identify frequency components of interest and cope with the non-linear and non-stationary fault features in the current signal, and go on to indicate its potential and suitability for WT CM.

Contents

List of Abbreviations

ANNs	Artificial Neural Networks
CM	Condition Monitoring
CMS	Condition Monitoring System
CWT	Continuous Wavelet Transform
DFIG	Doubly-Fed Induction Generator
EKF	Extended Kalman Filter
FFT	Fast Fourier Transform
FSCs	Fault Signature Components
IA	Instantaneous Amplitude
IDFT	Iterative Localized Discrete Fourier Transform
LFSCs	Lower Fault Signature Components
O&M	Operations and Maintenance
RMSE	Root Mean Squared Error
STFT	Short Time Fourier Transform
SCT	Spline-Kernelled Chirplet Transform
SVM	Support Vector Machine
SCADA	Supervisory Control and Data Acquisition
UFSCs	Upper Fault Signature Components
WT	Wind Turbine
WTs	Wind Turbines

List of Figures

List of Tables

Chapter 1

Introduction

1.1 Background

Wind power has been one of the fastest growing power sources in the world over the last two decades, growing from a tiny 7.6 GW in 1997 to 539.1 GW in 2017 [1]. According to the global wind statistics reported in [6], estimated by the global wind energy council (GWEC), wind power could reach 2,000 GW by 2030, and supply up to 17% -19% of global electricity by that time. By 2050, wind power could provide 25-30% of global electricity supply [7]. The WindEurope has projected that wind turbine (WT) installations in the European Union will increase 64% by 2020 compared to 2013 levels [8]. Furthermore, China foresees wind power capacity reaching 200 GW by 2020, 400 GW by 2030, and 1000 GW by 2050 [9].

Fig. 1.1 shows the global annual installed wind capacity from 2001-2017. There was five years of essentially flat markets from 2009-2013 due to the global financial crisis. Installations surpassed 50 GW per year in 2014, and have stayed over 50 GW per year for the last four years, with the Chinese market in 2015 pushing the total over 60 GW. Globally, cumulative installations passed 500 GW in 2017, ending the year at about 540 GW as shown in Fig. 1.2.

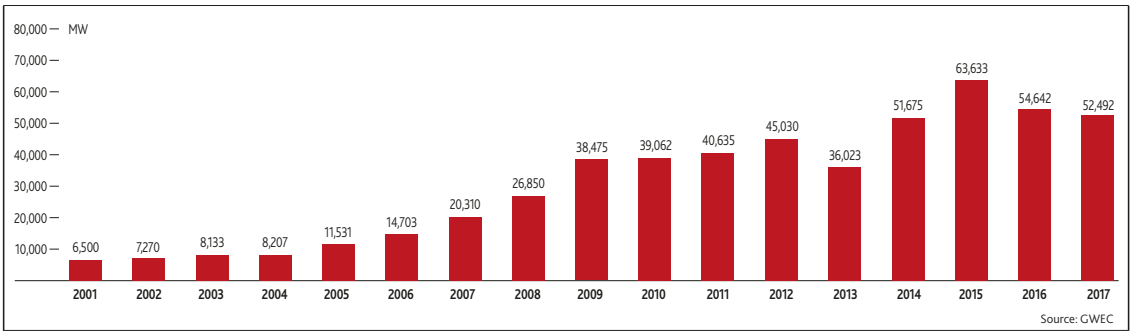

Figure 1.1 Global annual installed wind capacity 2001-2017 according to [1].

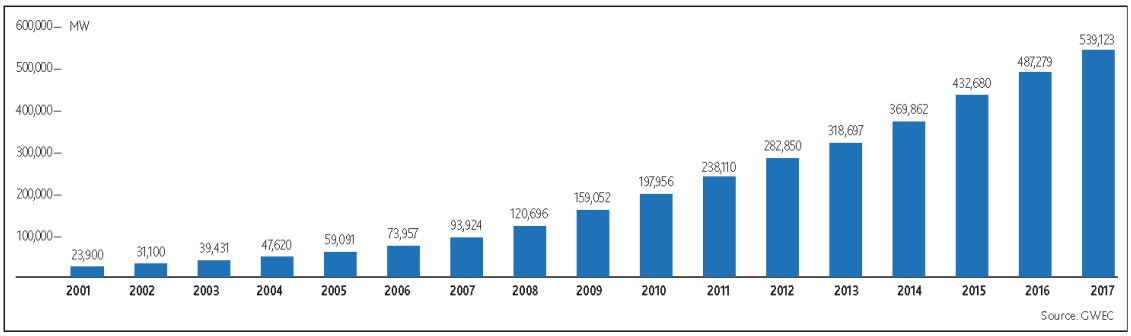

Figure 1.2 Global annual cumulative wind capacity 2001-2017 according to [1].

As a large number of WTs are being installed and connected to power systems, it becomes more and more challenging for manufacturers to monitor and maintain all of these machines. The cost of operations and maintenance (O&M) has been shown to be anything between 10% and 35% of the cost of energy from wind [10, 11], and there is a great demand to reduce O&M cost. In addition, a need arises for cost-effective predictive and proactive maintenance because the best wind resource is usually to be found in more remote locations including offshore. In order to make wind energy a competitive energy source in the energy market, the challenges of reliability and cost effectiveness should be addressed. To reduce the cost of wind energy, there is a need to improve WT availability and to reduce the maintenance cost [12]. This need is even more important in the offshore environment due to the harsh environmental conditions and the significant additional cost incurred by catastrophic failure should offshore machines not be maintained in a timely fashion.

For example, failure of a $1500 bearing in a WT drive-train could lead to a $100,000 gearbox replacement, a $50,000 generator rewind and another $70,000 in expenses to replace the failed components [13].

In recent years, the need to improve the reliability and the availability of wind turbines (WTs), particularly offshore has increased [14]. With this need has come different maintenance strategies to enable desired component performance by maintaining or returning the component's ability to function correctly. These maintenance strategies can be broadly divided into three categories: corrective maintenance, preventive maintenance, and condition-based maintenance. Table 1.1 summarizes the comparison between maintenance methods for WTs [15],[16]. To achieve condition-based maintenance, the use of remote WT condition monitoring (CM) is an effective means of not only increasing turbine reliability and availability but also reducing the costs and downtime associated with the operational and maintenance services [17].

Table 1.1 A Comparison of Maintenance Methods

Methods	Advantages	Disadvantages
Corrective maintenance	• Immediate corrective maintenance • Low maintenance costs • Maximum lifetime use of components	• Carried out after a failure event • High risk of consequential damages • Maintenance scheduling is not possible • Spare part logistics is complicated
Preventive maintenance	• Expected downtime is low • Maintenance can be scheduled • Spare part logistics is easy	• Carried out before a failure event • Components will not be used for the maximum lifetime • High maintenance costs
Condition based maintenance	• Full lifetime use of components • Low expected downtime • Low maintenance costs	• Reliable information of the component state is required • Additional CMS and software are required

To develop a successful WT condition monitoring system (CMS), there is a need for information to credibly describe the state of each monitored component and a reliable technique for fault feature extraction and fault diagnosis. In other words, the most important elements of a WT CMS are the measured signal and a technique to provide accurate interpretation of the measured signals. Generally, the signals used in WT CM include vibration, acoustic emission, strain, torque, temperature, electrical output, and supervisory control and data acquisition (SCADA) system signals [18, 19]. Among them, vibration is the most well-known signal used in a WT

CMS [20]. However, the analysis of the data can be complicated, and the sensors and data acquisition devices are expensive, and are themselves subject to failure. A survey of failures in wind power systems with focus on Swedish wind power plants during 1997-2005 showed that CMS sensor failures account for 14% of all wind turbine failures. This means sensor failures can cause unnecessary downtime and additional operation and maintenance costs. Generator current signals have been shown to have advantages over other signals for condition monitoring in terms of accessibility, cost, implementation, and reliability [21]. The costs and complexity involved in current measurements are significantly lower than many other signals such as vibration, because the current signals are already available and continuously measured in WTs and thus no additional sensors are required [22, 23].

However, the current-based approach is a new method for WT CM and diagnostics which requires further investigation to assess various challenges that will be discussed in the next section.

1.2 Scope of Research

The available literature indicates that each fault has its own characteristics (called a fault signature) in the frequency spectrum of WT current signals. Theoretical and analytical formulations of fault signature frequencies and their generation were attempted in [24–26] to define the signal spectral component that can be monitored for diagnostic purposes. To date, various WT condition monitoring (CM) techniques that aim to utilize these and similar diagnostic signals have been developed [18, 20]. However, an eefective method to detect the full range of WT faults in their early stages has not been achieved yet, and false alarms are still frequently reported from sites with the generator being a significant contributor [27], demonstrating the need to optimize these alarms. The root cause of generator false alarms can be related to the following problems:

- lack of clear understanding of the diagnostic information embedded in the stator current spectral content.

- lack of signal processing tools with sufficient sensitivity and reasonable computational efficiency to extract the instantaneous amplitude (IA) of fault signature components (FSCs) from the WT current signals.

The first problem has largely been addressed in [25, 28–30] with a comprehensive theoretical analysis of the stator current spectrum content for the machine operating in steady state, both with and without supply and/or winding asymmetries. The research reported in this thesis will focus on a potential solution to address the second problem where the FSCs in the WT current signals have nonlinear and non-stationary characteristics due to the constantly varying shaft rotating speeds caused by turbine variable loads [31]. Furthermore, a wide range of CM technique performance assessment under relevant transient conditions has not been widely reported in the literature, particularly when the machine operates at low load near to synchronous speed. As a result, in these conditions, the FSCs are particularly difficult to detect or differentiate using existing methods, which may lead to an increase in the false alarms for these conditions. This problem has not received attention in reported literature despite the fact that actual WTs frequently operate at low load conditions where the generator rotational speed is close to the synchronous speed, motivating the research in this study to propose potential solutions.

1.3 Research Objectives

To date, there is a need for an effective approach to address all the issues discussed in the previous section simultaneously. There has been much work to improve the detection quality, however, the computational time is compromised and vice versa. In addition, no such features identification and extraction technique exists in the available literature where an early indication of faults progression can be observed.

The primary objective of this thesis is to improve the cost-effective reliability and availability of CM techniques by using only the current measurements that have already been used by the control and protection systems of WTs, meaning that no additional sensors or data acquisition devices will be needed. This work attempts to target this research area by experimentally defining computationally efficient, highly sensitive signal processing methods to better interpret current signals for WTs operating in variable-speed conditions. The implementation of advanced signal processing techniques could allow for early detection of faults in WTs, allowing proactive decision making, minimizing downtime, and potentially forecasting the remaining useful life of a component given a diagnosed fault.

1.4 Original Contributions

Recently, the analysis of the generator current signal has been introduced as an effective means to detect early abnormalities in WTs. However, there are still potential challenges to analyse a large range of data rapidly at low cost and with modest computer hardware requirements in order to interpret the non-stationary characteristic features of faults. The work presented in this thesis is an effort to address these challenges by developing effective and reliable techniques that can be commercially applied to the generator current signals.

The reported experimental findings demonstrate clear and significant gains in both the computational efficiency and the diagnosis accuracy using the proposed techniques. The developed techniques are also proved capable of indicating the severity of a fault so that a judgement could be made as to when maintenance should take place. This is accomplished by identifying and tracking characteristic fault frequencies in WT CM signals using an adaptive extended Kalman filter (EKF) as the WT speed varies. The proposed technique has been validated experimentally on a WT drive train test rig with two fault levels of rotor electrical asymmetries at

three different driving conditions whose variability is representative of WT generator field operation. The EKF performance was compared with some of the leading WT generator CM techniques. The reported experimental findings demonstrate clear and significant gains in both the computational efficiency and the diagnosis accuracy using the proposed technique.

Another novel contribution of this thesis relates to improving the capability of the continuous wavelet transform (CWT) for the purpose of fault detection. This is accomplished by using an adaptable shape for the mother wavelet rather than the fixed shape in the conventional CWT to track only the fault signature frequencies from the non-stationary characteristics of the WT current signal, while other frequencies unrelated to the fault are left unprocessed. The shape with the number of oscillations of the proposed mother wavelet is adopted according to the oscillatory behaviour of the fault features in the WT current signals. The adaptive approach is tested using laboratory test rig data. The experimental data showed that the improved CWT overcame existing CWT limitations and was capable of correctly tracking characteristic fault frequencies. The improved CWT is then used to develop a new real-time CM technique dedicated to detecting early abnormalities in commercial WT current signals. The proposed technique is computationally efficient for on-line use, and shows promise in dealing with lengthy non-stationary current signals.

1.5 Thesis Outline

This thesis is organized as following:

In Chapter 2, some quantitative studies and literature surveys that have been carried out on reliability of WT components are introduced and discussed. In addition, this chapter features the current state of the art of commercial available

WT CM signal and signal processing techniques, their commercial advantages, challenges and limitations.

In Chapter 3, the characteristic signatures that relate to some faults in the current signal of the generator are presented and discussed. Then a WT model for representing a variable speed machine based doubly-fed induction generator (DFIG) is developed in order to describe how the fault signatures may occur in current signals, and potentially how they may deviate from a healthy and faulty state at fixed and variable speed conditions.

Chapter 4 discusses the capabilities, advantages and limitations of two commonly encountered signal processing techniques, and assesses their suitability for analysis of non-stationary signals. The concept of tracking particular frequencies of interest is also introduced using a recently introduced WT CM technique for extracting fault signatures from non-stationary CM signals. Finally, in Chapter 4, the application of Artificial Neural Networks for detecting faults is discussed to automate the fault detection in the light of the limitations of spectral analysis in processing signals subject to transient effects.

Chapter 5 introduces an effective approach based on an adaptive extended Kalman filter (EKF) that is better capable of dealing with the non-stationary and non-linear characteristics of the WT generator current signals. The proposed approach is used to iteratively track the strength of particular frequency components, characteristic of faults in the current signal. The proposed technique has been validated experimentally on a WT drive train test rig with two fault levels of rotor electrical asymmetries at three different driving conditions whose variability is representative of WT generator field operation.

Chapter 6 proposes a novel frequency tracking technique to analyse the non-stationary current signals by improving the capability of the continuous wavelet transform (CWT). Simulations and experiments have been performed to verify the proposed methods for detecting early abnormalities in WTs. The improved CWT is

then applied for developing a new real-time CM technique dedicated to detect early abnormalities in the generator current signals of a commercial WT. The results prove that the improved CWT overcomes existing CWT limitations and is capable of identifying frequency components of interest and coping with the non-linear and non-stationary fault features in the current signal.

Finally, conclusions are drawn and possible future research challenges are discussed in Chapter 7.

1.6 Summary

Chapter 1 presented the background that motivates the development of this thesis and establishes the research objectives. More specifically, this chapter highlighted the need for advanced WT CM techniques that could allow for early detection of faults in WTs, allowing proactive decision making, minimizing downtime, and potentially forecasting the remaining useful life of a component given a diagnosed fault. As the best wind resource is usually in more remote locations including offshore, a need arises for cost-effective predictive and proactive maintenance. For these reasons, there is a need to develop reliable and effective techniques for WT CM in order to avoid catastrophic failures and to reduce associated costs of unnecessary scheduled maintenance.

1.7 List of Journal and Conference Papers

One journal article has been published so far based on the research presented in this thesis:

- **R. K. Ibrahim**, S. Watson, S. Djurovic, and C. Crabtree, "An effective approach for rotor electrical asymmetry detection in wind turbine DFIGs,"

IEEE Transactions on Industrial Electronics, vol. 65, no. 11, pp. 8872–8881, Nov 2018.

The following peer-reviewed conference articles have been presented and published at international conference proceedings, which are listed below:

1. **R. K. Ibrahim** and S. J. Watson, "Wind turbine simulation model for the study of combined mechanical and electrical faults," in *Scientific Track Proceedings of European Wind Energy Association. EWEA*, Paris, Nov 2015.

2. **R. K. Ibrahim** and S. Watson, "Effect of power converter on condition monitoring and fault detection for wind turbine," in *Power Electronics, Machines and Drives (PEMD), 8th IET Conference*, Glasgow, Apr 2016.

3. **R. K. Ibrahim**, A. Daniyan, and S. J. Watson, "Adaptive fault detection and tracking for a wind turbine generator using kalman filter," in *Offshore Renewable Energy Conference-CORE*, Glasgow, Sep 2016.

4. **R. K. Ibrahim** and S. J. Watson, "Condition monitoring of permanent magnet synchronous generator for wind turbine applications," in *2016 3rd Conference on Control and Fault-Tolerant Systems (SysTol)*, Barcelona, Sep 2016, pp. 648–653.

5. **R. K. Ibrahim** and S. Watson, "Stator winding fault diagnosis in synchronous generators for wind turbine applications," in *5th IET International Conference on Renewable Power Generation (RPG)*, London, Sep 2016.

6. **R. K. Ibrahim**, J. Tautz-Weinert, and S. J. Watson, "Neural networks for wind turbine fault detection via current signature analysis," in *Proc. the WindEurope Summit Conference, Hamburg*, Sep 2016.

7. **R. K. Ibrahim** and S. J. Watson, "Advanced algorithms for wind turbine condition monitoring and fault diagnosis," in *Proc. the WindEurope Summit Conference, Hamburg*, Sep 2016.

Other:

1. **R. K. Ibrahim** and S. J. Watson, "Condition Monitoring and Fault Diagnosis of Wind Turbines Using Generator Output Signals," in *11th EAWE PhD Seminar on Wind Energy in Europe*, Poster, Stuttgart, Germany, September 2015.

2. **R. K. Ibrahim** and S. J. Watson, "Condition Monitoring and Fault Diagnosis of Wind Turbines Using Generator Output Signals," in *East Midlands Universities Association (EMUA) research student conference*, Poster, Lincoln University, United Kingdom, September 2015.

3. **R. K. Ibrahim** and S. J. Watson, "Offshore Wind Turbine Condition Monitoring and Fault Detection," in *Midlands Energy Consortium (MEC) Postgraduate Student Conference*, Poster, Loughborough University, United Kingdom, December 2015.

4. **R. K. Ibrahim** and S. J. Watson, "Online Wind Turbine Fault Detection via Stator Current Spectrum Analysis," in *12th EAWE PhD Seminar on Wind Energy in Europe*, Lyngby, Denmark, May 2016.

Chapter 2

Monitoring of Wind Turbines

2.1 Introduction

This chapter starts with a brief discussion of the reliability of WT components and the resulting interest in effective CM. Based on this discussion, the major WT components and subsystems for modern variable speed machines that require continuous monitoring are identified. This is followed by a brief description of the signals and signal processing methods that are used to monitor these components. The capabilities, advantages and limitations of the common WT CM signals and their processing techniques that have been successfully utilised by industry or studied by academia will be reviewed and compared.

2.2 Wind Turbine Reliability

2.2.1 Introduction to Reliability

Recently, wind energy has experienced a significant move towards offshore installations where a historical record of 4,331-MW of new offshore WTs were globally installed across different markets in 2017 as seen in Fig. 2.1. This represents an increase of 95% on the 2016 market.

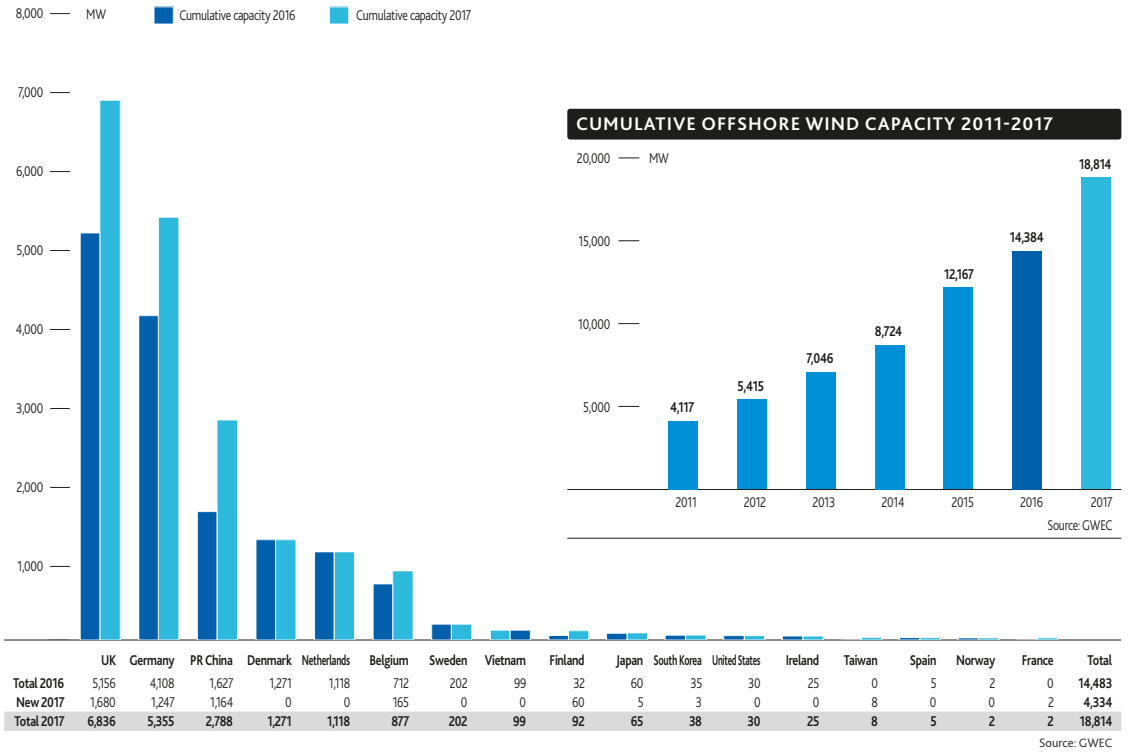

	UK	Germany	PR China	Denmark	Netherlands	Belgium	Sweden	Vietnam	Finland	Japan	South Korea	United States	Ireland	Taiwan	Spain	Norway	France	Total
Total 2016	5,156	4,108	1,627	1,271	1,118	712	202	99	32	60	35	30	25	0	5	2	0	14,483
New 2017	1,680	1,247	1,164	0	0	165	0	0	60	5	3	0	0	8	0	0	2	4,334
Total 2017	6,836	5,355	2,788	1,271	1,118	877	202	99	92	65	38	30	25	8	5	2	2	18,814

Source: GWEC

Figure 2.1 Global cumulative and annual offshore wind capacity end 2017 [1].

The figure shows that there are now 18,814-MW of installed offshore wind capacity in 17 markets around the world. For example, at the end of 2017, nearly 84% (15,780-MW) of all offshore installations were located in the waters off the coast of eleven European countries. The remaining 16% is located largely in China, followed by Vietnam, Japan, South Korea, the United States and Taiwan. The UK is the world's largest offshore wind market and accounts for just over 36% of installed capacity, followed by Germany in the second spot with 28.5%. China comes third in the global offshore rankings with just under 15%. Denmark now accounts for 6.8%, the Netherlands 5.9%, Belgium 4.7% and Sweden 1.1%. Other markets including Vietnam, Finland, Japan, South Korea, the US, Ireland, Taiwan, Spain, Norway and France make up the balance of the market. The main reasons for this significant move towards offshore wind energy globally are the increased wind resource, and the deployment of a new design and configuration of WTs, with large swept area and multi-MW output.

However, the move to offshore environments potentially presents significant challenges regarding operation and maintenance. For example, higher wind speeds in offshore environments can cause much greater mechanical loading of WT components than onshore turbines. In addition, the cost of operation and maintenance is substantially higher in offshore environments where the accessibility is restricted by bad weather conditions, e.g., storms, high tides, etc., which can prevent any repair actions for several weeks. In this case any small failure in turbine components may cause additional cost and significant downtime. These issues have led to a number of studies being performed so far to assess reliability of WT components.

2.2.2 Reliability Studies and Results

Several quantitative studies and literature surveys have been carried out over recent years on reliability of WT components. Amirat et al conducted a survey [32] describing different type of faults, such as generator, blade, gear, and bearing. Recently, Qiao and Lu [33] conducted a comprehensive survey focused on the common failure modes in the major wind turbine components and subsystems, e.g. bearing, electric motor, and control system which are used in multiple WT subsystems, such as pitch and yaw subsystems. In the literature, each component of the WT has its own failure modes and contribution to the downtime of the WT. Fig. 2.2 shows the annual failure frequencies of major WT subsystems and the average downtime caused by the failures of these subsystems based on two large surveys of onshore WTs in Europe over 13 years [2]. The comparison of the failure rate and downtime indicates that the worst contributors to WT failure frequency are the electrical system and electrical control areas with the mechanical subassemblies, gearbox, generator and blades, having a low impact. However, the gearbox, generator and blades have the highest downtime per failure among all the WT subassemblies.

Based on the failure data collected in Germany and Denmark [34], it was found that direct-drive WTs which do not have a gearbox might achieve a higher availability

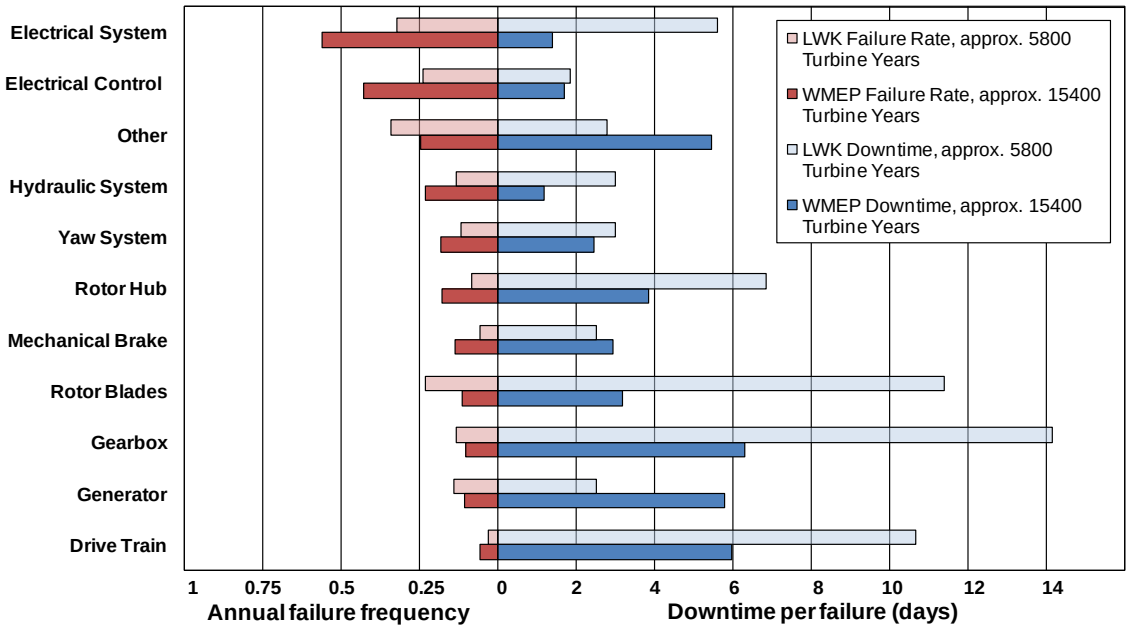

Figure 2.2 Failure frequencies of major WT subsystems and downtime caused by failures of these subsystems [2].

than indirect-drive WTs (with a gearbox). However, in large direct-drive WTs, the failure rate of generators is double that of indirect-drive WTs. The cause of this disparity in failure rates is not known yet. Therefore, the generator has been chosen in this thesis for further investigation because it is necessary for WT operation and central to the debate about turbine structure in terms of whether to use direct drive or geared WTs.

2.3 Reliability of Generators

As wind power has experienced substantial growth compared to other forms of power generation, wind energy conversion has employed variable speed configurations to maximize energy capture and reduce turbine loading. In the early 1990s, most of the installed WTs were designed using a squirrel cage induction generator running close to fixed speed and directly connected to the grid [35], meaning that whatever the wind speed would be, the rotational turbine speed was fixed and determined by the

frequency of the supply grid, the gear ratio and the generator design. During the past few years, the variable-speed WT has become the dominant type of installed WT based largely on doubly-fed induction generator (DFIG) technology, sharing the market with excited synchronous generators and new arrivals, namely permanent magnet synchronous generators. For a detailed analysis of generator types, the reader is referred to the standard literature in this field [36].

While alternative forms of power generation are emerging, a large proportion of currently installed and manufactured WTs continue to use induction generators. The DFIG in particular remains an attractive generator technology with a strong market position [37] due to its unique wide range variable-speed-constant-frequency operating capability coupled with low power electronic inverter rating requirements and effective power flow control. Undetected generator faults in DFIGs have been associated with high failure rates, replacement of major components and subsequent significant downtime [27]. The primary cause of this higher downtime in the offshore environment is the increased need for heavy-lifting vessels [38]. Usually, faults evolve from an incipient stage to a progressively more severe condition and eventually turn to failure. Early fault detection can hence avoid catastrophic failures and downtime reduction through careful condition based maintenance planning [39].

A study by Alewine analysed the reliability of generators [3]. The results of this analysis are compared in Fig. 2.3 with another reliability analysis of other rotating machines [4]. The results clearly show that rotor related faults and slip ring failures contribute significantly to total generator failures, particularly in small and medium-sized WT generators, despite the fact that bearing faults are dominant.

An analysis of failure statistics showed that 20% to 70% of the generator faults were related to bearings, 3% to 38% to the stator, 7% to 50% to the rotor and the rest were categorized as “others” [40]. Another study, which reviewed 80 journal papers published by the IEEE and IEE/IET on the subject of induction machine

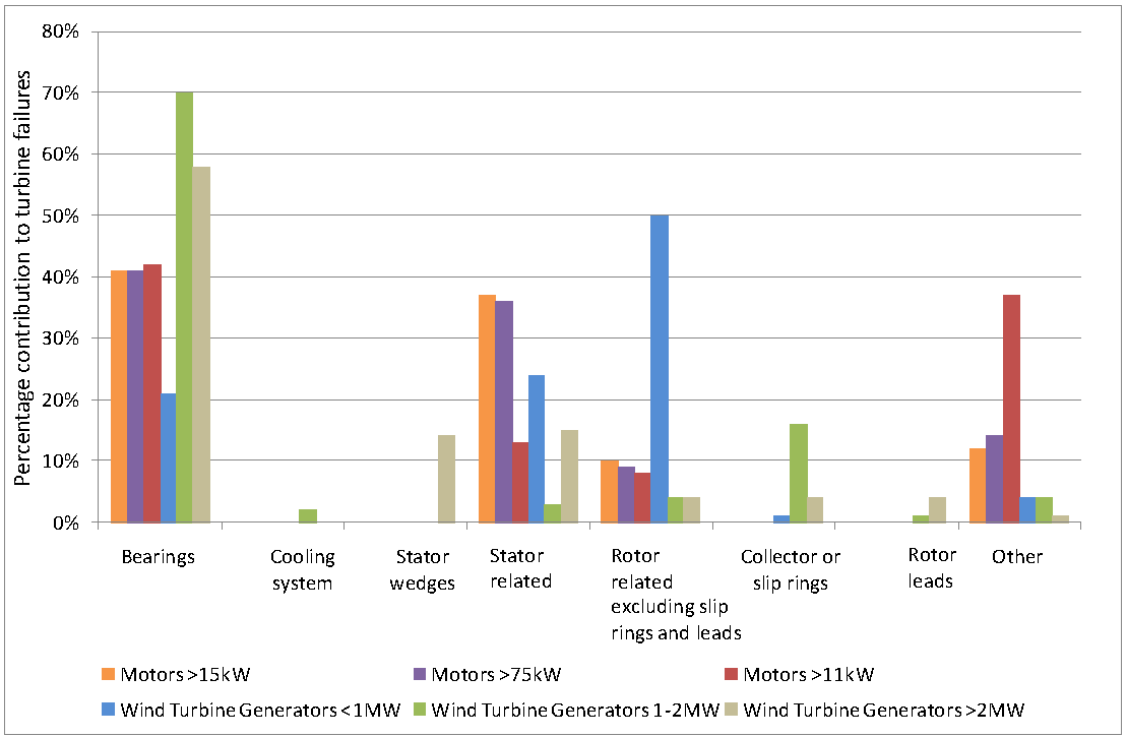

Figure 2.3 Comparison of failure contribution of WT generator components according to [3, 4].

failure statistics over the past 26 years, reported that 21% of generator faults were bearing problems, 35% stator related and 44% rotor related [4].

Rotor electrical unbalance is identified as an indicator of some of the major contributors to WT generator failure rate [24, 41]. This condition is representative of a number of recognized rotor electrical fault modes in DFIG systems such as brush gear degradation, rotor winding fault and/or improper connection between the slip ring unit and the rotor cable leads and its analysis and detection has been the topic of a number of studies conducted on representative academic scale test rig systems and MW size DFIG field applications [24, 25, 29, 39, 4, 40–43]. Undetected electrical faults may gradually develop into a major short circuit, and can cause severe damage to the machine and the system to which it is connected [44]. Early detection of rotor electrical unbalance faults of in-service generators is essential to

eliminate consequential damage. Thus, the detection of rotor electrical unbalance faults has been chosen for further investigation in this thesis.

2.4 Condition Monitoring System

Over the years, there has been much work to maximize energy capture, reduce costs and improve reliability of WTs [45]. With this work has come investment and the development of new technologies from WT manufacturers. Better design is of course one answer to increase the reliability and availability of WTs; the other is condition monitoring of the WT systems [46]. This allows for early detection of faults in wind turbines, allowing proactive decision making, minimizing downtime, and potentially forecasting the remaining useful life of a component given a diagnosed fault.

A WT condition monitoring system (CMS) can be defined as the process of monitoring and providing information on the condition of components in WTs before or during an early stage of abnormal operation. In other words, a CMS can be used as a tool to evaluate WT state of health during operation and measure WT performance indicating the need for remedial action when performance deteriorates. Most components in WTs are subjected to different sorts of failures. Over time, electrical and mechanical stresses can damage other components within the machine. For example, failure of a bearing could result in an entire gearbox replacement. If a particular damage is not detected or rectified, it can cause the WT to operate outside of its normal parameters and eventually a catastrophic failure will occur, causing potential damage to surrounding components and equipment, as well as lost revenue due to an unscheduled power outage. WTs cannot be maintained instantaneously in response to every problem that is detected. This is impractical and expensive, particularly in the offshore environment which requires forward planning and the use of an appropriate vessel, a particular crane or a helicopter.

It has been reported in [20, 32] that the CMS can potentially help by firstly, detecting incipient failures early. Secondly, it can be used to accurately evaluate component health conditions. Finally, it can be used to analyse root causes, which may provide the inputs for improved turbine operation, control strategy, and component design. The CMS is not able to avoid sudden failures, but the use of CMS allows maintenance to be planned, or other actions to be taken to avoid the consequences of catastrophic failure, before the failure occurs [47]. Moreover, success in detecting and repairing early faults not only avoids a catastrophic failure, but also has other system benefits, such as maintenance cost reduction, more efficient plant operation with consistent quality, plant availability and reliability improvement. Thus, a reliable CMS is required to detect and diagnose WT failures in their early stages.

In order to develop an effective CMS, there is a need for information to credibly describe the state of the monitored component and a reliable technique for fault feature extraction and fault diagnosis. In other words, the most important elements of a WT CMS are the measured signal and a signal processing technique to provide accurate interpretation of the measured signals. Therefore, the remaining part of this chapter will focus on signals and signal processing methods for WT CM. The capabilities, advantages and limitations of the common WT CM signals and their processing techniques that have been successfully utilised by industry or studied by academia will be reviewed and compared.

2.5 Signals Available for WT CM

The signals used for WT CM mainly include vibration, lubrication oil quality parameters, temperature, torque, acoustic emission, supervisory control and data acquisition (SCADA) system and electrical signals. They are acquired using appropriate sensors installed in various WT components. A brief description of the aforementioned signals is discussed in the next subsections.

2.5.1 Vibration

Most mechanical faults in the main components of WTs cause particular vibration and noise frequencies. These faults can be detected by using the signals acquired from vibration sensors. Vibration diagnostics have been used to detect mechanical faults [48, 49]. For example, vibration-based CM techniques are mostly applied to the rotor and blade, drivetrain shaft, gearbox, bearings and tower of the WT [20, 50]. These techniques usually employ the statistical analysis in the time-domain or the fault signature identification in the frequency-domain or joint time-frequency domain. The amplitude of the vibration signal or the fault signature can indicate the severity of a fault [6].

However, there are several challenges that must be addressed in order to use the vibration signals for WT CM. The first challenge with vibration monitoring is the high cost, owing to the requirement for additional sensors and hardware to be installed on the turbine [32]. Secondly, vibration signal analysis can be complicated, because the mechanical drive system is affected by turbulent wind conditions and load variation, particularly in wind farms situated in mountainous or hilly areas [51]. Furthermore, it has been reported that sensor failures contribute to 14.1% of the total failures of WTs [52] which can cause unnecessary downtime and additional operation and maintenance costs. In this case, the WTs might be turned off and go to downtime even at simple faults due to the wrong information collected from these sensors which is used for condition monitoring.

2.5.2 Lubrication Oil Parameters

Oil condition monitoring has been commonly used to detect potential cracks and mechanical wear in WT components which require lubrication such as the gearbox, generator, and main bearing. The principle behind lubrication oil condition monitoring is to use various sensing techniques to directly or indirectly monitor basic

lubricant degradation features. Basic degradation features includes oil oxidation, water contamination, particle contamination and oil dilution. For example, detecting and filtering the metal debris from cracked gearbox wheels or bearings is the current practice in oil debris monitoring [53]. In particular, the amount and type of metal debris can indicate the health of the component. Oil analysis is mostly performed off line (manually), by taking samples on at regular intervals , and then sent to a laboratory for analysis [54]. This is a time-consuming and labour-intensive process, especially with the increasing numbers of WTs.

Recent studies have tried to overcome the drawbacks of the offline monitoring by using oil sensors, such as viscometers, level sensors, particle counters, and thermometers, to monitor the oil condition in real time [55, 56]. However, most of these sensors need to be specially designed and fabricated which potentially increases the costs of the WTs. Additionally, not all the lubricant degradation features can be monitored in real time using such oil sensors [57]. Furthermore, there is a challenge to accurately interpret the real-time measurements of the oil parameters due to the impact of the variable operating conditions.

2.5.3 Temperature

The WT components have certain temperature values during normal operating conditions. Temperature-based monitoring tries to detect thermodynamic changes in the mechanical systems such as bearings and the gearbox which might indicate degradation and imminent failure. Temperature-based techniques have been also used to detect generator winding short-circuits, rotor over-speed and power converter faults. Model-based monitoring using techniques such as e.g. multi-linear regression, artificial neural networks or adaptive neuro-fuzzy inference systems has been demonstrated to be able to detect mechanical failures up to several months in advance [58–62]. Further approaches have tried to derive more physical models based on SCADA temperatures [63–65].

Temperature monitoring is usually accomplished either by installation of temperature sensors locally, or by using thermographic (infrared imaging) cameras [53]. Infrared thermography is a technique used to capture thermal images of components where each component emits infrared radiation according to its temperature and its emissivity.

However, changes in temperature associated with a fault can develop slowly and often such trends are not adequate to provide an early indication of the fault. For example, Feng et al. [66] monitored temperature signals from a gearbox over a period of time. The results showed a rising gearbox inefficiency in the 9 months before failure with a worsening trend presented 3 months before failure. Another drawback is that the measured temperature can be influenced by its surroundings. It has been reported that bearing temperature depends on the bearing fault, the amount of grease in the bearing cavity, the winding temperature, the ambient temperature, stator current heating, and rotational speed [67]. These factors are difficult to estimate in complex systems like WTs that operate in high noise environments. Therefore, further analysis is frequently required to find out the reason for abnormal temperature behaviour in a WT component.

2.5.4 Torque

Torque-based monitoring has been used to detect abnormal torque oscillations due to mechanical drive train faults. Torque measurements could be obtained using rotary torque sensors installed on WT mechanical components, such as the main shaft, gearbox, generator, etc. For example, using a test rig, with features similar to a wind turbine drive train, Wilkinson et al. [68–70] demonstrated that by monitoring the torque speed variation it was possible to detect faults in gearbox, shaft, main bearing, rotor unbalance and coil. In work [71, 72] statistical analysis of torque signal was used successfully to monitor turbine blade performance and rotor imbalance.

However, the torque signal is costly, very noisy and difficult to extract in practice [73]. For these reasons torque monitoring is rarely used in the wind industry.

2.5.5 Acoustic Emission

Acoustic emission monitoring is done by measuring and analysing acoustic emission signals which are emitted by certain components. This method is typically applied for fault detection in gearboxes, bearings, shafts, and blades [53]. For example, an intelligent sensing module, with the ability to detect developing faults in a gearbox at an early stage, is presented by [74]. The result of this work showed that there are a number of requirements for an effective system, namely: the number of sensors which need to be used, where sensors should be located, and the need for a high-specification Amplifier/Filter/ADC capable of processing high frequency and low amplitude acoustic emission signals with a high signal to noise ratio and the ability to select sampling frequency and sensor response. In recent work, acoustic emission monitoring has been applied to detect wind turbine blade defects [75, 76]. Some of the significant challenges of using acoustic emission for damage detection are that it is relatively expensive to implement and it can be difficult to extract the signal features. Other drawbacks are the difficulty of getting access to machinery for installation and only certain types of faults can be detected in the monitored high frequency range. Acoustic emission analysis is rarely used in isolation. It is far more common to combine the use of acoustic emission monitoring with vibration monitoring [77, 78]. Perhaps, one of the most significant challenges is processing the large amount of data which might be required in order to capture useful features which can indicate damage.

2.5.6 SCADA Signals

Commercial wind turbines are equipped with a Supervisory Control And Data Acquisition (SCADA) system that usually records operational data only in ten-

minute averages [79, 80]. The common setting of wind turbine SCADA systems to record 10-minute averages is motivated by the characteristics of wind. Wind varies significantly in time: from year to year, but also seasonally, in the scale of several hours up to few days (storms and weather systems) and during seconds and minutes (turbulence). If the spectrum is analysed, it can be seen that there is little energy in the range between 10-minute and 2-hours. Accordingly, 10-minute averages are a suitable choice to describe the wind resource without considering turbulence. The wind industry has used SCADA signals for WT CM and most wind farms now have a SCADA system providing data to remote control rooms. The recorded signals cover environmental and control parameters, e.g. wind speed, wind direction, pitch angle, rotational speed and three-phase power output. Although SCADA data were intended for control and performance monitoring in the first place. Multiple approaches of condition monitoring with these data have been proposed [81].

However, the main limitation of the common SCADA data lies in the very low time resolution. The setting of the SCADA system might be revised to enable data acquisition with a higher sampling rate for condition monitoring purposes. The selection of a specific sampling rate is a trade-off between higher accuracy with higher resolution and lower effort in terms of data acquisition, storage and post-processing for a lower rate. However, the benefit of higher resolution is not the same for different monitoring techniques.

2.5.6.1 Temperature-based monitoring

Temperature signals in the common 10-minute SCADA resolution are used to generate 'high temperature' warnings in real time which might lead to a shut-down of the turbine. However, these alarms can be considered as very late warnings [82]. If the temperature behaviour is monitored with normal behaviour models, slow developments can be detected and the resolution is usually further reduced by averaging over a longer period [60, 62].

Up to now, wind turbine condition monitoring with temperature signals of higher resolution than 10 minutes has not been investigated. It is doubtful that more frequent measurements would reveal new insights due to the thermal inertia of the system and also low accuracy if thermocouples are used.

2.5.6.2 Power-curve analysis

Most power curve monitoring studies have used 10-minute SCADA data to detect under performance. Gonzalez and Melero [83] investigated data with a sampling period of 4 s. The results indicated that the higher resolution monitoring was enabling detection of aerodynamic under-performance events associated with such as icing, yaw misalignment, etc.

However, it is unlikely that increasing the sampling rate further to multiple Hz will result in improved power curve monitoring as the system inertia and damping will significantly affect the response of the turbine to the wind load. As the input reference needs to have the same resolution as the power signal, the commonly used nacelle-top anemometer would not be a suitable tool to describe the wind at a resolution of multiple Hz [84]. Furthermore, the analyses would need to consider the sinusoidal time-series of the power signal.

2.5.6.3 Further monitoring approaches

Some manufacturers include tower-top and drivetrain acceleration measurements in the SCADA system. Such acceleration signals with a sampling period of 10 s have been used for investigating clustering and model-based monitoring approaches [85]. There might be potential for using higher resolution vibration and acceleration signals for further improving the fault detection capabilities. However, traditional frequency-domain vibration analysis might require a sampling rate of multiple kHz as used in CMS. The common setting of wind turbine SCADA systems to record 10-minute averages is motivated by the characteristics of the wind. Wind varies

significantly in time: from year to year, but also seasonally, on the scale of several hours up to few days (storms and weather systems) and over seconds and minutes (turbulence). If the spectrum is analysed, it can be seen that there is little energy in the range between 10 min and 2 h [86]. Accordingly, 10-minute averages are a suitable choice to describe the wind resource without considering turbulent fluctuations.

However, the collection of SCADA signals was initially intended for operational purposes, not really for the purpose of CM which is why these signals are recorded as 10-minute averages. As a result, the valuable and useful features of most WT faults are lost due to averaging over a relatively long interval. Thus, the detection and diagnosis of most WT faults cannot be done by monitoring 10-minute SCADA averages.

2.6 Electrical Signals

Voltage and current are electrical signals which can be acquired from the terminals of generators and motors in electrical machines. Electrical signal-based methods for CM have been well established, primarily motor current signature analysis, for condition monitoring and diagnosis of rotating electrical machine faults [4, 87–89]. Previous work [44, 89–94] has looked at the use of stator currents to detect induction motor faults, such as winding faults, unbalanced stator and rotor, broken rotor bars, eccentricity, and bearing faults. Instantaneous power (calculated using voltage and current signals) has also been used to monitor such faults [95–97]. Electrical signal-based monitoring has consequently been proposed as a general tool for WT condition monitoring and fault diagnosis [22, 23, 20]. For example, current signals have been applied for bearing fault detection in WTs [98–100]. Instantaneous power has also been used for bearing fault and generator fault detection in WTs [5]. More recently, work has been extended in this area to monitoring the phase stator current for fault diagnosis and prognosis of wind turbine drivetrain gearboxes [101]. Electrical signals

can also be used to detect wind turbine blade faults by using current measurements or power measurements [102, 103].

There are several advantages that monitoring the electrical signals offers when compared to other condition monitoring methods. For example, electrical analysis can provide a reliable indication of the presence of a fault for the monitored system; it can indicate the location and severity of the fault; it can give immediate information about the state of health of that system [104], in contrast with oil analysis, where several days may elapse between the sample collection and its analysis. Moreover, the main driver for using electrical signals is to reduce costs given that the electrical current and voltage are continuously measured [105, 106]. This would indicate that fault detection based on the measurement of electrical signals could be simpler, more comprehensive and cheaper compared to other techniques. This research will be based entirely on the use of current measurements for WT CM and fault detection. A summary of WT CM and fault detection methods are listed in Table 2.1.

Table 2.1 Summary of WT CMS and fault detection methods

Monitoring Technology	Main Components Monitored	Disadvantages
Vibration monitoring	Blade, gearbox, bearing, generator	High cost, intrusive
Oil monitoring	Gearbox, bearing	Limited, intrusive
Temperature monitoring	Gearbox, bearing, generator	Unreliable, intrusive
Torque monitoring	Blade, shaft, generator	High cost, high complexity, intrusive
Acoustic emission monitoring	Bearing, blade, gearbox	High cost, intrusive
Electrical monitoring	Blade, gearbox, bearing, shaft, generator	Low signal to noise ratio

To date, electrical signal-based monitoring has not achieved commercial application due to potential challenges. Firstly, it is a challenge to extract WT fault signatures from non-stationary current measurements, due to variable-speed operating conditions of WTs [20]. Moreover, the useful information in current measurements for a WT usually has a low signal to noise ratio, and thus is very difficult to extract

without advanced signal processing methods to interpret non-stationary current measurements [107, 31].

2.7 Signal Processing Methods for Feature Extraction

Electrical signal analysis has been shown to be a complex task and frequently involves the use of signal processing methods to facilitate fault features identification and extraction from the WT generator current and voltage signals. To monitor or detect faults, usually a threshold comparison is performed. If the monitored values of the fault features exceed a defined threshold, this indicates the presence of a fault. Probability analysis of failures using extracted fault features can be also used for WT CM and fault detection. The signal processing methods used for WT CM can be categorised into time-domain, frequency-domain and time-frequency analysis.

2.7.1 Time-Domain Methods

Classical time-domain analysis methods (e.g., statistical analysis, Hilbert transform, and envelope analysis) are the most simple methods that have been used for WT CM. The principle of these methods is often to simply obtain appropriate parameters, such as standard deviation, mean, root mean square (RMS), peak, peak-to-peak interval, etc., of the monitored signal acquired from a healthy WT. These features are firstly recorded as reference values at different operating conditions, and continuously monitored during the WT operation. Then if they deviate from their base thresholds, it may indicate the presence of a fault in the monitored WT.

Time domain statistical methods are usually used to analyse acoustic, temperature and vibration signals [59, 108, 109]. Time-domain analyses of electrical signals have focused on detecting wind turbine abnormalities through deriving a reference

power curve, showing the relationship between the wind speed and the generator output power during normal operating conditions [110–114].

The traditional methods based on time domain analysis are simple, easy to implement and mature techniques. On the other hand, these methods can mostly only be used to indicate the presence of a failure in a WT. It is difficult to employ these methods for early fault detection or to provide detailed information of the fault location or mode. This is due to the fact that many WT faults can cause very similar changes in the monitored feature, e.g. the power curve. Thus, frequency domain techniques and advanced time-frequency analysis techniques have been proposed in recent years in order to achieve better interpretation of the WT current signals.

2.7.2 Frequency Domain Methods

Frequency domain techniques used for WT CM (e.g., envelope analysis [115], cepstrum analysis[116], and spectral Kurtosis [117]) are based upon the fast Fourier transform (FFT). The FFT converts the time domain signal into a frequency domain signal in order to facilitate the extraction of fault component frequencies of interest from the time domain signal. The presence of certain frequency components in the frequency spectra of WT CM signals can be related to a particular fault. These components can be used as fault signatures for WT CM and fault diagnosis. Monitoring the magnitude of fault signatures can indicate the fault levels. It was reported in [118] that the FFT method can be used to extract the characteristic frequencies related to a bearing fault using the current signals of an electrical machine. In[29, 119, 120] the characteristic frequencies of certain WT generator faults were successfully extracted by applying the FFT method to generator current or power signals. The FFT method has also been applied to current signals to identify the characteristic frequencies of not only rotor blade unbalance [102, 103] but also gearbox and main bearing faults [98–101, 121].

However, the current signals from an operational WT are not stationary but are time-varying in nature because of the constantly varying loads and non-linear operation of the turbine. The FFT and those techniques developed based on it are not ideal for processing these signals because of inherent limitations (e.g. time-averaging effects). Therefore, a number of more advanced time-frequency analysis techniques have been proposed in recent years in order to achieve better interpretation of the WT current signals.

2.7.3 Time-Frequency Analysis Methods

Frequency domain methods are difficult to apply to non-stationary WT current signals and to explicitly interpret their time-varying nature. For this reason, time-frequency analysis methods have gained much more attention in the field of WT CM and fault diagnosis.

The Short Time Fourier Transform (STFT) is the simplest time-frequency method in the area of signal processing. The STFT analysis has been widely used to compute the spectrogram of a time signal giving the spectral density of a signal varying with time. This method has been successfully used to detect a variety of faults in induction machines, such as bearing deterioration [122, 123], rotor unbalance and a broken bar [124]. In [125, 126], the STFT was proposed as a means to detect rotor unbalance in a WT induction generator. One problem with the application of a STFT is that it analyses signals with fixed sized windows which yields limited frequency resolution that is not optimal for processing non-stationary WT CM signals with spectral resolution required for diagnostic purposes. This means that a good frequency resolution cannot be achieved using wide windows, which is desired for the analysis of low-frequency components. Also, a reasonable time resolution using narrow windows, which is desired for the analysis of high-frequency components, cannot be achieved. For this reason, the STFT is not suitable for time-frequency analysis of non-stationary WT current signals. Accordingly, more complex techniques

such as the wavelet transform have been proposed for tracking characteristic fault frequencies and extracting the necessary information to detect these faults and their severity [5, 127, 128].

The use of wavelet transforms in the analysis of current signals has been successfully established for detecting induction motor faults [94, 124, 129, 130]. These studies have employed the discrete (dyadic) wavelet transform (DWT) to decompose the current signal and extract the fault features in the signal. The DWT has limitations when analyzing non-stationary WTG current signals. Therefore, the continuous wavelet transform (CWT) based on, for example, a Morlet wavelet has been proposed for WT condition monitoring [5, 131]. This transform in previous work was mainly used to track a single variable frequency component at twice slip frequency divided by pole pairs ($2ksf_1/p$) in order to determine its magnitude as an indicator of a fault. However mechanical and electrical faults frequently manifest themselves as changes in the magnitude of several spectral components [4, 132].

It has been reported in [20, 31, 98] that high time resolution and high frequency resolution cannot be achieved simultaneously using a CWT and thus even this transform still cannot provide accurate interpretation of non-stationary WTG signals. Another drawback inherent to the wavelet transform is that it represents the analysed signal in terms of predefined functions (e.g. mother wavelet functions) that are defined in advance based on experience to extract the target diagnostic feature in the signal that varies in time. In the light of the previous research mentioned above, satisfactory results have not been achieved today using the CWT. Moreover, the computational time required for the CWT analysis to produce useful results for a signal recorded over long intervals and with wide frequency ranges is prohibitive.

To better process the WT CM signals, the spline-kernelled chirplet transform (SCT) was proposed recently[133], and an improved SCT developed [134] to extract the instantaneous amplitude (IA) of a nonlinearly varying fault signature component. The improved SCT proved capable of detecting mechanical and electrical fault

signatures in a WT drive train in less than half of the time needed by the conventional SCT. However, the required computational time is still considerable as the results in [134] show that the improved SCT required 135s to extract the IA of one frequency component related to the fault from 300s of the power signal. This significantly limits a more extensive application of the SCT in WT CM. Despite recent progress in SCT development, further improvement of WT CM techniques with accurate interpretation of the measured signals and minimization of the computational time still remains a current research goal.

In light of the previous work, satisfactory results have not been achieved today using time-frequency analysis techniques. Thus, an effective and computationally efficient signal processing technique is still needed to interpret non-stationary current signals acquired from variable-speed wind turbines for a cost-effective WT CM system.

2.7.4 Artificial Intelligence Methods

Signal processing is mainly used in WT fault studies to facilitate the extraction of fault-related features in the monitored signals, and then, the fault detection can be automated via threshold comparison or probability analysis. The fault level and location can then be identified by an artificial intelligence method. The term artificial intelligence involves various different techniques, such as expert systems, artificial neural network (ANN), and fuzzy logic, support vector machine (SVM), which can all be used individually or in a combination, to improve their efficiency. Although these methods require an initial training phase, they have adequate capacity to process a large amount of data. The training phase requires a comprehensive set of expected scenarios to avoid erroneous or produce results which are limited to a set of examples.

ANNs have been primerly used as a fault classifier for analyzing and predicting faults associated with different WT components, such as gearboxes [135, 136],

bearings [137, 138], generator, power electronics, rotors, blades and pitch angle control [139, 140]. The main drawbacks are the amount of inputs required, over-training of the networks, the extrapolation errors and the difficulties of optimizing the network [141].

Fuzzy logic systems have been used for WT CM and fault diagnosis in many studies. In [142], a small-sample WT fault detection method with the synthetic fault data was presented to detect WT faults. In [143], a fault diagnosis method based on identified fuzzy models was proposed. In [144], a fuzzy synthetic model based on a real-time condition assessment method was developed. In [145], based on the fuzzy theory, a generalized anomaly detection model which integrated different data prediction models was proposed. Fuzzy logic systems are designed to perform certain rules to deal with reasoning based on fuzzy sets of linguistic rules. Fuzzy logic rules are set to extract information related to faults and then used for fault diagnosis. However, setting the rules requires comprehensive background knowledge of faults conditions and variables (i.e., fault modes, locations, and severities), which is usually not available in practice. Failure to set accurate and robust rules can cause false diagnostic results. In addition, more sophisticated rules will increase the size of a fuzzy logic system and making it computationally expensive.

Recently, a combination of the two previous techniques called neuro-fuzzy technique has been developed to obtain optimal weights in ANNs and to optimise the rules setting in fuzzy logic systems. This optimisation of rules is performed using training examples, by minimizing expert intervention during the formulation of conditional rules. [146] and [147] have shown that this combination achieve higher accuracy in comparison with ANNs for diagnosing and monitoring WTs. However, neuro-fuzzy techniques are sensitive to the size of training data. To develop an effective neuro-fuzzy model that is capable of estimating a certain output, large historical operational data is required, which is potentially challenging to a newly-built wind farm particularly in offshore.

SVMs have been proposed for WT fault detection and isolation. In [148], a method of WT fault classification and detection based on Cuckoo search optimization SVM parameter was proposed. In [149], the application of SVM algorithms to predict WT generator bearing failure through analysis of high-frequency vibration data was presented. In [150], a model for alarms-related WT fault detection based on kernel SVMs was developed. However, SVMs are also a data-driven heuristic technique and, therefore, have similar shortcomings of ANNs [20].

2.8 Summary

This chapter presented some relevant literature on the reliability of WT components. The basic ideas of WT CM and fault diagnosis were discussed, and the most predominant WT CM signals that have been used or studied were reviewed and compared. The functions, capabilities, and limitations of signal processing methods that have been employed for the analysis of WT CM signals were comprehensively described in the literature overview. Special attention was paid to the use of signature analysis of electrical signals in order to arrive at a better understanding of some of the challenges of CM a non-stationary signal. This thesis will be focused entirely on the use of current measurements for WT CM and fault detection, and the solution of major problems faced to identify and track spectral fault signatures in current signals under variable speed operation in order to enable non-intrusive online fault detection.

Chapter 3

Current Signature Analysis to Detect WT Fault Conditions

3.1 Introduction

The current signals in electrical machines carry dynamic information about the machine. These signals have potential to be used for WT CM by the wind power generation industry. In this chapter, the characteristic signatures that related to certain faults in the current signal of the generator are presented and discussed. Then to describe how the fault signatures may occur in current signals, and potentially how they may deviate from a healthy state, firstly under steady state, constant speed test operation and secondly under transient, variable speed conditions, a WT model for representing a variable speed machine based doubly fed induction generator (DFIG) is developed. The model performance is validated against experimental data from a test rig under healthy and faulty conditions. The WT model is then run under actual variable conditions recorded over a period of a two-year measurement campaign on an operating WT to investigate the kind of results expected under such conditions.

3.2 Characteristic Signatures in Current Signals

Monitoring the signatures in the WT current signal is based on the principle that each fault has its own characteristics in the current signals in the form of particular frequency components. While there has been a wide range of faults studied in the literature, the Author limits this introduction and discussion to rotor electrical asymmetry and rotor eccentricity as both are common faults in a WT DFIG. Rotor electrical asymmetry has been shown to be a significant indicator of WT generator faults, caused by common winding, brush gear, broken rotor bars and high resistance connection faults [29, 4, 41, 151, 152]. Rotor eccentricity has been shown to be a significant indicator of bearing faults, caused by shaft misalignment, unbalanced torque and wearing of bearings [153–156]. Thus, early detection of rotor electrical asymmetry and rotor eccentricity is essential to significantly reduce WT downtime and plan maintenance in advance. In addition, a fully satisfactory method to detect the full range of WT faults in their early stages has not been achieved yet, and false alarms are still frequently reported with the generator being a significant contributor [27], demonstrating the need to develop reliable techniques for feature extraction that can subsequently be suitable for real-time applications.

3.2.1 Rotor Eccentricity

Rotor eccentricity can be classified into two forms of eccentricity: static or dynamic. In the case of static eccentricity, the airgap has a fixed minimal position, whereas dynamic eccentricity occurs when the center of the rotor is not at the center of rotation and the position of minimum air-gap rotates with the rotor [157]. The causes of either type of rotor eccentricity are many, such as a bent shaft, mechanical resonances at critical speeds, or bearing wear and movement [4, 156]. Moreover, it has been reported that eccentricity related faults commonly occur as a result of

bearing faults [158, 159]. Thus, the detection of rotor eccentricity faults in WTs could potentially be a good indication of bearing failure.

The presence of static and dynamic air-gap eccentricity induces additional frequencies called fault signature components (FSCs) around the fundamental frequency components in the current signal. The equation that describes the frequency components is given by [159, 157]

$$f_{ecc} = \left((kR \pm n_d) \frac{(1-s)}{p} \pm v \right) . f_s \tag{3.1}$$

where $n_d = 0$, in the case of static eccentricity, and $n_d = 1, 2, 3$, in the case of dynamic eccentricity, R is the number of rotor slots, s is the slip, v is the order of the stator time harmonics that are present beside the fundamental frequency components in the current signal, and p is the number of pole pairs.

3.2.2 Rotor Electrical Unbalance

Rotor electrical unbalance is one of the major contributors to WT generator failure rate [160]. Usually, the cause of rotor electrical unbalance is inter-turn, winding insulation and brush gear faults [151, 4]. Undetected inter-turn faults may gradually develop into a major short circuit, and can cause severe damage to the machine and the system to which it is connected. Therefore, early detection of rotor electrical unbalance faults during operation is essential to eliminate consequential damage.

It has been experimentally shown in [29, 30] that rotor electrical unbalance faults in a WT DFIG actually induce additional FSCs in the current signals given by:

$$f_b = \left(\frac{k(1-s)}{p} \pm i \right) . f_s \tag{3.2}$$

where f_b and f_s are detectable spectral components due to the fault and fundamental frequency components, respectively, k is the harmonic order (k= 1, 2, 3, 5...),

s is the slip, i is a constant which relates to air-gap field space harmonics resulting from the layout of the machine and p is the number of pole pairs.

The analysis of the stator current signal under rotor eccentricity and rotor electrical unbalance $I_s(t)$ can be modeled by adding the fault signal $\bar{I}_f(t)$ to the stator current signal under the steady state $\bar{I}_s(t)$:

$$\begin{aligned} I_s(t) &= \bar{I}_s(t) + \bar{I}_f(t) \\ &= I_{max}\sin(2\pi f_s t + \phi) + I_f \sin(2\pi k f_f t + \phi_f) \end{aligned} \tag{3.3}$$

where I_f is the maximum amplitude of the additional FSCs during the fault at each k. Note that the number of additional FSCs can be determined by the parameter k in equations (3.1) and (3.2). During the rotor eccentricity event, the stator current signal can be represented as:

$$I_s(t) = I_{max}\sin(2\pi f_s t + \phi) + I_f \sin(2\pi k\Big((kR \pm n_d)\frac{(1-s)}{p} \pm v\Big).f_s t + \phi_f) \tag{3.4}$$

For the rotor electrical unbalance fault, the stator current signal can be represented as:

$$I_s(t) = I_{max}\sin(2\pi f_s t + \phi) + I_f \sin(2\pi k\Big(\frac{k(1-s)}{p} \pm i\Big).f_s t + \phi_f) \tag{3.5}$$

3.3 Wind Turbine DFIG Modelling: Case Study

One of the challenges to conduct this investigation using only a laboratory test rig is the need for extra equipment and instruments leading to additional cost and complexity. The time and development costs can be avoided considerably by developing a WT model with sufficient level of accuracy. For this purpose, a WT

dynamic model for representing a variable speed machine based doubly-fed induction generator (DFIG) has been developed and validated against laboratory tests made on a physical test rig under healthy and faulty conditions. The WT model is driven at actual variable speed conditions to investigate the impact of the variable speed on the fault signatures. The proposed WT model was implemented in MATLAB/Simulink, including wind speed, rotor, pitch control system, drivetrain and generator sub-models as illustrated in Fig. 3.1. Mathematical models for the representation of these sub-models have been extensively developed with a sufficient level of accuracy in the literature for a detailed description, the reader is referred to the standard literature in this field [161–163]. Some components, including yaw systems, tower, bearings, brakes and power converter have not been considered in the proposed model. This should not be a problem, as the purpose of this work is to identify electrical and mechanical faults in electrical signals, and the impact of those components on the stator current can be assumed to be rather limited.

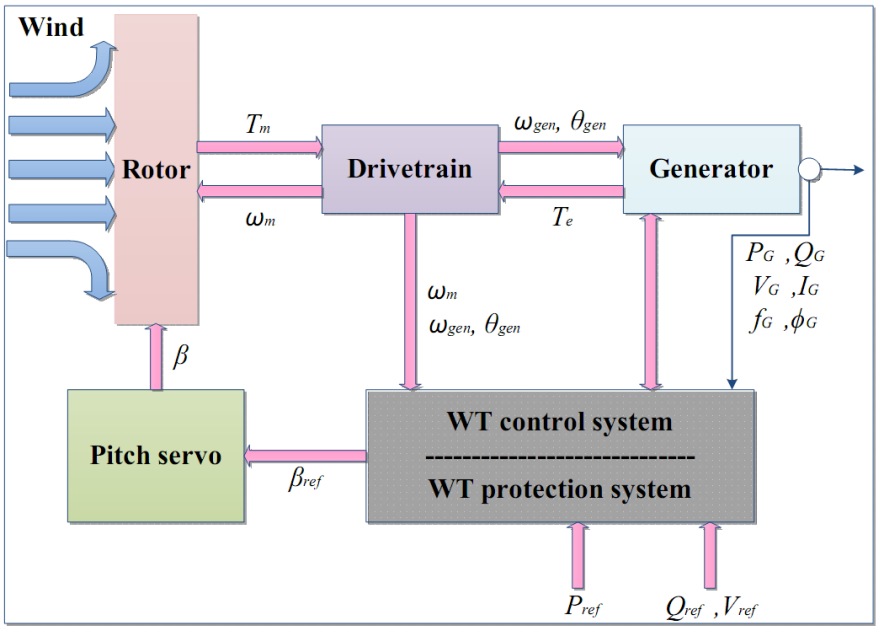

Figure 3.1 Overview of the WT model

3.3.1 Wind Speed Model

A wind model is used to generate short-term wind speed variations with certain characteristics, such as mean wind speed or turbulence intensity, which a WT will experience. A simple random walk is used of the form [164]:

$$U_{t+1} = rU_t + (1 - r)\bar{U} + \varepsilon_t \tag{3.6}$$

U_{t+1} is the value of wind speed at time $t + 1$, U_t the value at t, $\bar{U}$ the desired mean wind speed value, r the auto-correlation at unit lag and ε_t a Gaussian noise term. An example of a wind speed sequence generated using this approach is shown in Fig. 3.2.

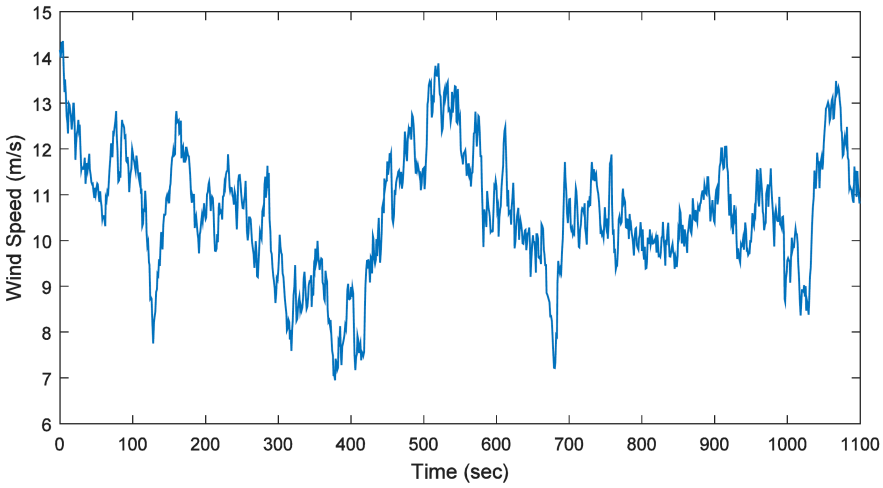

Figure 3.2 Illustration of the wind speed sequence used in the model.

3.3.2 Rotor Model

The WT rotor, that transfers the kinetic energy from the wind into mechanical energy is a complex aerodynamic system. To solve this problem, a simple rotor model is used based on the following equation:

$$P_w = \frac{1}{2}\rho\pi R^2 C_P(\lambda, \beta)v_w^3 \tag{3.7}$$

where P_w is the power extracted from the wind; ρ is the air density (1.225 kg/m^3); R is the rotor radius [m]; C_P is the performance coefficient or power coefficient; λ is the tip-speed ratio; β is the blade pitch angle [deg]; and v_w is the mean wind speed [m/s]. A WT has a theoretical maximum level of power which can be extracted from the wind, i.e. $C_P = 0.593$, the so-called Betz limit. In practice the coefficient of performance is less than this and also depends on the specific WT design, the wind velocity, the turbine rotor speed, and the turbine blade pitch angle [165]. For example, the power coefficient C_P for a 2MW machine is defined as a function of the tip-speed ratio λ and the blade pitch angle β in [166].

$$C_P(\lambda, \beta) = 0.5(\frac{116}{\lambda_i} - 0.022\beta^2 - 5)\exp(-0.17\frac{v_w}{\omega_m}) \tag{3.8}$$

The tip-speed ratio λ and the optimal tip-speed ratio λ_i are given by

$$\lambda = \frac{R\omega_m}{v_w} \tag{3.9}$$

$$\frac{1}{\lambda_i} = \frac{1}{\lambda + 0.08\beta} - \frac{0.035}{\beta^3 + 1} \tag{3.10}$$

Equations (3.8), (3.9) and (3.10) show how the aerodynamic behavior of the turbine rotor can be modelled in more detail where the power efficiency coefficient is a function of the tip-speed ratio, the blade pitch angle, the turbine rotational speed ω_m and the wind speed. Accordingly, if we need to calculate the tip-speed ratio λ from Equation (3.9) which is needed with the blade pitch angle β in order to calculate the optimal tip-speed ratio λ_i in Equation (3.10), then the calculated value of optimal tip-speed ratio and the blade pitch angle are used to calculate the power coefficient. This is a complex process and raises several questions as to how it should be performed. In these circumstances it is convenient to be able to identify the power efficiency coefficient directly as a function of wind speed instead of several

variables (i.e. ω_m, λ, λ_i and β). Therefore, the power coefficient is directly defined as a function of wind speed using the following expression:

$$C_P = \begin{cases} a_1 e^{a_2 v_w} + a_3 e^{a_4 v_w}, & 4 \leq v_w < 11 \\ \\ c_1 e^{-(\frac{v_w - c_2}{c_3})^2} + c_4 e^{-(\frac{v_w - c_5}{c_6})^2}, & 11 \leq v_w \leq 25 \end{cases} \tag{3.11}$$

Fig. 3.3 compares the power coefficient curve using this approach with the power curve of the commercial Nordex N80-2.5MW. This power curve is used to model the aerodynamic behaviour of the turbine rotor.

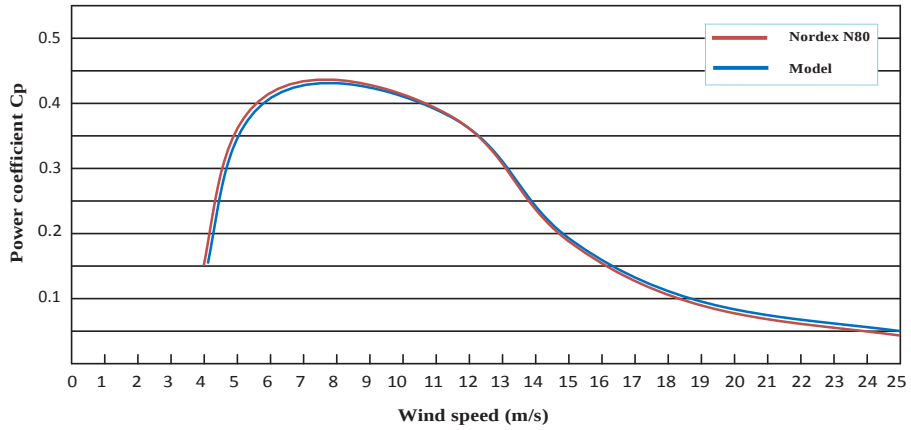

Figure 3.3 Comparison of the numerical approximation of the power curve with the power curve of the commercial Nordex N80-2.5MW wind turbine.

In variable-speed WTs, the pitch control system controls the rotor speed by changing the blade angle. The control system has a blade reference angle and the pitch servo is the actuator, which changes the turbine blades to the desired angle. The pitch control system is active only at higher wind speeds to diminish the aerodynamic performance of the turbine and limit the power extraction.

In order to simulate a simple model for the pitch control, Equation (3.11) is used to obtain the power coefficient to limit the mechanical power extracted from the wind. The pitch control is modeled as shown in Fig. 3.4, by a PI controller that generates a reference rate of change of the power efficiency coefficient. Although a

PI controller is used and tuned using try and error, there is a slight over-speeding of the rotational speed above its nominal value which can be tolerated and does not cause a significant problem to the WT.

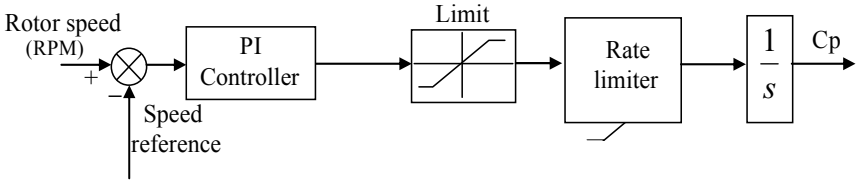

Figure 3.4 Pitch control system.

3.3.3 Drivetrain Model

The drive train is modeled in this work by a two-mass model. The drive train is used to transfer torque from the rotor to the generator. The two-mass representation is described by the equations [164]

$$\begin{aligned} J_t \frac{d^2}{dt^2}\theta_t &= -K(\theta_t - \theta_g) \\ J_g \frac{d^2}{dt^2}\theta_g &= -K(\theta_g - \theta_t) \end{aligned} \tag{3.12}$$

J_t, J_g are the moments of inertia of the turbine and generator respectively (kgm^2), ω_g is the rotational speed of the generator (rad/s), θ_t, θ_g are the rotational displacements of the turbine and generator respectively (rad) and K is the shaft stiffness (Nm/rad).

3.3.4 Generator Model

The DFIG is the dominant generator used in WTs at the present time with the largest share of the market [37]. The DFIG runs at a certain limited range of speeds above or below the synchronous speed. The principle of the DFIG is that rotor

circuit receives the magnetic field from a power converter so that it does not require any excitation from the grid or permanent magnets. In normal operation, balanced voltages applied to stator windings provide a rotating magnetic field at synchronous speed ω_s (rev/min). The synchronous speed is expressed as:

$$\omega_s = \frac{60 f_s}{p} \tag{3.13}$$

where f_s (Hz) denotes the stator current frequency and p is the number of poles pairs. In principle, the DFIG always transmits power to the network through the stator, but when the DFIG operates in super-synchronous mode, the rotational stator flux will induce currents in the rotor windings which are taken off externally through the brushes. This will lead to additional power from the rotor being delivered via the power converter to the network. However, the rotor voltage that is induced in the rotor windings depends on the relationship between the stator flux rotational speed and the actual rotor shaft speed. The angular frequency of these voltages can be expressed as follows:

$$\omega_2 = \omega_s - \omega_r \tag{3.14}$$

where

ω_s= the speed of the rotating magnetic field in stator (rad/s)

ω_r= the actual rotor speed (rad/s)

ω_2= the slip speed (rad/s)

The relation between the speed of the rotating magnetic field in the stator and the actual rotor speed is defined by a commonly used term called the slip, s:

$$s = \frac{\omega_s - \omega_r}{\omega_s} \tag{3.15}$$

The sign of the slip is used to determine three different operating modes of the DFIG:

$$\omega_r = \omega_s \Rightarrow \omega_2 = 0 \Rightarrow s = 0 \Rightarrow \text{synchronous}$$

$$\omega_r < \omega_s \Rightarrow \omega_2 > 0 \Rightarrow s > 0 \Rightarrow \text{sub-synchronous}$$

$$\omega_r > \omega_s \Rightarrow \omega_2 < 0 \Rightarrow s < 0 \Rightarrow \text{super-synchronous}$$

The DFIG equivalent electric circuit with different stator and rotor frequencies in the steady state can be ideally represented in Fig. 3.5. The electric parameters of the DFIG are given as:

$\bar{v}_s, \bar{v}_r =$ Supplied stator and rotor voltages

$\bar{E}_s, \bar{E}_r =$ Induced stator and rotor emf

$\bar{I}_s, \bar{I}_r =$ Induced stator and rotor currents

$\bar{\psi}_s, \bar{\psi}_r =$ The stator and rotor fluxes

$\bar{R}_s, \bar{R}_r =$ Stator and rotor resistances

$\bar{X}_s, \bar{X}_r =$ Stator and rotor reactances

$\bar{L}_s, \bar{L}_r, =$ Stator and rotor leakage inductances

$\bar{L}_m =$ Magnetic inductance

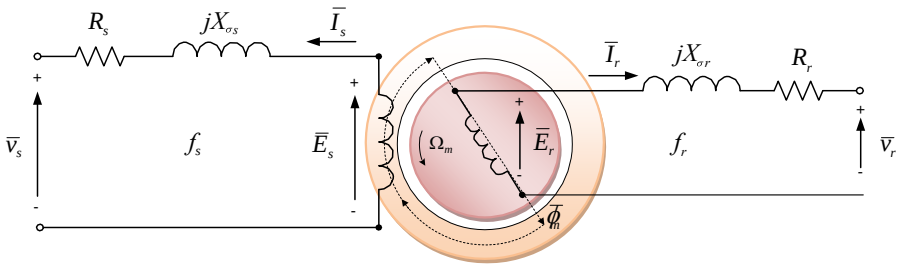

Figure 3.5 DFIG equivalent electric circuit with different stator and rotor frequencies.

The induced voltage in the stator and rotor winding can be expressed as:

$$\bar{E}_s = \omega_s k_s N_s \bar{\phi}_m = 2\pi f_s k_s N_s \bar{\phi}_m \tag{3.16}$$

$$\bar{E}_r = \omega_r k_r N_r \bar{\phi}_m = 2\pi f_r k_r N_r \bar{\phi}_m \tag{3.17}$$

Where k_s and k_r are winding factors of the stator and rotor, N_s and N_r are number of turns of the stator and rotor, respectively, and $\bar{\phi}_m$ is the magnetizing flux [Wb].

The induced RMS voltages are:

$$\bar{E}_s = \frac{2}{\sqrt{2}}\pi f_s k_s N_s \bar{\phi}_m = 4.44 f_s k_s N_s \bar{\phi}_m \tag{3.18}$$

$$\bar{E}_r = \frac{2}{\sqrt{2}}\pi f_r k_r N_r \bar{\phi}_m = 4.44 f_r k_r N_r \bar{\phi}_m \tag{3.19}$$

Hence, by dividing Equation (3.19) by Equation (3.18), the relation between the induced voltage in the stator and rotor winding can be expressed as:

$$\frac{\bar{E}_r}{\bar{E}_s} = \frac{f_r k_r N_r}{f_s k_s N_s} \tag{3.20}$$

Where $f_r = s f_s$, $k_s \cong k_r$ and $s = 1/$ at standstill speed then we have:

$$\frac{\bar{E}_r}{\bar{E}_s} = \frac{N_r}{N_s} = n \tag{3.21}$$

Equation (3.21) indicates that a DFIG can equivalently be treated as the primary and secondary windings of a transformer which can be used to refer the rotor electric quantities to the stator windings as shown in Fig. 3.6. Hence, the rotor electrical quantities referred to the stator by factor n, can be expressed as:

$$\begin{aligned} \bar{E'}_r &= \bar{E}_s \quad = \frac{\bar{E}_r}{n} \\ \bar{v'}_r &= \frac{\bar{v}_r}{n} \\ \bar{I'}_r &= n.\bar{I}_r \end{aligned} \tag{3.22}$$

Similarly, the rotor's resistance and inductance referred to the stator side, can be calculated as:

$$\begin{aligned} \bar{R'}_r &= \frac{\bar{R}_r}{n^2} \\ \bar{X'}_r &= \frac{\bar{X}_r}{n^2} \end{aligned} \tag{3.23}$$

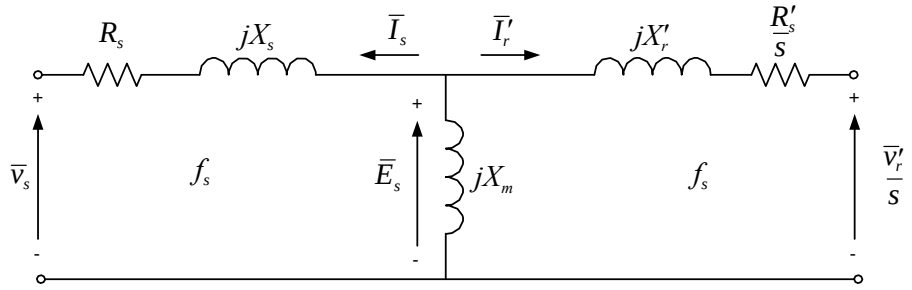

Figure 3.6 DFIG equivalent electric circuit referred to the stator.

It is important to highlight that the stator currents and voltages have different frequencies compared to the currents and voltages in the rotor windings. The stator frequency of the currents and voltages is always fixed to the grid frequency, whereas the rotor frequency is variable and proportional to the actual speed of the rotor.

The DFIG machine dynamic equations represented in the excitation reference frame can be described by [167]:

$$\begin{aligned} \bar{v}_s &= R_s\bar{I}_s + \frac{d\bar{\psi}_s}{dt} + j\omega_s\bar{\psi}_s \\ \bar{v'}_r &= R'_r\bar{I'}_r + \frac{d\bar{\psi'}_r}{dt} + j(\omega_s - \omega_r)\bar{\psi'}_r \\ \bar{\psi}_s &= L_s\bar{I}_s + L_m\bar{I'}_r \\ \bar{\psi'}_r &= L_m\bar{I}_s + L_r\bar{I'}_r \end{aligned} \tag{3.24}$$

The parameters used in the proposed WT model are listed in Table 6.1.

Table 3.1 Model Parameters.

DFIG	
Cut-In, Rated, Cut-Out Wind Speed	3 m/s, 12 m/s, 25 m/s
Rated Tip Speed	80 m/s
Rotor Diameter	90 m
Gearbox Ratio	1:77.4
Stator voltage (RMS)	690v
Frequency	50Hz
Pole Pairs	3
Rated Generator Speed (RPM)	1000
Magnetising inductance (H)	0.0025
Stator phase resistance (ohm)	0.029
Stator leakage inductance (H)	$85 * 10^{-}6$
Rotor phase resistance (ohm)	0.026
Rotor leakage inductance (H)	$85 * 10^{-}6$

3.4 The Impact of Varying Load Conditions

In electrical machines, the current signal contains non-linear components due to the corresponding electromagnetic force produced by the non-linear interaction of the linkage flux [168]. The current signals tend to change with speed and load of the machine. A constant speed and load will typically generate stationary signals if the machine remains in a normal condition. In this case, the current signal presents non-stationary characteristics related to the operating process, machine run-up, shutdown and driving conditions. However, the main differences that characterise the operation of WTs in comparison to other forms of generation are the variable speed and load operation. This makes the WT current signal analysis a complex and costly task.

In this section, simulation results obtained from the WT dynamic model will be presented to describe the difficulties that may arise for WT CM under rapidly varying speed and load conditions. It should be mentioned that the WT model presented

in this work is first validated using experimental data from a test rig run under alternately healthy and faulty conditions and then is used to investigate the kind of results expected under actual variable conditions which is potentially challenging to perform using a test rig. The results according to the driving conditions are described in the following subsections.

3.4.1 Experimental Driving Conditions

The University of Durham has experimentally investigated rotor electrical asymmetry faults under constant and variable speed [21, 169]. The collected data have been provided to the Author for further analysis and processing. The test rig comprises a DC motor, rated at 50 kW; a two stage gearbox; and a two pair poles DFIG.

The test rig, although in a healthy state, had an inherent level of eccentricity due to manufacturing and assembly imperfections. In the experiments, the rotor electrical unbalance fault was simulated on the test rig by adding two additional external resistances to one phase of the rotor circuit. The value of the external resistances corresponds to two levels of rotor electrical unbalance of 23% and 46%, respectively, given as a percentage to the original rotor phase resistance. The driving conditions selected to run the simulation model are shown in Fig. 3.7. The three phase stator currents from an induction motor are measured from the terminals of the generator. The frequency of the stator current was 50.05 Hz in the measurements. Data were sampled at 5 kHz.

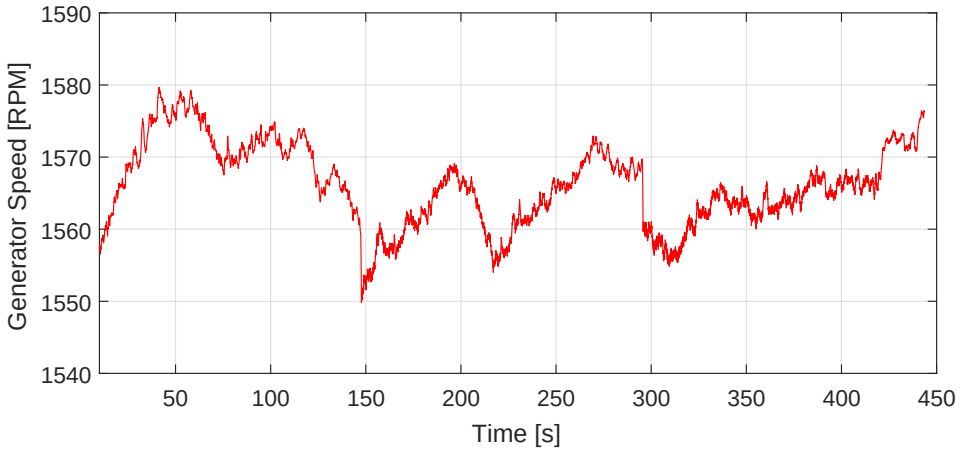

Figure 3.7 Experimental variable speed driving conditions.

In order to show the validation results of the developed WT model against the test rig, a fast Fourier transform (FFT) is used to convert the time series of the current signals into the frequency domain. Fig. 3.8 shows the result of this FFT for the stator current from both the test rig and the proposed WT model operating in a normal healthy case. Fig. 3.8(a) is actual measured data and Fig. 3.8(b) is the developed WT model run at the same parameters to the test rig. Due to the inherent static eccentricity, the healthy machine clearly shows the components predicted by equation (3.1). The inherent eccentricity related components are simulated to be present in the healthy case in our WT model similar to the test rig as shown in Fig. 3.8(b), where the results of the developed WT model are quite similar to the test rig.

Fig. 3.9 shows similar spectra, but this time the rig and the WT model are subject to a rotor electrical unbalance conditions, and due to the fault some additional sideband harmonics are clearly seen around the fundamental frequency components. These frequencies respond as expected in Equation (3.2) and are consistent throughout the simulation results. The magnitude of these harmonics increases with the severity of the rotor electrical unbalance fault, as illustrated in Table 3.2. Note that LFSCs and UFSCs denote the lower and upper sideband harmonics, respectively.

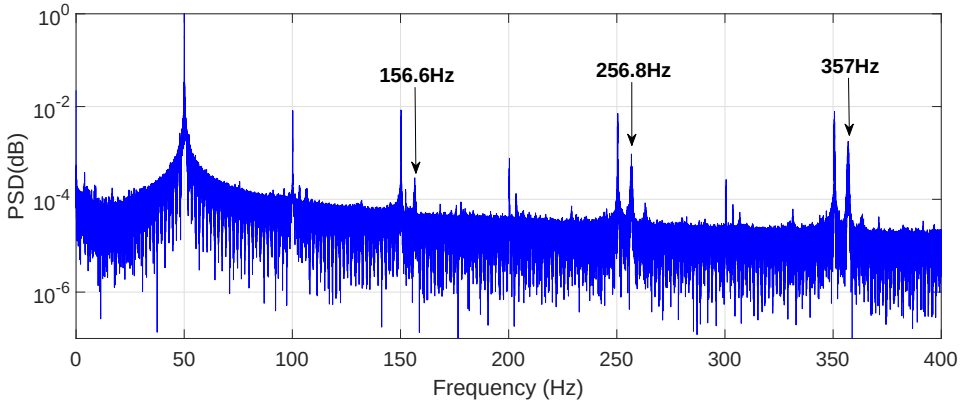

(a) Measured data

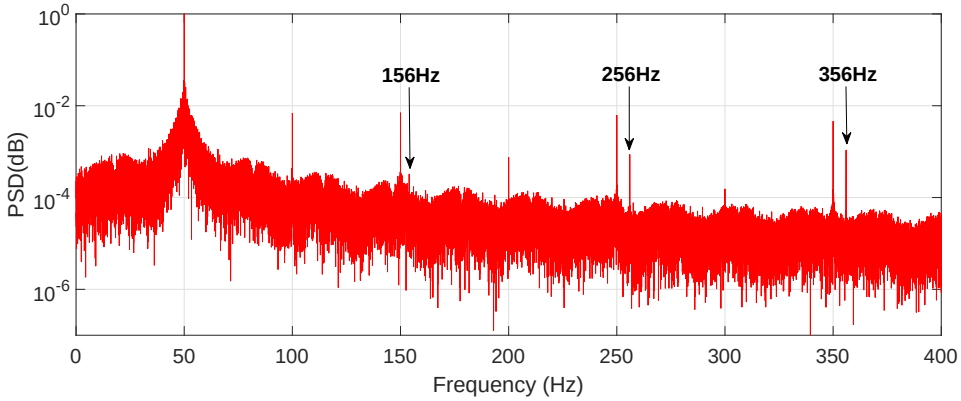

(b) Simulated data

Figure 3.8 Normalized stator current spectra with inherent static eccentricity.

Also, it can clearly be seen that by increasing the fault level of rotor electrical unbalance in Fig. 3.9(c), the magnitudes of the FSCs related to the fault increase significantly compared to those in Fig. 3.9(b). Thus, the WT model presented here is able to successfully replicate the effects of static eccentricity and rotor electrical unbalance conditions in an actual machine under fixed speed operations.

Table 3.2 Comparison between measured and simulated results.

Harmonic Order (k)	FSCs (mA) for the test rig		FSCs (mA) for the WT model			
	23% of rotor electrical unbalance		23% of rotor electrical unbalance		73.6% of rotor electrical unbalance	
	LFSCs	UFSCs	LFSCs	UFSCs	LFSCs	UFSCs
1	-	8.44	-	7.36	-	14.51
2	0.59	0.94	0.58	0.96	0.9	3.4
3	-	1.76	-	1.7	-	3.5
5	0.61	0.2	0.59	0.24	1.51	0.56
7	-	0.51	-	0.58	-	1.48

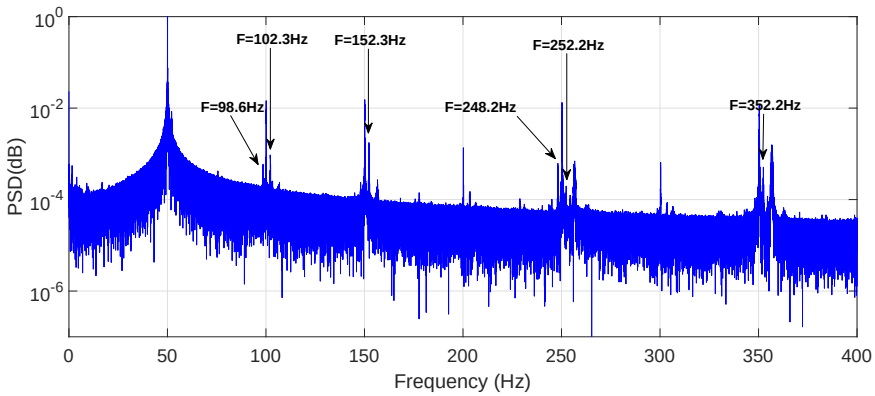

(a) Measured data under 23% of rotor electrical unbalance

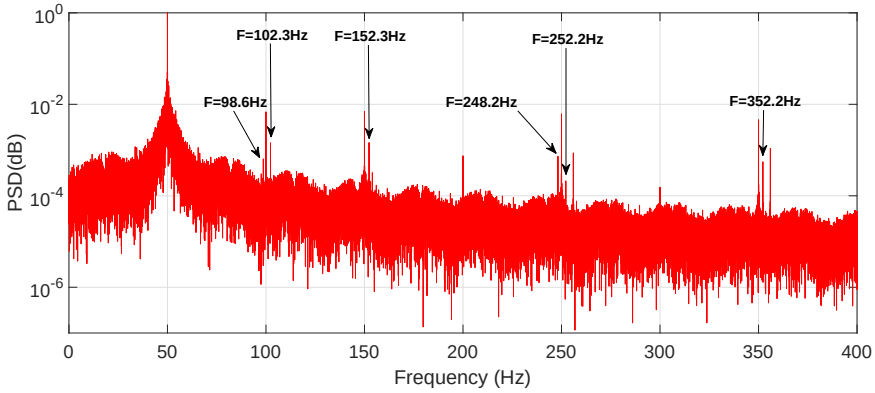

(b) Simulated data under 23% of rotor electrical unbalance

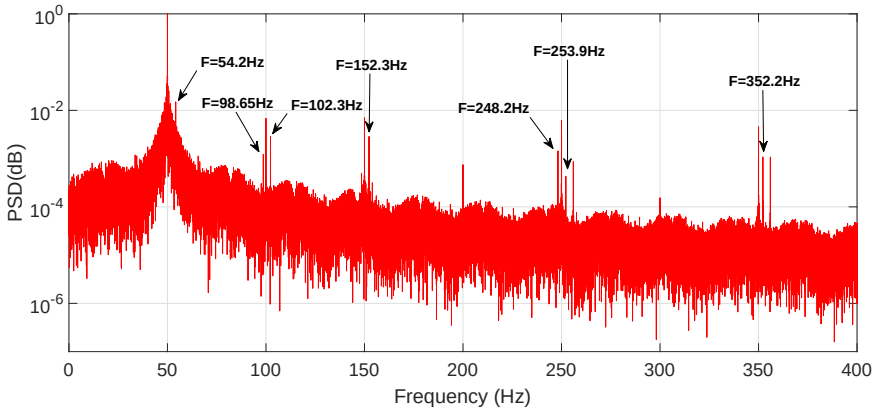

(c) Simulated data under 73.6% of rotor electrical unbalance

Figure 3.9 Normalized stator current spectra under different fault levels.

The Root Mean Square Error (RMSE)is used to compare the performance of the WT model against the test rig. The RMSE metric is defined as follows:

$$RMSE = \sqrt{\frac{1}{N}\sum_{i=1}^{N}(y_i - \hat{y}_i)^2} \tag{3.25}$$

where the y_i and $\hat{y}_i$ are, respectively, the magnitudes of the FSCs measured and simulated values for the ith output N of data samples. The results of the RMSE in Table 3.3 show that the response of the model was found to be in very good agreement with the measured results.

Table 3.3 Agreement evaluation between measured and simulated results.

FSCs for 23% of rotor electrical unbalance	RMSE Values
LFSCs	0.016
UFSCs	0.485

3.4.2 Actual Variable Speed Driving Conditions

As previously mentioned, rotor eccentricity and rotor electrical unbalance in the steady state have been investigated in a number of previous studies, however, their detection under a wide range of actual variable speed conditions has not been examined. Since the WT model has been validated against the experimental data, the model this time is run under actual variable speed conditions. By doing this, we can investigate the impact of the variable speed on the fault signature frequencies.

Wind turbine DFIGs are machines which operate under highly variable load and speed conditions as shown in Fig. 3.10 where load and speed data recorded from an operational variable speed WT are presented. It can be seen that it is potentially challenging to run a test rig under such driving conditions, but this is a relatively simple task for a simulation model. The model developed in this work was initialized using actual variable speed conditions. Operational data from five 2.5MW turbines were recorded by the standard Supervisory Control And Data Acquisition (SCADA)

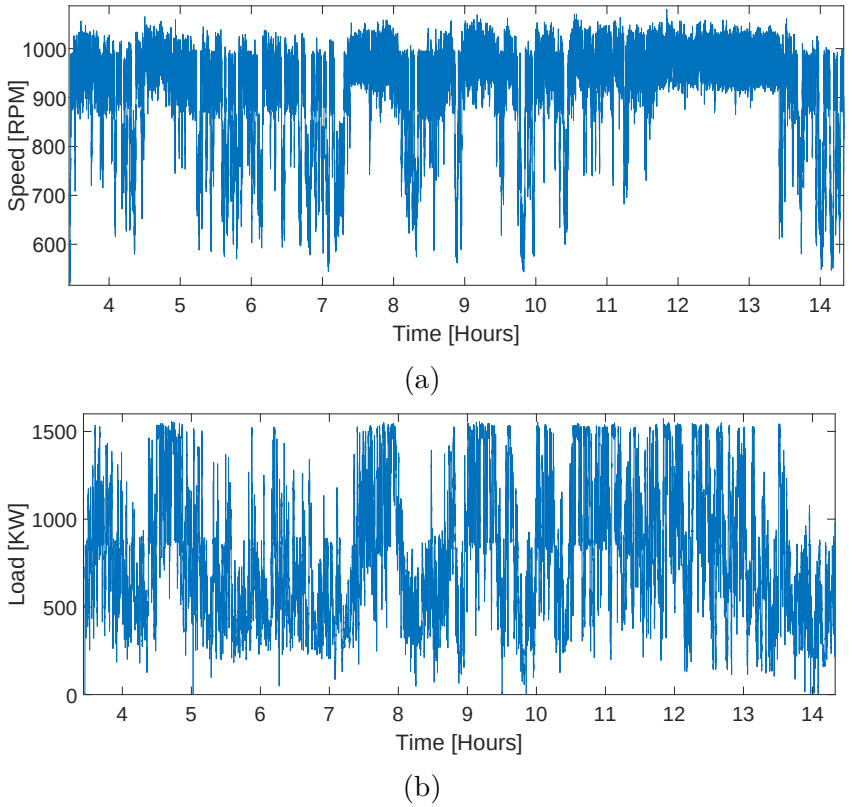

Figure 3.10 Operational data from a 2.5 MW variable speed WT
(a) Generator speed and (b) Load.

system and by a bespoke high frequency monitoring system over the period of 1 year. The measured data were recorded at 10-min intervals with 32Hz sampling frequency and included wind speed, wind direction, pitch angle, rotational speed and three-phase power output. To show the accuracy of the model, its response to a measured 10-minute wind speed time sequence is presented in Fig. 3.11 for one of the turbines. It is worth noting that the rotor and drivetrain act as a low-pass filter to the high-frequency wind speed variations, due to their relatively high moment of inertia.

Fig. 3.12 shows the simulated stator current spectrum of the model operating under varying speed conditions, driven by the wind speed time series recorded for one of the 2.5MW turbines. Even though the turbine was known to be operating normally with no known fault, there is still some inherent rotor electrical unbalance with static eccentricity. If these components were of a sufficient magnitude, then

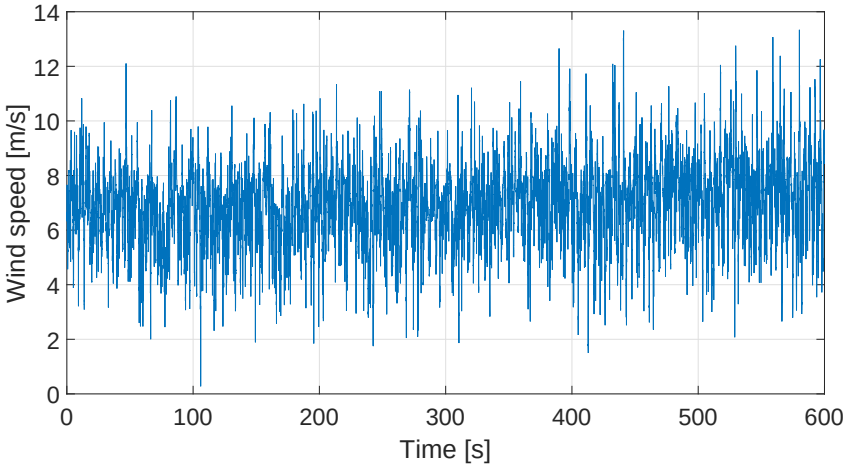

(a) Measured wind-speed time series

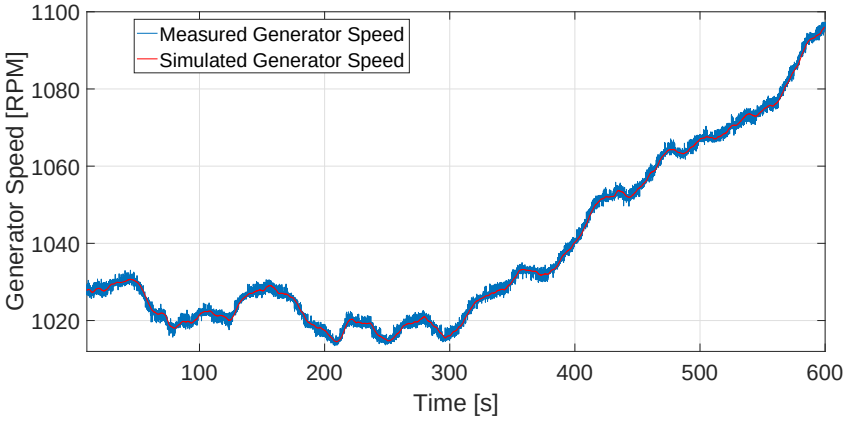

(b) Model validation considering generator speed

Figure 3.11 Actual variable speed driving conditions.

they could be considered as indicative of a fault requiring intervention. Because of the varying shaft rotating speed of the WT, the FSCs related to the rotor electrical unbalance vary and overlap with the inherent static eccentricity components, and both are corrupted in other wide-band dominant frequency components of the current signal unrelated to any unbalance and eccentricity. The unrelated sideband frequencies can be related to Equation (3.1). These sideband frequencies are a function of the slip, so they are present in proportion to the rotational speed. As a result, the FSCs related to any actual fault cannot be identified by simply using the FFT algorithm for the stator current signal. This fact makes the detection of such faults in the current spectrum problematic. This problem is discussed in [5], and the authors used a continuous-wavelet-transform (CWT) to track the magnitude of the

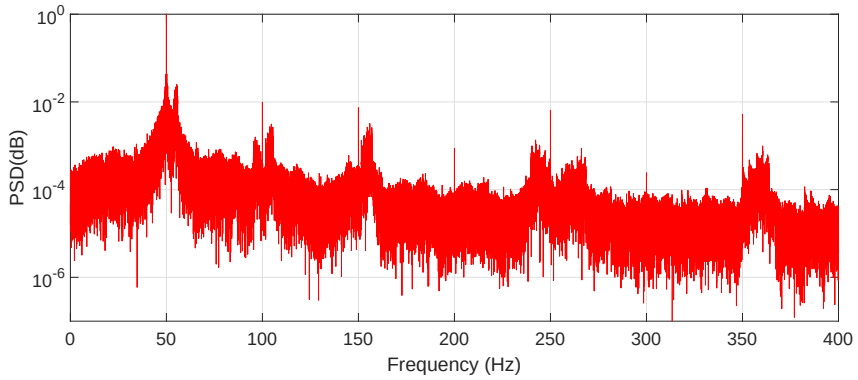

Figure 3.12 Simulated stator current spectra with inherent static eccentricity and rotor electrical unbalance at variable speed conditions.

component at twice slip frequency divided by pole pairs ($2sf1/p$) as an indicator of rotor eccentricity in a test rig, however, the detection of these faults and others under actual variable speed and load conditions has not been investigated. Moreover, it has been reported in [31, 33, 98] that high time resolution and high frequency resolution cannot be achieved simultaneously using a CWT and so this transform cannot necessarily provide accurate interpretation of non-stationary WT signals. It therefore follows that a more advanced signal processing technique needs to be developed in order to better interpret WT CM signals. This will be the subject of the next chapter.

3.5 Summary

In this chapter, fault signatures in WT generator current signals were described briefly. A WT model was implemented to investigate how the fault signatures may occur in current signals, and potentially how they may change when a generator deviates from a healthy to a faulty state when operating under variable speed conditions. The performance of the model was validated by experimental measurements made on a physical test rig under healthy and faulty conditions. The WT model was then initialized using actual variable speed conditions collected from operational WTs

to produce generator signals exhibiting similar noise, variability and information content as those which would be seen on such operational turbines had direct high frequency measurements of the generator current been available. The results of this investigation showed that potential fault signatures in the WT current signals are non-stationary with a low signal to noise ratio due to the constantly varying shaft rotating speeds and varying loads. This means that more sophisticated analysis methods should be chosen. In the next chapter, more advanced signal processing techniques for time frequency analysis will be presented.

Chapter 4

Time-Frequency Analysis and Neural Networks in WT CM

4.1 Introduction

The previous chapter showed that fault signatures in a WT generator current signal have non-stationary characteristics with low signal to noise ratio due to the constantly varying shaft rotating speeds and varying loads. It therefore follows that more advanced techniques need to be developed in order to achieve better interpretation of WT CM signals that are varying with time.

This Chapter begins with a brief discussion of the commonly applied standard signal processing techniques, namely the short-time Fourier transform (STFT) and the continuous wavelet transform (CWT). The concept of tracking particular frequencies of inter of Artificial Neural Networks (ANNs) for detecting faults is discussed to automate the fault detection in the light of the limitations of spectral analysis in processing signals subject to transient effects. The capabilities, advantages and limitations of these techniques are outlined. Conclusions are drawn about their effectiveness to analyse non-stationary signals.

4.2 Common Time-Frequency Analysis Techniques

The emphasis of this thesis is on the analysis of non-stationary WT generator current signals for CM and fault diagnosis. Hence the principles and applications of two common time-frequency techniques are discussed.

There are many signal processing techniques based on time-frequency analysis which have been developed. Among them, the STFT and CWT are the most well-known techniques used in WT CM. These techniques are the basis for the new frequency tracking algorithms developments attempted in this thesis which introduced in the next two chapters.

4.2.1 The Short-Time Fourier Transform

The limitations of the direct application of the Fourier transform method, and its inability to localize a signal in both the time and frequency domains, was realized very early on in the development of radar and sonar detection methods. The Hungarian electrical engineer and physicist G´abor D´enes (Physics Nobel Prize in 1971 for the discovery of holography in 1947) was the first person to propose a formal method for localising information in both the time and frequency domains [170]. His method is known as the short-time Fourier transform (STFT), the STFT of a continuous-time signal $\mathbf{x}(t)$ is defined as:

$$\mathbf{STFT}(f,\tau) = \int_{-\infty}^{\infty} \mathbf{x}(t)\mathbf{g}(t-\tau)e^{-j2\pi ft}\,dt \tag{4.1}$$

where $\mathbf{g}(t-\tau)$ is the window function whose position is translated in time by $\boldsymbol{\tau}$. The integration over the parameter $\boldsymbol{\tau}$ slides the time-filtering window along the entire signal in order to pick out the frequency information at each instant of time. Fig. 4.1 gives a clear illustration of how the time filtering scheme of the STFT works.

In this figure, the time filtering window is centred at $\boldsymbol{\tau}$ with a width **a**. Thus the frequency content of a window of time is extracted and $\boldsymbol{\tau}$ is modified to extract the frequencies of another window. Thus, the STFT is able to capture the entire time-frequency content of the signal.

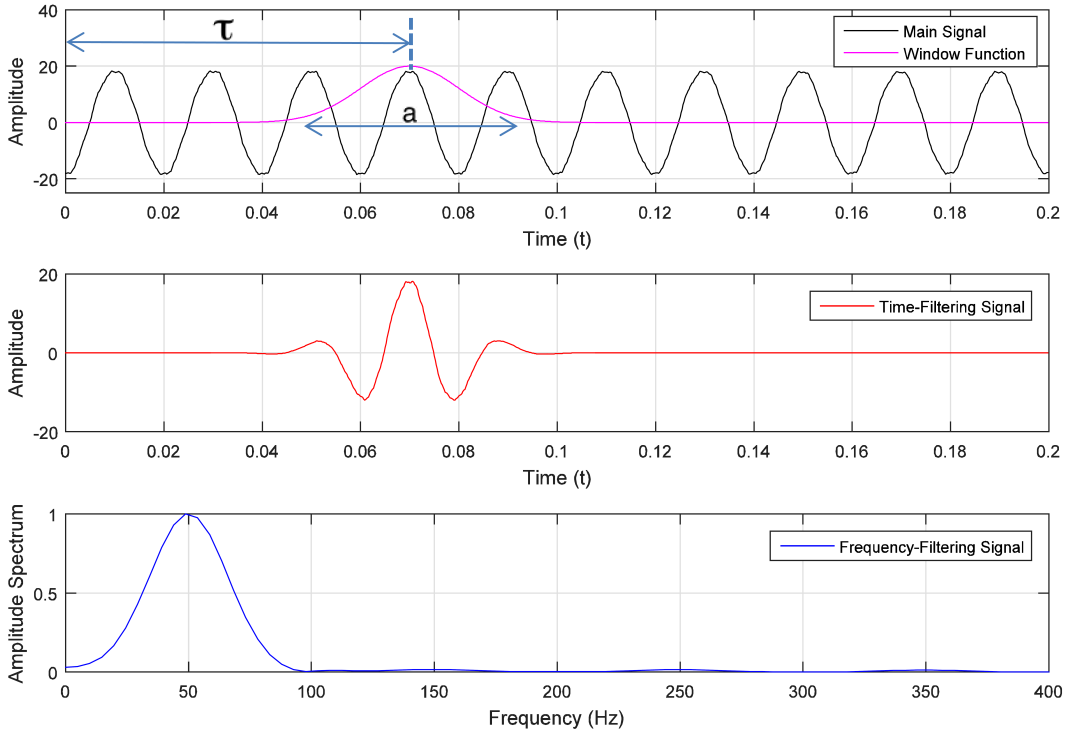

Figure 4.1 Graphical illustration of the STFT for extracting the time-frequency content of a measured signal.

The next stop is for the STFT is to multiply the time filter function with the original signal in order to produce a windowed section of the signal. The Fourier transform of the windowed section then gives the local frequency content in time. To demonstrate the advantage of the STFT over the conventional FFT, a time varying sinusoidal signal is simulated. It is formulated as follows:

$$\mathbf{x}(t) = \begin{cases} \sin(2\pi f_1 t) & 0 \leq t \leq 50\ s \\ +\ 0.2\sin(2\pi f_2 t) & 0 \leq t \leq 20\ s \\ +\ 0.4\sin(2\pi f_3 t) & 0 \leq t \leq 30\ s \end{cases} \tag{4.2}$$

with f_1 =50 Hz, f_2 = 100 Hz, and f_3 = 150 Hz.

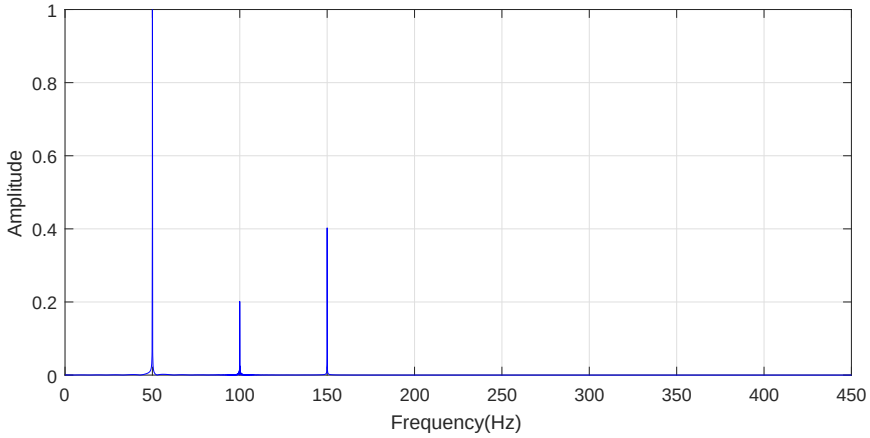

(a) Spectrum of complete signal

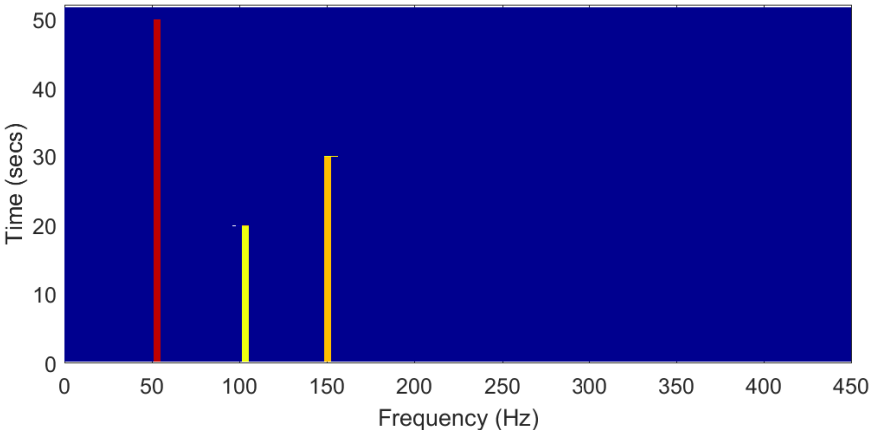

(b) Spectrogram of complete signal

Figure 4.2 Analysis of a non-stationary signal via the (a) FFT and (b) STFT.

In Fig. 4.2(a), the results of the FFT show that throughout the entire period of the signal three frequency components are present with different amplitudes. On the other hand, the results of the STFT in Fig. 4.2(b) shows that the three frequency components are correct in their values but these frequencies are not actually present throughout the entire time domain signal. This is the advantage of the STFT and its capability to localize the frequency components of the original signal in time domain through iterative analysis of short time intervals of the analysed signal, whereas the FFT is unable to localize the signal in both the time and frequency domains so that all time information of the original signal is lost.

However, the STFT has some limitations in time-frequency resolution due to the signal segmentation where there is a trade off in the choice of window size. On the one hand, the window width has to be narrow in order to localize an event in time. On the other hand, the frequency resolution requires a longer time window to obtain an accurate representation of the frequency content of the entire signal. This means that STFT has a constant resolution for all frequencies since the same window size is used for the analysis of the entire signal. Therefore, an accurate representation of frequency content using a wide window, and an accurate time localization using a narrow window, cannot be achieved based on the STFT analysis. In reality, WT generator current signals are non-stationary because of both the rotating machine itself and the nature of the wind and so a more advanced time-frequency analysis than the STFT should be used in order to accurately locate dynamically varying frequency components in time.

4.2.2 The Continuous Wavelet Transform

As mentioned in Section 4.2.1, the STFT uses translation of a short-time fixed window along the entire signal in order to pick out the frequency information at each instant of time. The fixed window size imposes a fundamental limitation on achieving simultaneously high time and frequency resolution. A simple modification to the STFT is to use a varied time-frequency window to obtain better resolution simultaneously in the time and frequency domains. By doing this, the low frequency components (with relatively poor time resolution) are firstly captured using a wide scaling window. The scaling window is then subsequently shortened to capture higher frequency components with better time resolution. This is the basic principle of the continuous wavelet transform (CWT). The term wavelet usually refers to a little wave that originates by picking out smaller and smaller pieces of waves from the original signal using a scaling window.

A CWT analysis requires the choice of an analysing function $\boldsymbol{\psi}$ known as the mother wavelet. An example of such an analysing function is the Morlet wavelet described by a modulated Gaussian function:

$$\boldsymbol{\psi}(t) = \frac{1}{\sqrt{\pi f_b}}\mathbf{exp}(\frac{-t^2}{f_b})\mathbf{exp}(i2\pi f_o t) \tag{4.3}$$

where f_b is the bandwidth parameter and f_o is the wavelet centre frequency. The Morlet wavelet and its Fourier transform are shown in Fig. 4.3(a) and Fig. 4.3(b).

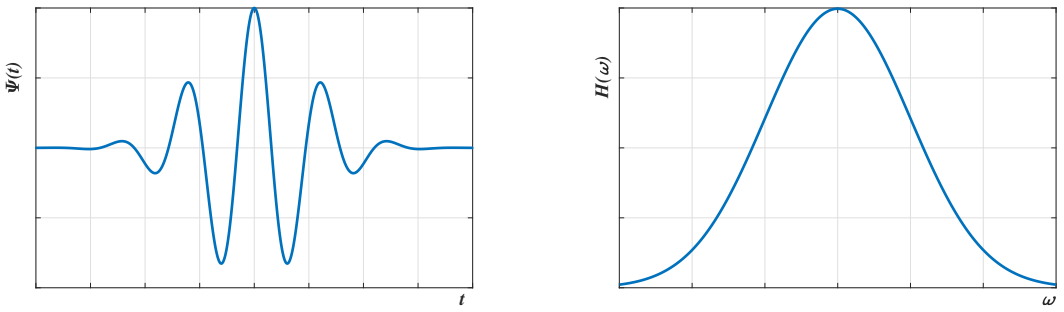

(a) (b)

Figure 4.3 (a) Morlet wavelet in time domain and (b) frequency domain.

The corresponding family of wavelets $\boldsymbol{\psi}_{a,\tau}$ is generated from shifted and scaled copies of $\boldsymbol{\psi}$ defined as follows:

$$\boldsymbol{\psi}_{a,\tau} = \frac{1}{\sqrt{a}}\boldsymbol{\psi}\left(\frac{\boldsymbol{t-\tau}}{\boldsymbol{a}}\right) \tag{4.4}$$

The wavelets $\boldsymbol{\psi}_{a,\tau}$ can be viewed as a copy of the mother wavelet $\boldsymbol{\psi}$ rescaled by $\mathbf{a}$ and centred around the time $\boldsymbol{\tau}$. The CWT of a signal $\mathbf{x}(t)$, which is a real continuous function of time, can then be defined by the inner product between $\mathbf{x}(t)$ and $\boldsymbol{\psi}_{a,\tau}$.

$$\mathbf{C}_{a,\tau}(t) = \int_{-\infty}^{+\infty} \mathbf{x}(t)\boldsymbol{\psi}^*_{a,\tau}(t)\mathbf{d}t \tag{4.5}$$

where $*$ denotes the complex conjugate. By substituting (4.4) into (4.5) the CWT coefficients $\mathbf{C}_{a,\tau}(t)$ of $\mathbf{x}(t)$ can also be written as a correlation between the signal and the scaled wavelets $\boldsymbol{\psi}_{a,\tau}$:

$$\mathbf{C}_{a,\tau}(t) = \int_{-\infty}^{+\infty} \mathbf{x}(t)\frac{1}{\sqrt{a}}\boldsymbol{\psi}^*\left(\frac{t-\tau}{a}\right)\mathbf{d}t \tag{4.6}$$

The position of the CWT coefficient in the time domain is given by $\boldsymbol{\tau}$, whereas its position in the frequency domain is given by $\mathbf{a}$ (the relationship between the scale and the frequency is explained later). The CWT, by mapping the original series into a function of $\boldsymbol{\tau}$ and $\mathbf{a}$, provides information simultaneously in the time and frequency domains. The main difference between the wavelet transform and the Fourier transform is that, the Fourier transform does not have a time localization parameter like the mother wavelet. In the case of the mother wavelet, its position is translated in time by $\boldsymbol{\tau}$ and integration over this parameter leads to the sliding of the mother wavelet along the entire signal in order to pick out the frequency information at each instant of time.

Using the properties of the Fourier transform, the CWT can be represented as:

$$\mathbf{H}_{a,\tau}(\boldsymbol{\omega}) = \frac{\sqrt{a}}{2\pi}\int_{-\infty}^{+\infty} \boldsymbol{\Psi}^*(a\omega)\mathbf{X}(\omega)\mathbf{e}^{-j\omega\tau}\mathbf{d}\omega \tag{4.7}$$

Equation (4.7) shows that in the frequency domain the wavelet is scaled by $1/a$ and multiplied by a phase factor $\mathbf{e}^{-j\omega\tau}$. It is also clear that the amplitude of the scaled wavelet is proportional to $\mathbf{a}^{-1/2}$ in the time domain, whereas it is proportional

to $\mathbf{a}^{1/2}$ in the frequency domain. This is the main advantage of the CWT where the low frequency (worse time resolution) components are firstly extracted using a larger scale parameter. The scale parameter is subsequently reduced in order to extract higher frequency components with better time resolution localisation.

4.2.3 Comparison of Techniques

To demonstrate the advantage of the CWT compared to the STFT, a non-stationary signal is simulated as an example, i.e.,

$$\begin{aligned}\mathbf{x}(t) = &\sin[50\pi t_1 + 20\pi \sin(t_1)] \sin(68.4\pi t_2) \\ &+ \sin[66\pi t_1 + 20\pi \sin(t_1)] \sin(84.4\pi t_2) \\ &+ \sin\left\{16\pi t + 6\pi \arctan[(t-5)^2]\right\}\end{aligned} \tag{4.8}$$

with $0 \leq t_1 < 6\ s$, $6 \leq t_2 < 10\ s$, and $0 \leq t < 10\ s$.

Fig. 4.4(a) shows the results of the STFT of a 10 s non stationary signal sampled at (1kHz). The information obtained from the STFT indicates that there are three frequency components (f_1, f_2 and f_3) present over the entire time period of the signal. It can also be seen that the STFT has divided the non-stationary signal into segments to ensure that the window size adopted always coincides with the stationary time-scales but the time-frequency representation obtained is still not well concentrated. By contrast, the CWT avoids this problem and can better characterize the time-frequency content of the non-stationary signal as shown in Fig. 4.4(b).

However, the CWT had difficulty capturing component (f_1) between 3.25-5.75 s because this component has strong non-stationary characteristics for a short period compared to the other components. Another drawback inherent to the CWT is that its analysis involves more intensive convolution calculations than the STFT, making it more difficult to analyse lengthy online data, such as WT monitoring signals.

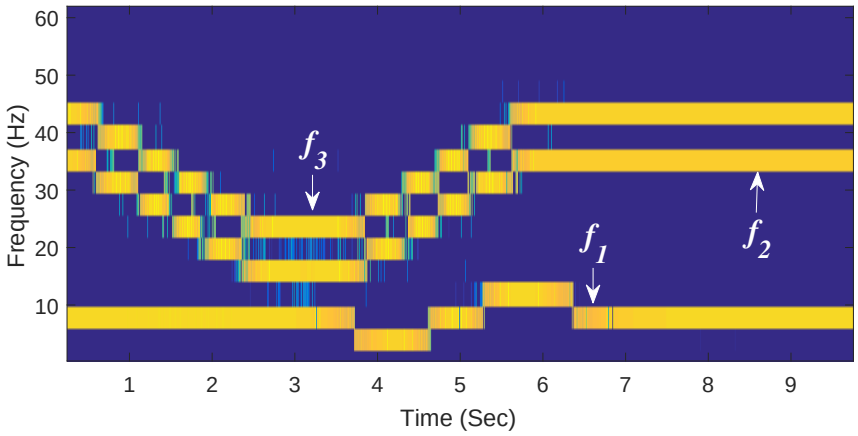

(a)

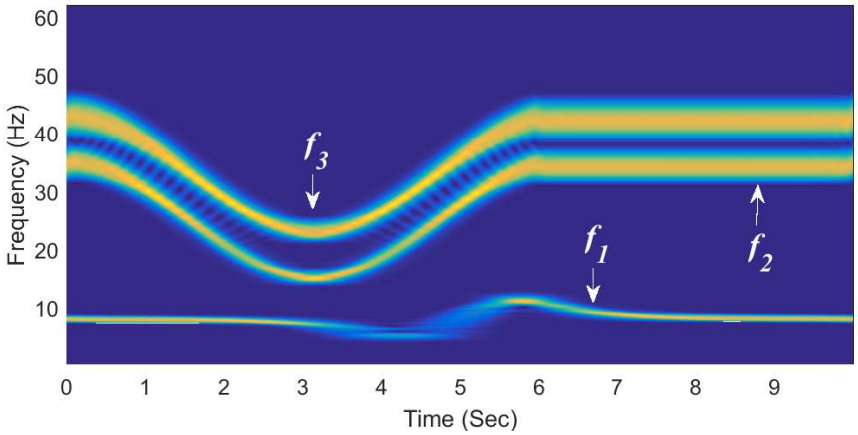

(b)

Figure 4.4 Non-stationary signal analysed via the (a) STFT and (b) CWT.

These deficiencies significantly limit the application of the CWT in commercial WT CM systems. One possible methodology to reduce the computational time is the idea of frequency tracking which will be discussed in the next section.

4.3 Fourier Transform-Based Frequency Tracking

Effective CM using time-frequency analysis on highly non-stationary WT signals depends on techniques that can successfully extract CM features accurately and quickly from lengthy CM records. Traditional time-frequency methods such the the STFT and the CWT are unable to meet such a requirement because of their

complex calculations and the windowing technique. This has to be addressed when considering on-line WT CM of a large fleet of machines.

To improve WT CM signal analysis, there has been research to explore the potential of frequency tracking. The main idea behind frequency tracking techniques is to reduce processing times by extracting individual fault-related frequency components instead of analysing all frequency components. For example, a tracking algorithm based on the CWT was applied in [169] to track a given variable frequency component at twice slip frequency $2sf$. In this study, the algorithm was shown to be capable of detecting mechanical and electrical faults in WT-based DFIG. However, high computational time is still needed to obtain good results, making it unsuitable for large size data analysis.

To overcome this, another frequency tracking methodology was proposed in [24] using the iterative localized discrete Fourier transform (IDFT) algorithm to extract the fault frequency of interest over time. Similar to the STFT, the IDFT employs a development of the discrete Fourier analysis to analyse the entire signal with short time segments. The steps followed for this tracking method are:

- Divide the measured generator rotational speed and the stator current data points into a number of time segments
- Calculate the mean speed and slip
- Calculate the stator current spectrum using an FFT
- Calculate discrete constants from frequencies of interest
- Calculate amplitudes for each constant
- Extract maximum amplitude and its frequency
- Repeat the process starting with next sampling interval

4.4 Simulation Verification of IDFT

The WT model in Chapter 3 was used to test the IDFT algorithm and its ability in interpreting non-stationary signals. The WT model was driven by variable speed data derived from one of the operational 2.5 MW WTs described briefly in Chapter 3 to produce signals of similar noise, variability and information content as those encountered on operational turbines. The IDFT algorithm was then applied to extract both the instantaneous amplitude and frequency of fault signature components in the stator current under rapidly varying speed and load conditions. Fig. 4.5 shows the driving conditions selected for testing.

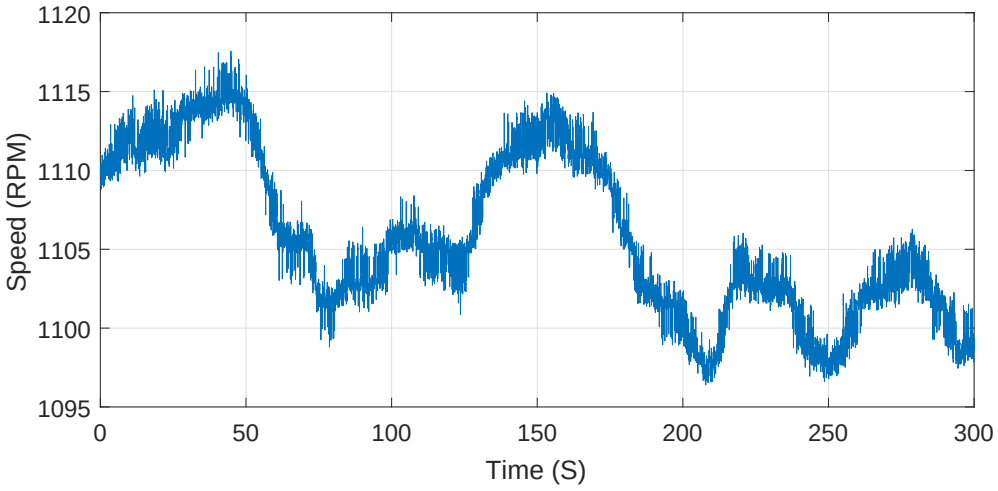

Figure 4.5 Generator speed for analysis using the IDFT algorithm.

A case study of the modelled WT under rotor unbalance of 23%, given as a percentage of the rotor balanced phase resistance, was performed. One phase stator current of the WT was recorded in the simulations before and after the presence of the 'fault'. To observe the effect of the fault, the model was run from 0 to 150 s in a healthy condition (no unbalance) and from 150 s to 300 s with a rotor unbalance. It was shown in the previous chapter that rotor unbalance fault gave rise to a number of side-band components in the current spectrum but monitoring all components would be impractical in an operating environment, so only four upper sideband harmonics

have been selected to be tracked using the IDFT. These sideband harmonics are labelled as C_1, C_2, C_3 and C_4 in Fig. 4.6. The results of tracing the instantaneous amplitude of these components are shown in Fig.s 4.7 and 4.8.

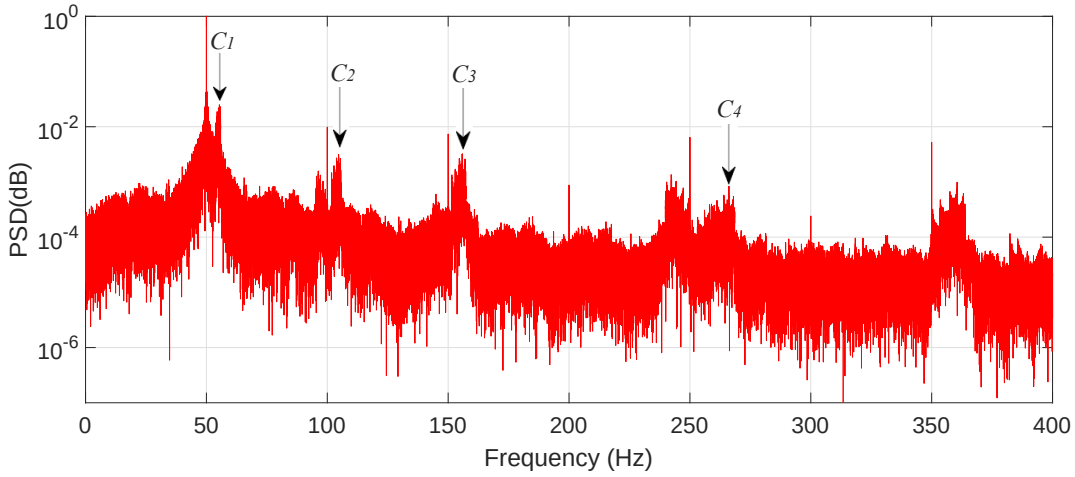

Figure 4.6 Simulated stator current spectra with inherent static eccentricity and rotor electrical unbalance at variable speed conditions.

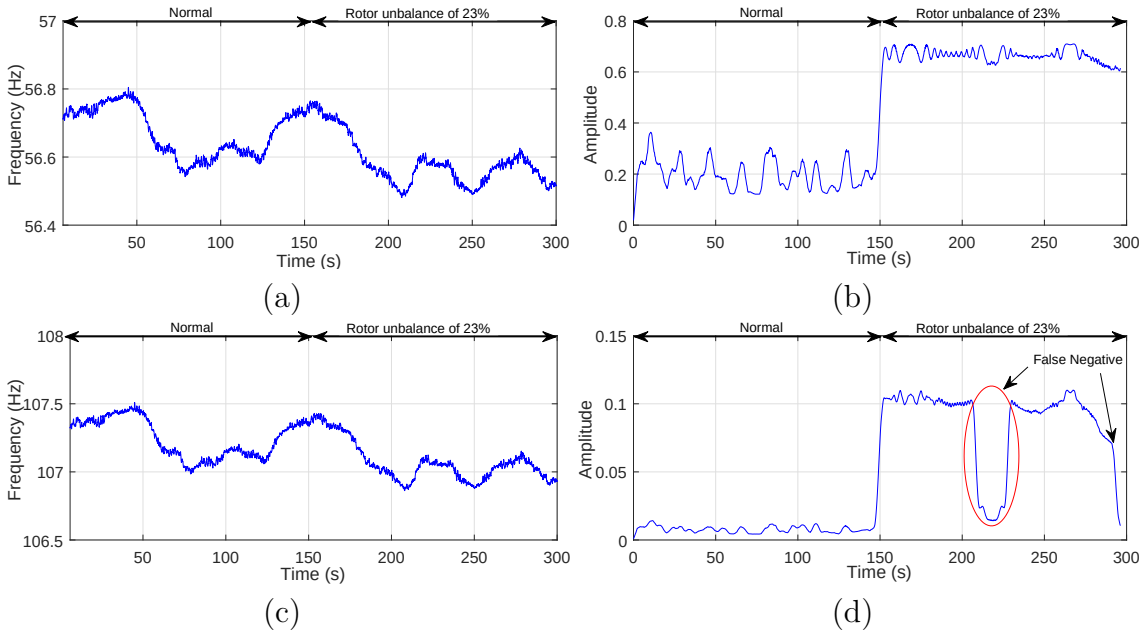

Figure 4.7 The analysis of the characteristic frequencies in the current signal using the IDFT under variable speed conditions (a) C_1 (b) Its amplitude over time (c) C_2 (d) Its amplitude over time.

It is worth noting if the tracked component shows a step change in magnitude when the fault condition was present, then it can be said that the IDFT method

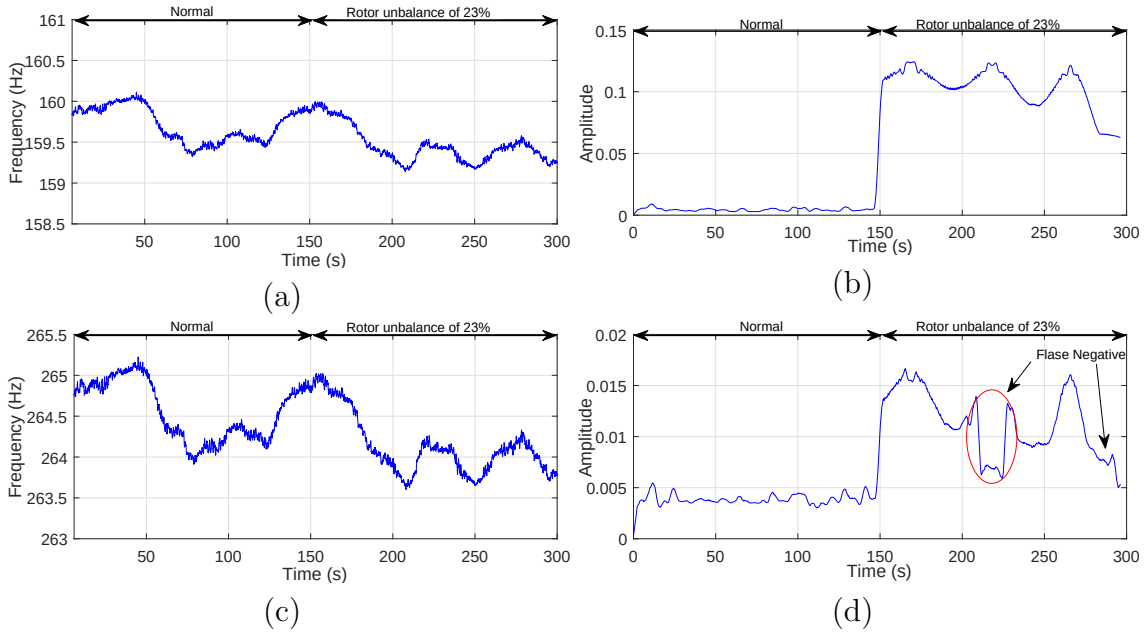

Figure 4.8 The analysis of the characteristic frequencies in the current signal using the IDFT under variable speed conditions (a) C_3 (b) Its amplitude over time (c) C_4 (d) Its amplitude over time.

has successfully captured the component frequency related to the fault. The results presented in Fig. 4.7 and Fig. 4.8 clearly show that the C_1, C_2, C_3 and C_4 components vary in frequency as the slip of the generator varies in response to changes in rotor speed. Although the rotational speed was not varying over a wide range and for long time, these components have non-stationary frequencies and amplitudes. The results show that the IDFT is able to capture fault components of interest where their magnitudes did show a marked change when the fault condition was applied at 150 s. However, the magnitudes of C_2 and C_4 show a reduce amplitude for a period where the tracking results would seem to indicate no presence of the fault for a period even when in reality it is present. This is due to the fact that the fault signature components may overlap with the fundamental frequencies when the machine operates at low load near to the synchronous speed. As a result, the fault signature components are difficult to detect or differentiate using the IDFT method, posing a risk of missing the detection of a fault when in this operating region. This demonstrates, that further improvement of WT CM techniques with

accurate interpretation of the signals and minimization of computational time is still an area that requires more research.

4.5 Application of Neural Networks in WT CM

The attractive feature of Artificial Neural Networks (ANNs) for CM is their ability to represent complex, nonlinear relationships through learned pattern recognition or signal regression. ANNs have been successfully used to identify changes in the relationships between WT CM signals that indicate the development of a failure.

The application of ANNs for detecting faults is discussed in this section to automate the fault detection in the light of the limitations of spectral analysis in processing signals subject to transient effects. The main purpose of using ANNs is to identify changes in the current signal which have non-stationary characteristics due to the variable-speed operating conditions of WTs, and to provide online fault detection in advance of catastrophic failures. The methodology behind the ANN fault detection is discussed in the subsections.

4.5.1 Automated Fault Detection with ANNs

A simple detection threshold for the fault frequencies is not feasible due to the variable speed operation and accordingly shifting frequencies. ANNs are useful for automated processing and finding non-linear relationships. With data-driven training, ANNs learn to weight different inputs in a way to deliver the required output. Problem-specific settings have to be found in particular for the number of neurons and the amount of training required.

The rotational speed ω of a WT varies significantly. Fault detection for all possible rotational speeds is not feasible with a single ANN. A framework is proposed, in which different networks are used for different ranges of rotational speeds, as sketched in the workflows in Fig. 4.9 and Fig. 4.10. In the training phase, n sets of different

rotational speeds (Ω) with defined limits ω_{min} and ω_{max} are used for simulation of the current signals. The sets are selected in a way that all possible speeds are covered. For each of the sets, an ANN is trained to detect a fault. In the detection phase, maximum (max), minimum (min) and-standard deviation (σ) are calculated for each two second record. If the variation in the rotational speed is relatively high, the frequency spectrum becomes indistinct. Accordingly, the standard deviation of the set has to go below a defined limit σ_L to allow further processing. The appropriate ANN for fault detection with the FFT of the current signal is selected with the information of the rotational speed extrema.

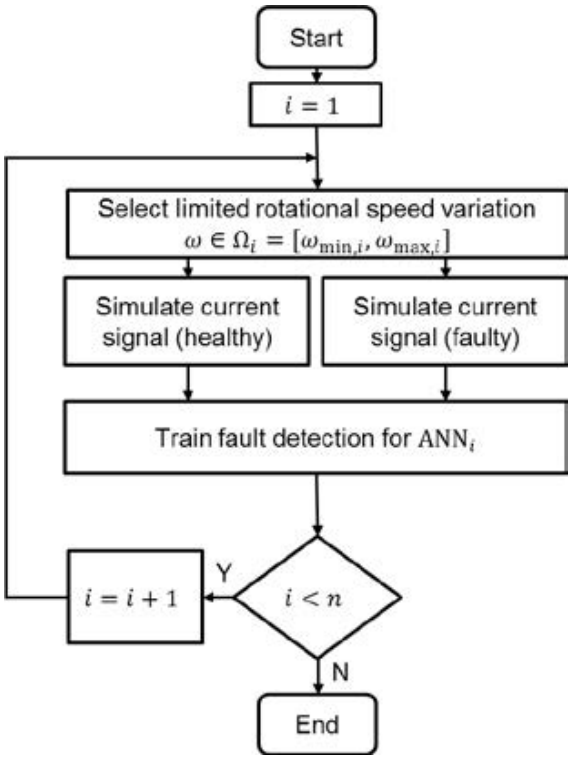

Figure 4.9 Workflow for training of fault detection algorithm.

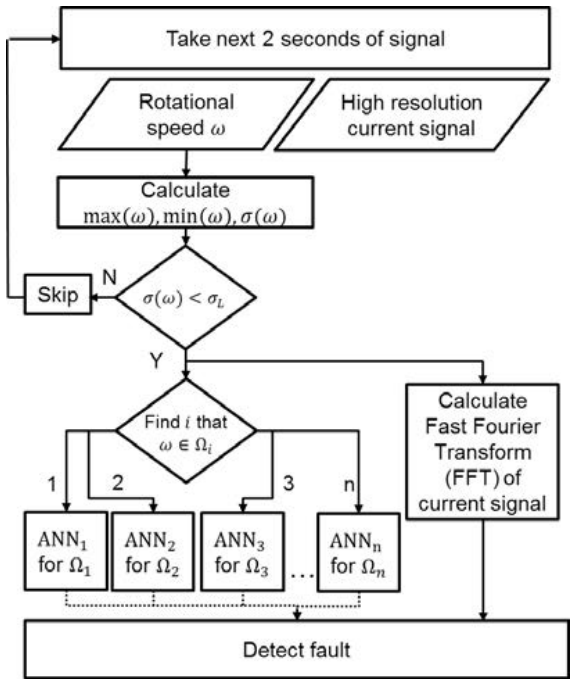

Figure 4.10 Workflow for fault detection after training.

The feasibility of the framework is discussed by investigating the training of one network for a limited rotational speed variation. In a first simulation study the ability to differentiate between healthy and faulty stages is tested. The second study investigates fault degree detection with different fault strengths where the fault level has been simulated by increasing the magnitude of the sideband harmonics as an indication to the fault with higher level.

4.5.2 Fault Classification

The WT simulation model is run for healthy and faulty condition with a selected variable speed variation between 924 and 937 rpm as shown in Fig. 4.11. For each condition, the current signal is recorded for 300 seconds at 5 kHz sampling frequency. Periods of two seconds of data are selected for analysis using the Fast Fourier Transform (FFT) algorithm. This window length is identified as the shortest possible with a sufficient resolution to capture all harmonics of interest. The frequency spectrum of each window consisting of 250 amplitudes acts as a 'sample'

for ANN fault detection. All samples from healthy and faulty stages are mixed and randomly split in training and testing. A classification as 'healthy' or 'faulty' is trained with scaled conjugate gradient backpropagation. The number of neurons and training samples are varied in a sensitivity study. Network training is repeated a number of times to investigate the impact of the random selection of training samples.

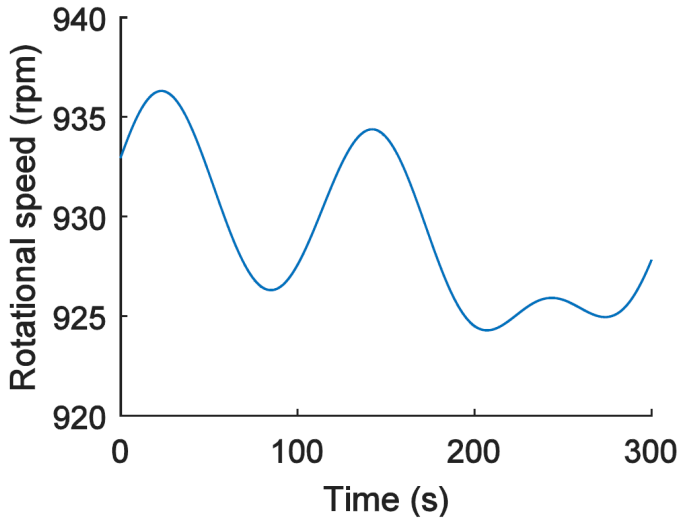

Figure 4.11 Rotational speed variation in simulation study.

The results of the simulation study with current signals from healthy and faulty conditions are presented in Table 4.1 considering accuracy as correct classification of both 'healthy' and 'faulty' stages. The median detection accuracy between 93.5 and 98% for different ANN and training length configurations distinctly higher than random classification (50% accuracy) shows that ANN fault detection using current signals under non-stationary conditions is feasible.

4.5.3 Fault Degree Detection

Additional to the above described two simulations representing permanent healthy and faulty condition, two further runs are used to investigate fault development. The first simulation applies a linear increasing fault during 300 seconds. In the second

Table 4.1 Accuracy of ANN condition detection from frequency spectrum given as median percentage from 250 training repetitions.

Number of neurons used:	Training with 100 samples, testing with 200 samples	Training with 150 samples, testing with 150 samples	Training with 200 samples, testing with 100 samples
2	93.5	96.7	98.0
5	94.5	96.7	98.0
10	95.5	97.3	98.0
25	95.5	97.3	98.0
50	95.0	97.3	98.0

run a fault occurs only at a certain point in the simulation. A fitting neural network with a tansig transfer function in the output layer is used to predict a fault degree between 0 and 1. All samples from the first simulation plus 100 randomly selected samples of the linear increasing fault simulation are used for training the ANN. Network training is repeated with identical data to illustrate differences resulting from suboptimal training.

Results of the transient and variable fault detection are presented in Fig. 4.12 and Fig. 4.13. Although the significant differences between three ANNs trained with the same input indicate that further optimisation of training and algorithm settings might be reasonable, the general fault development is successfully detected. Unsurprisingly, the fault degree detection is less accurate than the simple healthy or faulty classification. Regardless, even the rough detection of the strength of a fault enables better monitoring of condition changes.

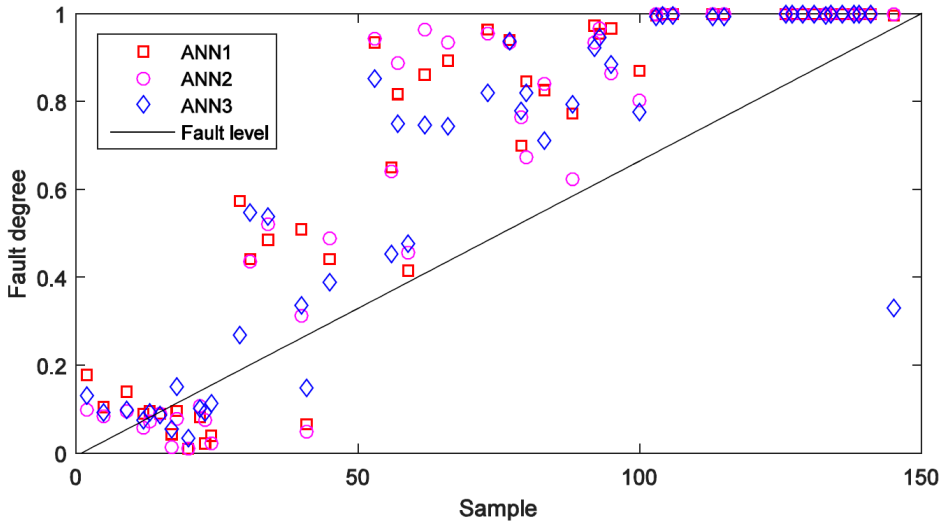

Figure 4.12 ANN fault degree detection of a linear increasing fault.

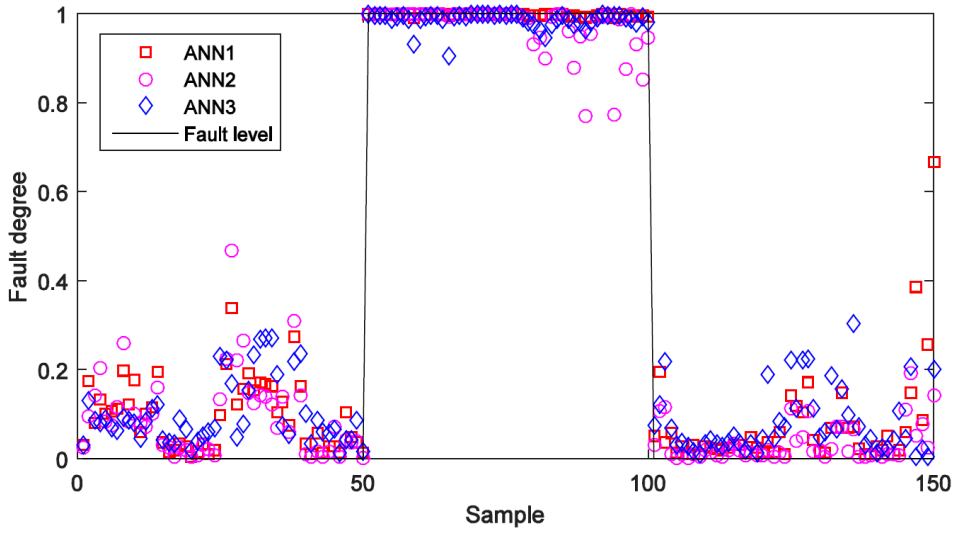

Figure 4.13 ANN fault detection of a transient fault.

4.6 Summary

Two standard techniques for time-frequency analysis have been introduced in this chapter in terms of their capability and complexity when used for detecting faults in a WT generator. Having examined these techniques, it seems that the time-frequency representations obtained by STFTs and CWTs appear to be unsuitable

for WT CM and fault diagnosis because they cannot provide accurate interpretation of non-stationary signals. However, the CWT was more successful in detecting anomalies in the time domain across different frequency bands from the analysis so far.

The central idea behind frequency tracking techniques was introduced and the commonly applied IDFT method was used as an example in this chapter. This frequency tracking technique proved successful on a simulation case study for a WT running under variable speed conditions. The IDFT has good computational efficiency by applying a discrete Fourier analysis over a narrow band around the potential fault frequency of interest to extract its peak amplitude. However, the problem with this technique is that the fault frequencies do not always have their maximum amplitude especially when they are corrupted by other components unconnected to the fault or when they are hidden in other high amplitude components such as the supply frequency and its harmonics, making the use of the IDFT impractical for continuous application on large WT populations.

A technique to detect faults in variable speed WTs via ANNs has been also introduced. A framework is discussed for training of fault detection with simulated signals from faults for later online detection in real WTs. For each set of limited rotational speed variation a separate ANN will detect the fault. In a simulation study of a rotor imbalance under varying rotational speed as expected in 5 minutes operation the feasibility of the fault detection approach is demonstrated. Simple classification of healthy or faulty condition is achieved with a high accuracy. In a further step towards fault prognosis, the severity of the fault is successfully detected. However, the dependency of ANNs on training data and manually set thresholds can result in undetected changes or frequent false alarms. Thus, further investigation has to be done to validate the fault detection algorithm with experimental data. A full test of the proposed framework has to be conducted including different sets of rotational speed variation. In terms of fault prognosis, optimisation of the ANN

settings might increase the fault degree detection accuracy. It is unlikely that the full range of fault's progression will be available in any training data period in practice. This demonstrates, that further improvement of WT CM techniques is still an area that requires more research to achieve effective real-time detection in real WTs.

One of the purposes of this research is to fill a gap in terms of finding a reliable method which can efficiently and consistently detect and track fault frequencies. The next two chapters will illustrate the theory behind new techniques that are better able to fill this gap.

Chapter 5

Extended Kalman Filter-Based Frequency Tracking

5.1 Introduction

In the previous chapter, the concept of time-frequency analysis to interpret non-stationary signals was discussed and the IDFT frequency tracking technique was used as an example. Despite the improvement in computational efficiency offered by this method, the FSC can be difficult to isolate accurately due to the fact that the WT frequently operates with the generator close to synchronous speed, resulting in FSCs manifesting themselves in the vicinity of the supply frequency and its harmonics, making their detection more challenging using methods such as an IDFT. To address this challenge, this chapter introduces an effective approach for WT CM and fault diagnosis where the detection of rotor electrical asymmetry in WT DFIGs is used as an illustrative example. Firstly, the analytical expressions defining a rotor electrical asymmetry fault signature in the DFIG stator current described in [30, 29] have been used to enable FSCs to be recalculated over time as a function of machine speed. Secondly, an adaptive extended Kalman filter (EKF) tracker has been proposed to extract the IAs of the FSCs based on the corresponding machine speed signal

and the estimated error covariance. At each time step, the calculated FSCs along with those extracted from the measured current signal are processed by the EKF to predict the future state of the FSCs, and continuously update the IAs of the FSCs as real-time monitored signal data samples become available. The proposed technique has been validated experimentally on a WT drive train test rig with two fault levels of rotor electrical asymmetries at three different driving conditions whose variability is representative of WT generator field operation. The performance of the proposed approach is compared with some of the leading WT generator CM techniques [128], [29]. The reported experimental findings demonstrate clear and significant gains in both the computational efficiency and the diagnosis accuracy using the proposed technique. The contents of this chapter has been published as an IEEE paper [119].

5.2 EKF for Frequency Tracking

The EKF is an efficient recursive algorithm widely applied in the fields of radar tracking [171] and adaptive control [172]. The conventional Kalman filter assumes a linear system dynamics model with Gaussian noise in the measurements, which is not always realistic in many applications. The EKF on the other hand is an extension of the conventional Kalman filter to non-linear system dynamics and has been used for state estimations of induction motors and WT DFIGs [173, 174]. In this section, the observed FSC $\boldsymbol{y}_k$ at time k is first modelled. The mathematical formulation of the EKF used to iteratively estimate the FSCs is then briefly presented. Theoretically, the stator current waveform in one phase (e.g., phase A) of DFIG can be expressed as:

$$\boldsymbol{z}_k(t) = \sum_i A_i \cos(2\pi f_i t_k + \theta_i) \tag{5.1}$$

where A_i and f_i are the amplitude with initial phase θ_i and the frequency of the ith sinusoid, respectively. A Fourier transform to convert the time description of the

stator current waveform into an equivalent function in the frequency domain has been used:

$$\boldsymbol{z}_k(f) = \sum_i A_i[\delta(f_k + f_i) + \delta(f_k - f_i)] \tag{5.2}$$

The one-sided Fourier transform of (5.2) at (f_s) the main supply frequency can be written as:

$$\boldsymbol{z}_k(f) = A\delta(f_k - f_s) \tag{5.3}$$

As previously mentioned in Chapter 3 that rotor electrical imbalance faults in a WT based doubly fed induction generator (DFIG) can induce additional frequency components in the frequency spectra of the stator current signals given by

$$f_f = \left(I \pm \frac{k(1-s)}{p}\right).f \tag{5.4}$$

where f_f are the series of fault signature components (FSCs) related to the fault, f is the fundamental frequency, k is the component order (k= 1, 2, 3...), s is the slip, I is a constant which relates to air-gap field space harmonics and p the number of pole pairs.

From equation(5.4), the main supply frequency can be represented as:

$$f_s = \Big(\frac{p}{pI \pm k(1-s)}\Big) f_f \tag{5.5}$$

By substituting (5.5) into (5.3), the representation of the FSCs in the frequency domain can be obtained:

$$\begin{aligned} \boldsymbol{z}_k(f) &= A\delta\Big(f_k - \Big(\frac{p}{pI \pm k(1-s)}\Big) f_f\Big) \\ &= A\delta(f_k - \alpha f_f) \end{aligned} \tag{5.6}$$

where α is a constant defined as:

$$\alpha = \Big(\frac{p}{pI \pm k(1-s)}\Big) \tag{5.7}$$

A system whose physical process can be mathematically modelled as it changes or evolves over time is known as a dynamical system. In making inference for such a system, two models are usually considered, a state model and a measurement model.

5.2.1 State Model

The state model is otherwise known as the state evolution model. In this case, it describes the motion model of the FSC profile, i.e. how the amplitude of a particular fault signature frequency evolves at time index k based on the previous time step, $k-1$.

$$\boldsymbol{x}_k = \mathbf{f}(\boldsymbol{x}_{k-1}, \mathbf{u}_k) + \mathbf{w}_k \tag{5.8}$$

where $\mathbf{f}$ is a non-linear function of states, $\mathbf{u}_k$ is the control vector, $\mathbf{w}_k$ is a white noise driving function to account for the dynamic variation of the state variables.

5.2.2 Measurement Model

The observed FSC $\boldsymbol{y}_k$ at time k with the additive noise $\boldsymbol{v}_k$ can be described as follows:

$$\boldsymbol{y}_k = \mathbf{z}_k + \mathbf{v}_k \tag{5.9}$$

and can be represented by the following linear stochastic system:

$$\boldsymbol{y}_k = \begin{bmatrix} 1 & 1 \end{bmatrix} \begin{bmatrix} A \\ \alpha f_f \end{bmatrix} + \mathbf{v}_k \tag{5.10}$$

The above linear representation is also equivalent to the following non-linear stochastic system:

$$\textbf{State equation } \boldsymbol{x}_{k+1} = \mathbf{f}(x_k) + \mathbf{w}_k \tag{5.11}$$

$$\textbf{Measurement equation } \boldsymbol{y}_k = \mathbf{H}\boldsymbol{x}_k + \mathbf{v}_k \tag{5.12}$$

where

$$\boldsymbol{x}_k = \begin{bmatrix} x_k(1) & x_k(2) \end{bmatrix}^T = \begin{bmatrix} A & \alpha f_f \end{bmatrix}^T \tag{5.13}$$

$$\mathbf{f}(x_k) = \begin{bmatrix} x_k(1) & x_k(1)x_k(2) \end{bmatrix}^T = \begin{bmatrix} A & A\alpha f_f \end{bmatrix}^T \tag{5.14}$$

$$\boldsymbol{H} = \begin{bmatrix} 1 & 1 \end{bmatrix} \tag{5.15}$$

5.2.3 Implementation

This formulation leads to the EKF algorithm in order to linearize the above system which is slightly different from a standard linear Kalman filter model. The recursive tracking process of a series of fault frequencies at any time step from k equal to zero is outlined as follows:

Step 1) Predict the estimates of the state variables $\hat{\boldsymbol{x}}_{k+1|k}$ and the error covariance $\mathbf{M}_{k+1|k}$

$$\hat{\boldsymbol{x}}_{k+1|k} = \mathbf{f}\hat{\boldsymbol{x}}_{k|k} \tag{5.16}$$

$$\mathbf{M}_{k+1|k} = \mathbf{F}\mathbf{P}_{k|k}\mathbf{F}^T + \mathbf{Q}_k \tag{5.17}$$

Step 2) Update the Kalman gain $\mathbf{K}_k$

$$r_k = |\boldsymbol{z}_k - \hat{\boldsymbol{z}}_k| \tag{5.18}$$

$$\mathbf{S}_k = \mathbf{H}_k \mathbf{P}_{k|k-1} \mathbf{H}_k^T + r_k \tag{5.19}$$

$$\mathbf{K}_k = \mathbf{P}_{k|k-1} \mathbf{H}_k^T \mathbf{S}_k^{-1} \tag{5.20}$$

where

$$\begin{aligned} \mathbf{F}_k = \mathbf{f}(x_k) x_k \Big|_{x_k = \hat{x}_{k|k}} &= \begin{bmatrix} 1 & 0 \\ \hat{x}_{k|k}(2) & \hat{x}_{k|k}(1) \end{bmatrix} \\ &= \begin{bmatrix} 1 & 0 \\ (1-\varepsilon)(\alpha \hat{f}_f)_{k|k} & \hat{A}_{k|k} \end{bmatrix} \end{aligned} \tag{5.21}$$

Step 3) Update the state variables $\hat{\boldsymbol{x}}_{k|k}$

$$\hat{\boldsymbol{x}}_{k|k} = \bar{\boldsymbol{x}}_{k|k-1} + \mathbf{K}_k [\boldsymbol{y}_k - \mathbf{H}_k(\bar{\boldsymbol{x}}_{k|k-1})] \tag{5.22}$$

Step 4) Update the error covariance

$$\begin{aligned} \mathbf{P}_{k|k} &= (\mathbf{I} - \mathbf{K}_k \mathbf{H}) \mathbf{P}_{k|k-1} + q\mathbf{B} \\ \mathbf{B} &= \begin{bmatrix} 0 & 0 \\ 0 & 1 \end{bmatrix} \end{aligned} \tag{5.23}$$

where the symbols $\bar{\mathrm{L}}$ and $\hat{\mathrm{L}}$ stand for the predicted and updated values, respectively. $\mathbf{I}$ is the identity matrix. The vector $\boldsymbol{z}_k$ is the observed FSCs which is obtained by applying the Fast Fourier Transform (FFT) algorithm for each interval of interest from the current signal in the time domain, and $\hat{\boldsymbol{z}}_k$ is the expected normal state which represents the calculated FSCs in equation 5.4. r_k denotes the measurement innovation.

The design of a stable EKF was largely addressed in [175, 176] which report theoretically supported design guidelines to characterize the EKF design by a vector of three parameters (r, ε, q). An easier and more transparent tuning of EKFs is introduced in[177] where the results showed that ε must be set to zero to achieve the basic property of unbiasedness, and that the performance of the EKF tracker then only depends on the ratio $\lambda = r/q$; Ref. [177] proceeds to suggest that $q = 1$ (and hence $\lambda = r$) for a further significant simplification of the tuning procedure. Hence, the task of tuning the design parameters of the EKF tracker (parametrized with r, ε, q) is reduced to the fact that only a single parameter ($\lambda = r$) has to be chosen [177]. This EKF tuning approach was followed in this chapter where, r is set to be the difference between the observed FSCs and the calculated FSCs in order to (a) limit the variation of the innovation vector, (b) cope with spurious measured values, (c) enhance the estimated accuracy and (d) help the EKF to provide proper weighting.

In the implementation of the EKF, we assume that at time k an initial estimate of the state variable is known and is denoted by $\boldsymbol{x}_{k-1|k-1}$ and that its associated covariance matrix is also known and denoted by $\mathbf{M}_{k-1|k-1}$. The estimated variables are not affected by this assumption because the EKF is not sensitive to moderate changes in the initial covariance [178].

The principal stages of the tracking method based on the EKF to iteratively estimate the FSCs in the stator current signal are

• Input the initial measured generator rotational speed and the stator current data points, the initial value of the state variables $\boldsymbol{x}_0$ and its associated covariance matrix $\mathbf{M}_0$, and covariance of the measured error r_0 at a sampling interval Δt_k

• Calculate the mean speed for the sample and the slip

• Calculate the stator current spectrum using an FFT

• Calculate discrete constants from frequencies of interest,k

• Calculate amplitudes for each constant,k

• Extract maximum amplitude and its frequency $\boldsymbol{z}_k$

• Calculate the FSCs of interest using equation 5.4 $\hat{\boldsymbol{z}}_k$

• Predict the estimates of the state variables and the error covariance using equations (5.16) and (5.17)

• Calculate covariance of the measured error r_k using (5.18)

• Compute the Kalman filter gain $\mathbf{K}_k$ using (5.20)

• Update the estimates of the state variables and the error covariance with the measurement $\boldsymbol{z}_k$ using (5.22) and (5.23)

• Project ahead using equations (5.16) and (5.17)

• Repeat the process starting with next sampling interval Δt_{k+1}

5.3 Application of EKF to WT CM

The proposed approach has been applied to the generator current signals collected from a purpose built WT drive train test rig. As shown in Fig. 5.1, the test rig comprises of a 54-kW DC variable-speed drive connected via a two-stage gearbox to a four-pole DFIG that was rated for the experiment at 30-kW. The rotational speed of the DC motor is controlled by an external model incorporating the properties of a 2-MW WT operating under closed-loop conditions, driven by realistic wind conditions at a variety of wind speeds and turbulence intensities. The rotor circuit of the generator is coupled via slip rings to an external three-phase resistive load bank so that electrical imbalance can be applied to the generator rotor. The test rig was instrumented and controlled using LabVIEW.

In the experiments, a rotor unbalance fault was implemented on the test rig by adding two additional external resistances to one phase of the rotor circuit through an external load bank. In the healthy state, the rotor resistance was 1.3 Ω per phase and additional resistances of 0.3 Ω and 0.6 Ω were successively added to one phase to create two fault levels. These correspond to two levels of rotor unbalance of 23%

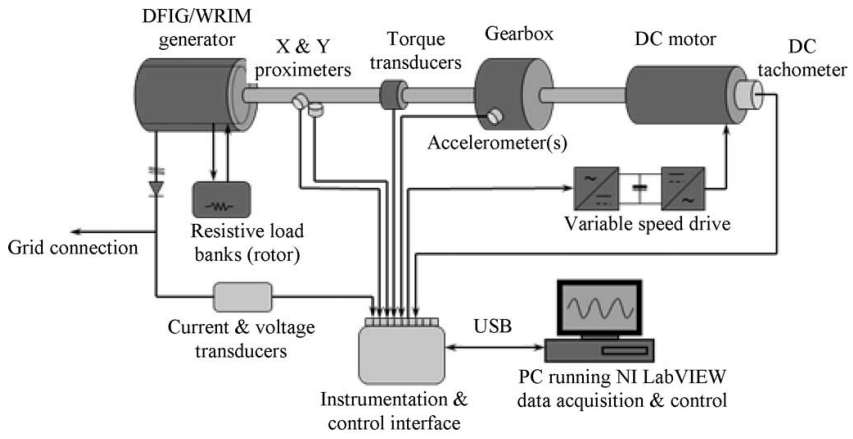

Figure 5.1 Schematic representation of the test rig[5].

and 46%, respectively, given as a percentage of the rotor balanced phase resistance. The test rig enables the generator to be driven at a desired pre-programmed wind speed profile that emulates realistic WT transient behavior and is achieved by providing a pre-defined speed reference profile to the controller. The relevant signals for condition monitoring were collected from the terminals of the generator at a sampling frequency of 5 kHz. An example of the measured current signal under faulty conditions is shown in Fig. 5.2.

It can be seen that the amplitude of the current-time waveform gave no indication of abnormal conditions. Consequently, an FFT algorithm is used to convert the generator current signal from the time domain into the frequency domain in a healthy condition (no unbalance) and with a rotor unbalance as shown in Fig. 5.3. As is generally expected for any grid connected machine the supply frequency (50 Hz) and its harmonics are clearly seen in the spectra. There are also spectral components present around the even and odd harmonics even when operating in a healthy state. This is believed to be caused by pre-existing low level rotor excitation imbalance commonly induced by inherent manufacturing imperfections [28, 29]. However, the comparison of healthy and faulty data indicates a significant rise in magnitude of a number of twice slip frequency $2sf$ sideband components on the current harmonics

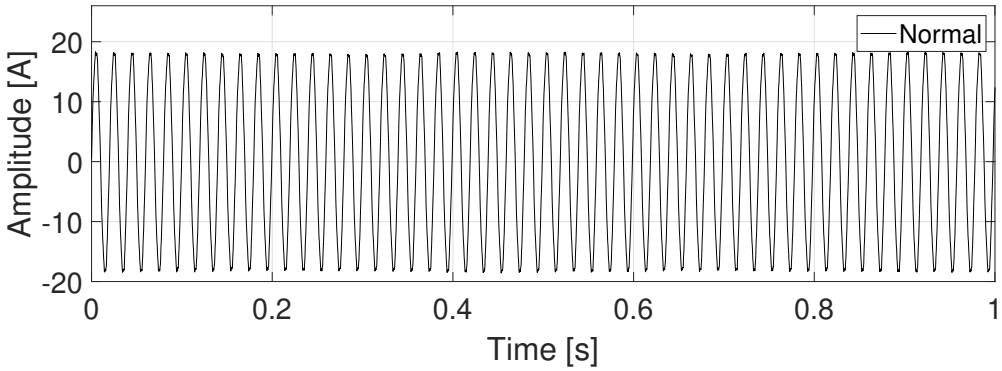

(a)

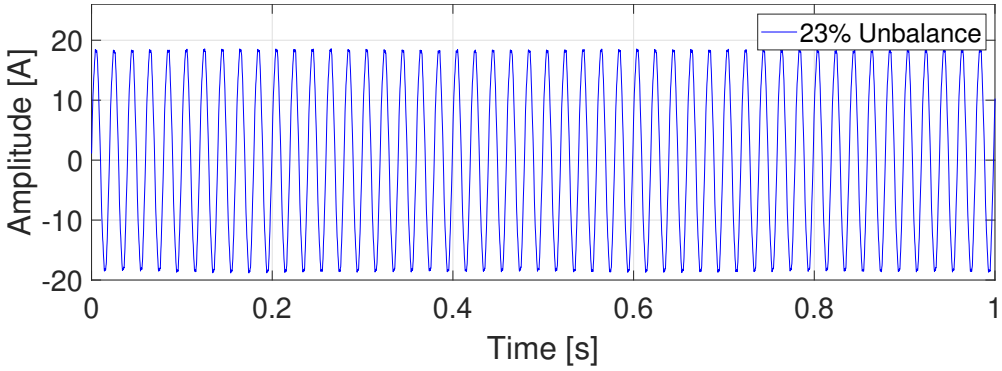

(b)

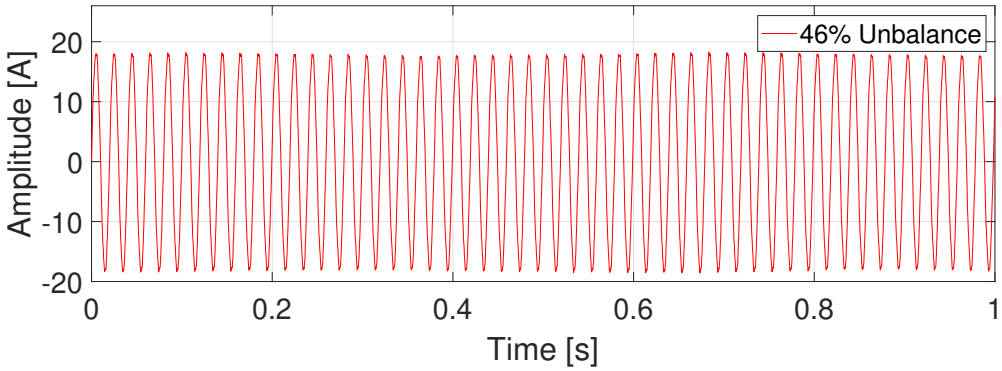

(c)

Figure 5.2 Comparison of the current-time waveform for healthy case, 23% rotor unbalance case and 46% rotor unbalance case.

which can be clearly observed when the 23% and 46% unbalance are applied to the generator rotor.

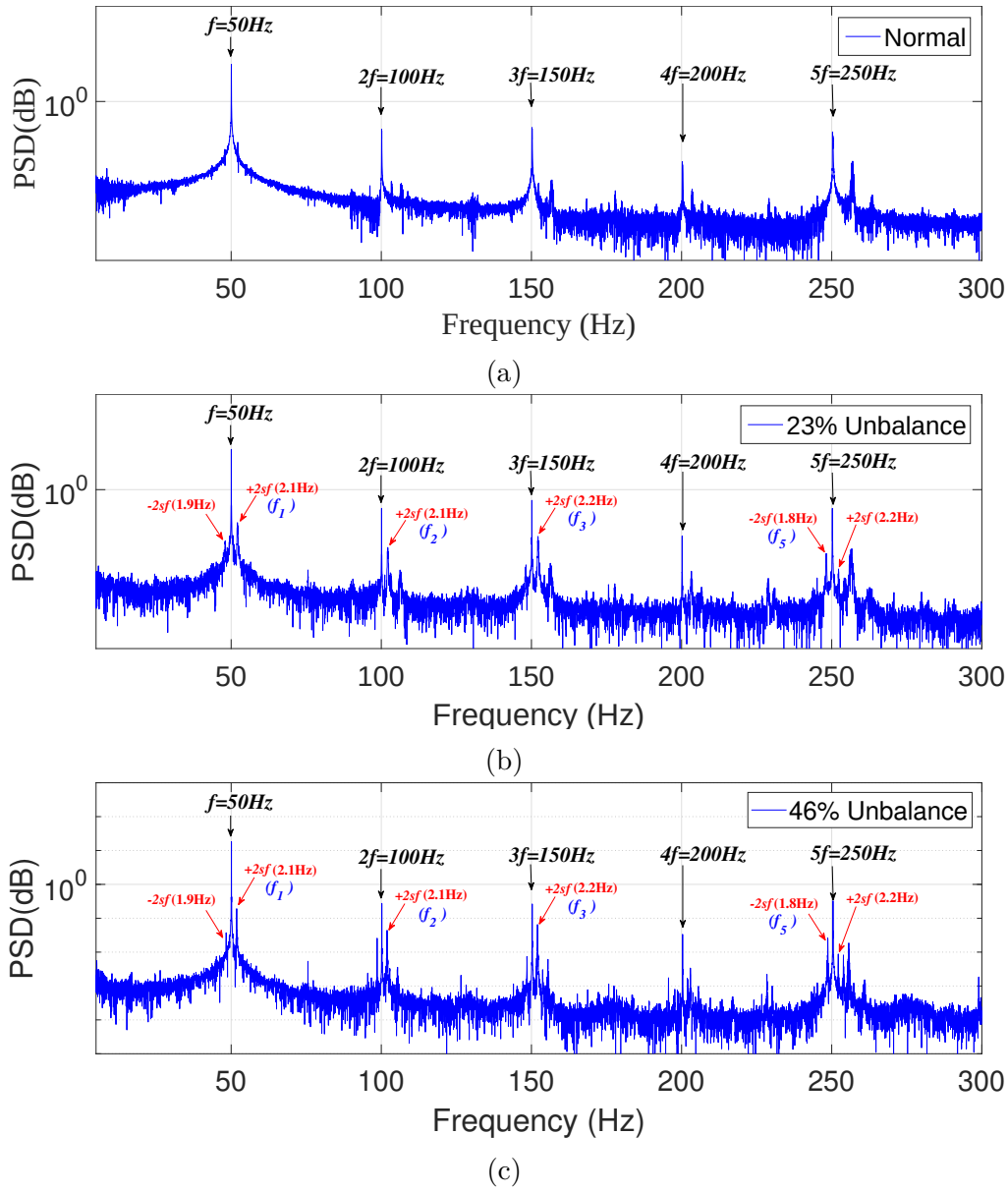

Figure 5.3 Comparison of the current spectra for healthy case, 23% rotor unbalance case and 46% rotor unbalance case.

In Fig. 5.3, the FFT algorithm cannot reveal the time information of any frequency changes i.e. no time domain information is available regarding fault occurrence and progression. Thus, an EKF has been proposed to detect faults by monitoring the magnitudes of the FSCs over time, taking into account variable operating conditions. The rotor unbalance fault gave rise to a number of side-band

components in the current spectra. Monitoring all components would be impractical in an operating environment, so a series of FSCs was selected that exhibit the highest magnitude. The FSCs of interest to be tracked using the EKF algorithm are labelled as f_1, f_2, f_3, f_5 in Fig. 5.3.

5.4 Experimental Results

In order to show the effectiveness of the proposed approach based on an EKF, the CWT and IDFT have been selected, used in [128, 29] for WT generator CM, for comparison. The algorithms are tested under varying rotational speed conditions representative of the operating regimes seen by a hypothetical wind turbine out in the field. At each test, the test rig was run for a period of 150 s after which the 23% and 46% unbalance fault conditions were applied at 150 s and 300 s, respectively. The driving conditions selected for testing are shown in Fig. 5.4, corresponding to the following WT operating conditions:

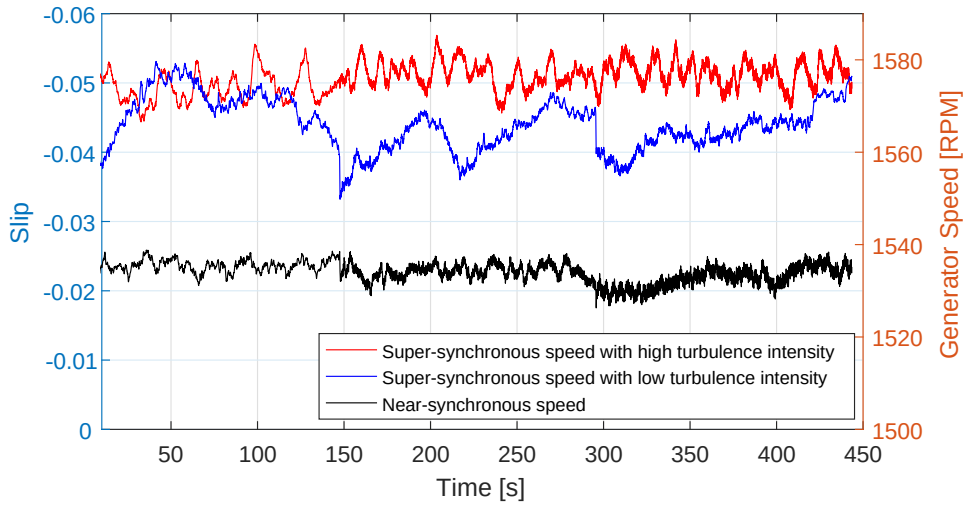

Figure 5.4 Generator speed test conditions.

5.4.1 Test case 1

Super-synchronous speed with high turbulence intensity: In this test, a high mean wind speed (15 m/s) with high turbulence intensity (20%) was applied to the test rig via a dc motor, the speed of which was controlled by an external model incorporating the properties of a 2 MW exemplar turbine model developed by the University of Strathclyde as part of the Supergen Wind Energy Technologies Consortium [29]. The CWT, IDFT and EKF methods have been applied to the current spectra in Fig. 5.3 to extract the IAs of the four defined frequencies of interest (f_1, f_2, f_3, f_5) for the detection of rotor unbalance. The results under super-synchronous speed with high turbulence intensity are shown in Figs. 5.5, 5.6 and 5.7. Note, if the tracked FSC of each method shows a step change in magnitude when the fault condition was present or has changed, then the method has successfully captured the component frequency related to the fault.

In Fig. 5.5, the conventional CWT is able to capture fault components f_1 and f_2 where their IAs did show a marked change when the fault condition was applied or has changed. The CWT failed to capture other components due to the influence of the window function on the results, where the window size is well matched with the oscillation of component f_1 and f_2 but as the fault frequency increases the window is no longer able to capture the variation of the fault components. A more robust window design is necessary in order to improve simultaneously high time resolution and high frequency resolution. But, this is not an easy task as the difference between the f_1, f_2 and f_3 components is about 50 Hz and increases to 100 Hz for component f_5. In addition, these components overlap with the main supply frequencies and other dominant frequency components of the current signal that are irrelevant to the fault. To overcome these shortcomings, the IDFT algorithm was applied to extract the magnitude of the FSCs. The results are shown in Fig. 5.6.

In Fig. 5.6(b), it is seen that the IDFT method has successfully tracked the magnitude of the four fault-related frequencies with increasing fault severity (i.e.,

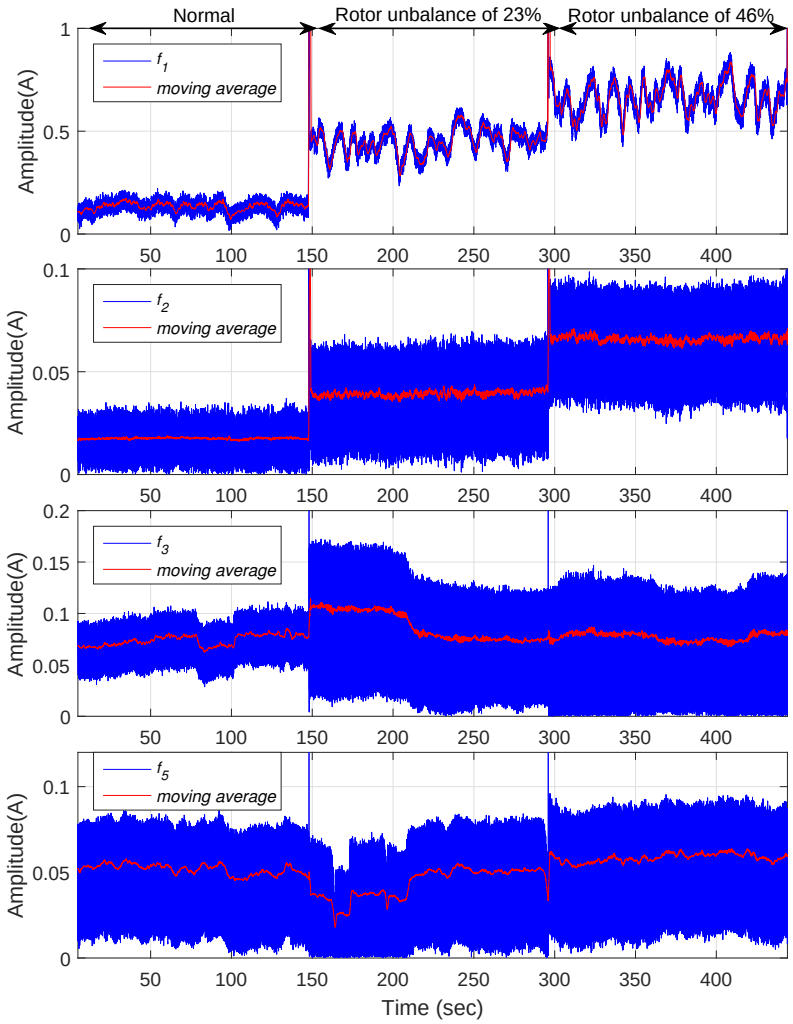

Figure 5.5 Tracking the magnitude of fault signature frequencies of interest using the CWT for test case 1.

from 300 s to 450 s) despite the fact that the shaft speed was varying continuously throughout the experiments. Similar to the IDFT results, the EKF algorithm has successfully picked up the four FSCs that are changing proportionally to the rotational speed as shown in Fig. 5.7. The results show that the EKF is able to track the fault frequencies, giving quantitative information about the fault progression.

However, the tracking results of each algorithm follow different variation tendencies due to the fact that the current signals from an operational WT are not stationary but are time-varying in nature because of the constantly varying generator speed, making the detection of FSCs by the tracking algorithms more challenging. In

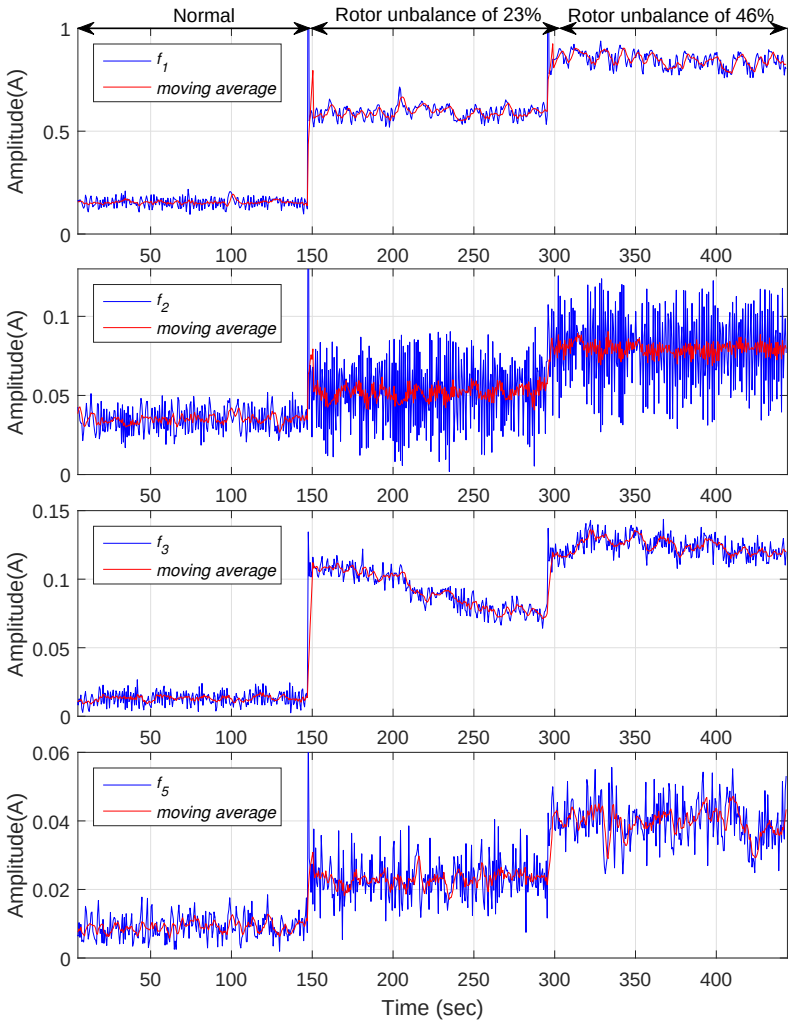

Figure 5.6 Tracking the magnitude of fault signature frequencies of interest using the IDFT for test case 1.

order to demonstrate the best achieved performance for detecting the rotor unbalance fault and revealing the actual fault degree, the performance of all diagnostic methods during the fault event is evaluated using root mean squared error (RMSE) values. Since the increase in the degree of rotor unbalance can be calculated from the IA variations of the FSCs extracted by the diagnostic methods, a general expression is derived for machine operation with rotor unbalance degree $\hat{\eta}_k$ by calculating the difference between the IA for each component under healthy and faulty conditions divided by the order of the component order times the average under healthy conditions as follows:

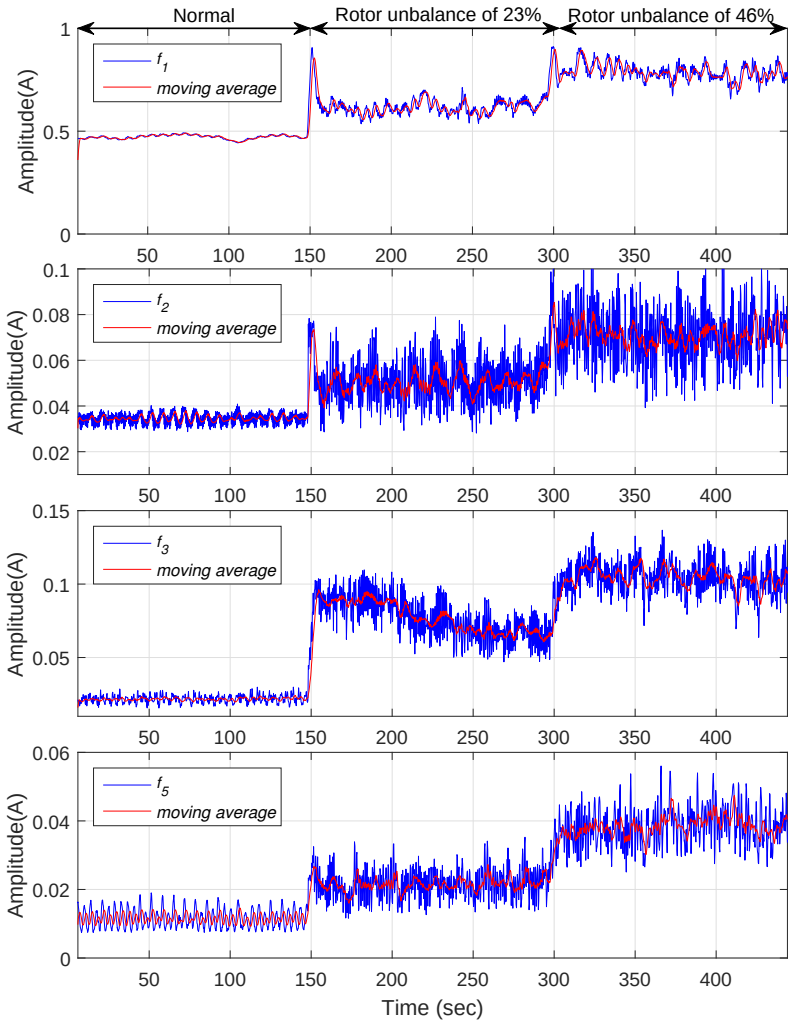

Figure 5.7 Tracking the magnitude of fault signature frequencies of interest using the EKF for test case 1.

$$\hat{\eta}_k = \frac{A_f - A_h}{k.A_h}.100\% \tag{5.24}$$

where the A_h and A_f are the IA at any time step k for each component under healthy and faulty conditions respectively and **k** is the component order (**k**= 1, 2, 3...). The RMSE is given by

$$RMSE = \sqrt{\frac{1}{N}\sum_{i=1}^{N}(\eta_i - \hat{\eta}_i)^2} \tag{5.25}$$

where the η_i is the degree of the fault during the experiment, corresponding to the two levels of rotor unbalance of 23% and 46%. Table 5.1 summarizes the results of the performance evaluation. It is clear from the table that the IDFT and EKF methods perform best in terms of the RMSE for all FSCs. The CWT is incapable of detecting the fault by tracking the components f_3 and f_5, but the RMSE values for components f_1 and f_2 are lower than the same components for the IDFT. The comparison between the three methods shows that the RMSE for all FSCs is much lower when using the EKF method.

Table 5.1 RMSE of the tracking methods for test case 1.

Fault Signature Components	RMSE Values (%)		
	CWT	IDFT	EKF
f_1	1.967	2.135	0.325
f_2	1.134	1.301	0.258
f_3	N/A	2.115	0.441
f_5	N/A	0.420	0.236

5.4.2 Test case 2

Super-synchronous speed with low turbulence intensity: This test represents 7.5 m/s mean wind speed with low turbulence intensity 6%. The slip for this state differs significantly from case 1 with a wide range as seen in Fig. 5.4. Similar results to the previous test case are observed as shown in Figs. 5.8, 5.9 and 5.10, where the CWT is only able to track the fault component f_1 and f_2. This explains why in [128], [5] only the fault component f_1 which is the twice slip frequency was tracked using the CWT. In contrast, both the IDFT and EKF methods can successfully show the presence of the fault. It is also clear that the variation tendencies of the IAs at the four characteristic frequencies have been correctly extracted despite the time-varying features due to the variable speed operation and the disturbance of the components unrelated to the fault.

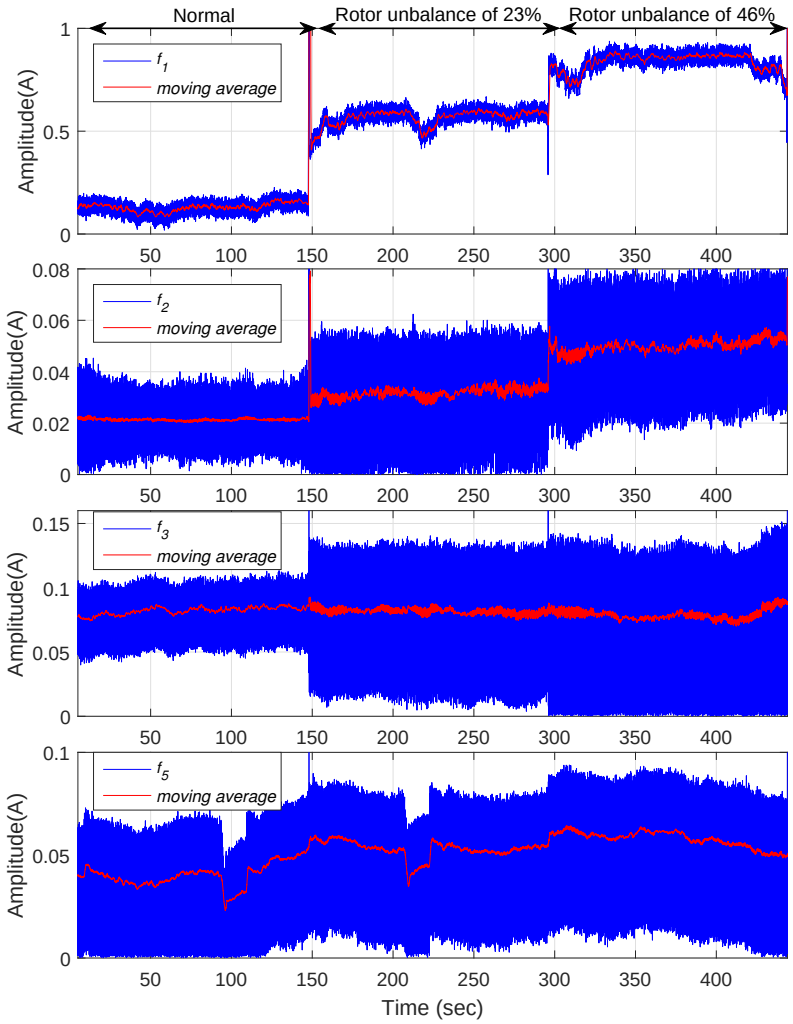

Figure 5.8 Tracking the magnitude of fault signature frequencies of interest using the CWT for test case 2.

The performances of the three methods are summarized in Table 5.2. Again, the performance of the IDFT and EKF is better in terms of the RMSE values for all FSCs. Compared to the CWT and IDFT, the EKF proved capable of dealing with different variable speed driving conditions with lower RMSE values. In addition, the components f_1 and f_2 for the CWT show higher RMSE values compared to the results in case 1 as larger variation in rotational speed for test case 2 makes it more challenging to track the FSCs. It can be concluded that the EKF not only showed the best performance overall in terms of RMSE metric, but also in terms of the rotor unbalance fault detection at different driving conditions, whereas the CWT method

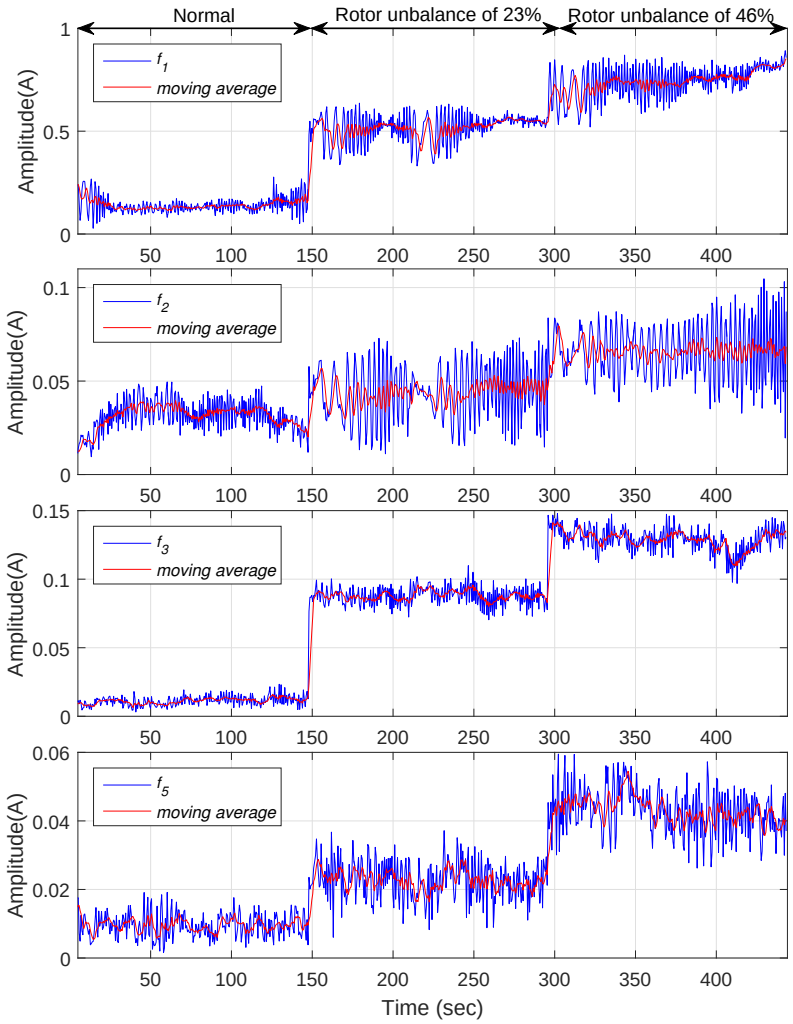

Figure 5.9 Tracking the magnitude of fault signature frequencies of interest using the IDFT for test case 2.

performed worst. One explanation for the poor performance of the CWT method can be the windowing technique which has been influenced by the speed variations.

5.4.3 Test case 3

Near-synchronous speed: Following the successful detection of the fault conditions at super-synchronous speed, it is important now to verify the CM capability of the algorithms when the machine operates near to the synchronous speed. In this case, the slip will be near to zero so the FSCs in equation 5.4 will be very close to the supply frequency(50 Hz) and its harmonics (both odd and even), making CM

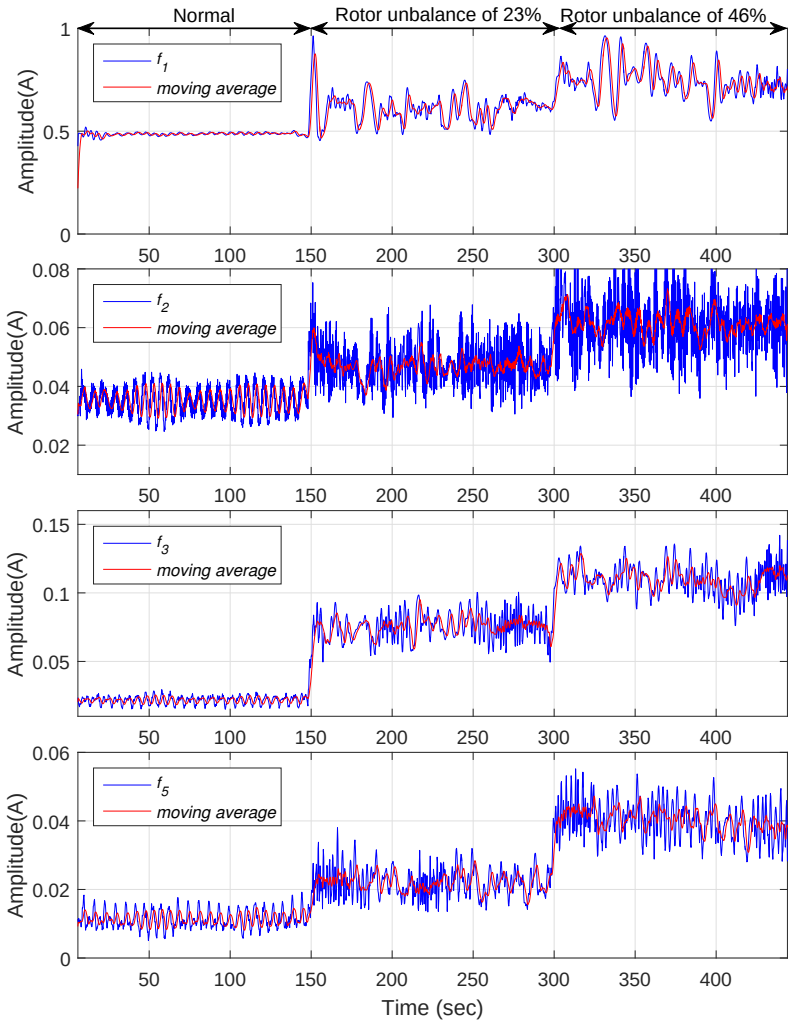

Figure 5.10 Tracking the magnitude of fault signature frequencies of interest using the EKF for test case 2.

and fault detection more challenging even though this condition occurs frequently for an operational wind turbine. The results of such a scenario are shown in Figs. 5.11, 5.12 and 5.13.

Both the CWT and IDFT algorithms, shown in Figs. 5.11 and 5.12 have failed to effectively track the FSCs; the shortcoming of the CWT and IDFT methods is that both use windowing technique, and do not have an observer to avoid tracking the FSCs when they are so close as to be effectively merged with the supply frequency and its harmonics.

Table 5.2 RMSE of the tracking methods for test case 2.

Fault Signature Components	RMSE Values (%)		
	CWT	IDFT	EKF
f_1	2.757	2.413	0.318
f_2	2.213	0.608	0.276
f_3	N/A	2.067	0.382
f_5	N/A	0.388	0.234

On the other hand, the EKF shows much better resolution of the varying fault conditions, as shown in Fig. 5.13. The results clearly show that the amplitude of the fault-related frequencies jumps sharply when the 23% unbalance fault is introduced at 150s. A similar jump occurs for the 46% unbalance condition introduced at 300s that shows clear differences between healthy and faulty conditions particularly for components f_2, f_3 and f_5. The performances of the FSCs tracked by the EKF in terms of the percentage RMSE values are found to be 0.378, 0.244, 0.386 and 0.352 for the f_1, f_2, f_3 and f_5, respectively. It can be seen that the EKF shows more accurate fault tracking across all the driving conditions and the RMSE values for all FSCs are very close. Over the three cases, the EKF shows better fault resolution compared to the CWT and IDFT as it does not use any windowing technique, rather it uses the Kalman gain ($\mathbf{K}_k$). The Kalman gain acts as a relative weight given to the current extracted and measurement values, and its value is continuously tuned to get the correct estimation value of the FSCs and their magnitude from the non-stationary current signal. At each time step, the $\mathbf{K}_k$ is calculated from the covariance. The constantly varying generator speeds and non-linear operation lead to an increase or decrease of the Kalman gain, so with a high gain the filter places more weight on the most recent measurements, and thus follows them more responsively to avoid tracking the noise (i.e. the supply frequency and its harmonics or other dominant frequency components of the current signal) which are irrelevant

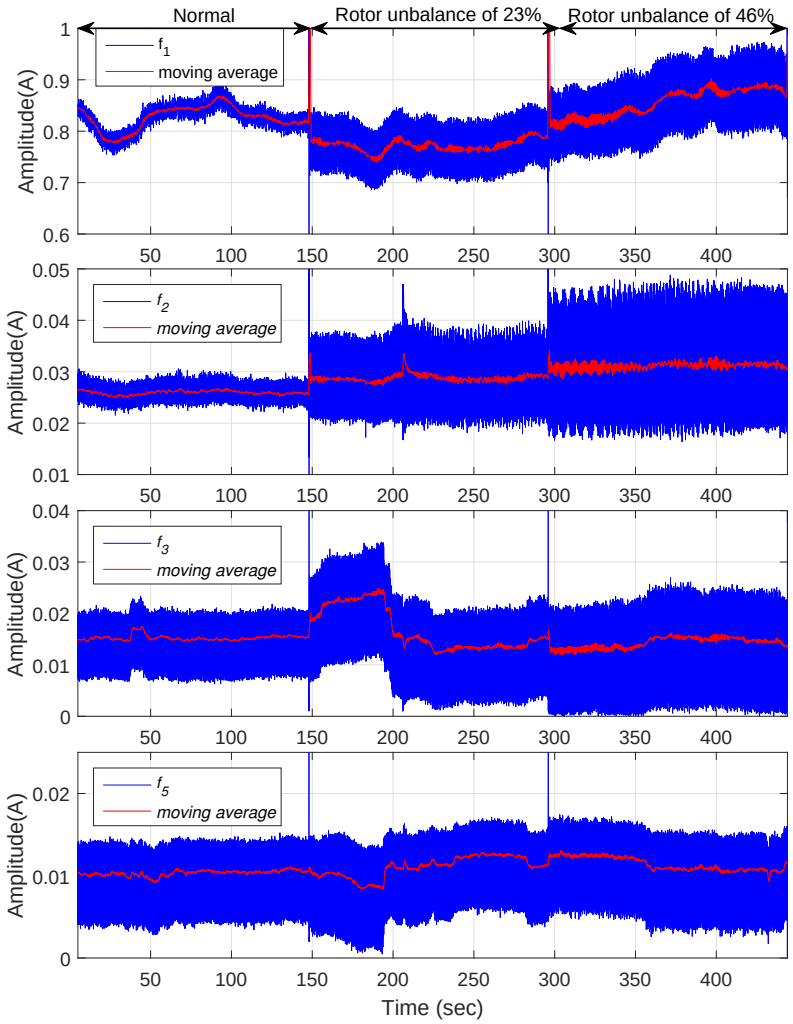

Figure 5.11 Tracking the magnitude of fault signature frequencies of interest using the CWT for test case 3.

to the fault. With a low gain, the filter follows the model predictions more closely to track the fault signatures and smooth out the noise.

To show the effectiveness of the proposed EKF, we compare in Fig. 5.14 the tracking results of the EKF associated with the spectral component frequencies against the actual frequencies, described by equation5.4, across all driving conditions. As it can be seen from Fig. 5.14, that the tracking frequencies are different from the actual frequencies in normal operation when there is no fault because the magnitude of the actual frequencies is very small and merged with the noise so they are difficult to detect or differentiate. Once, the fault has been applied, the EKF immediately

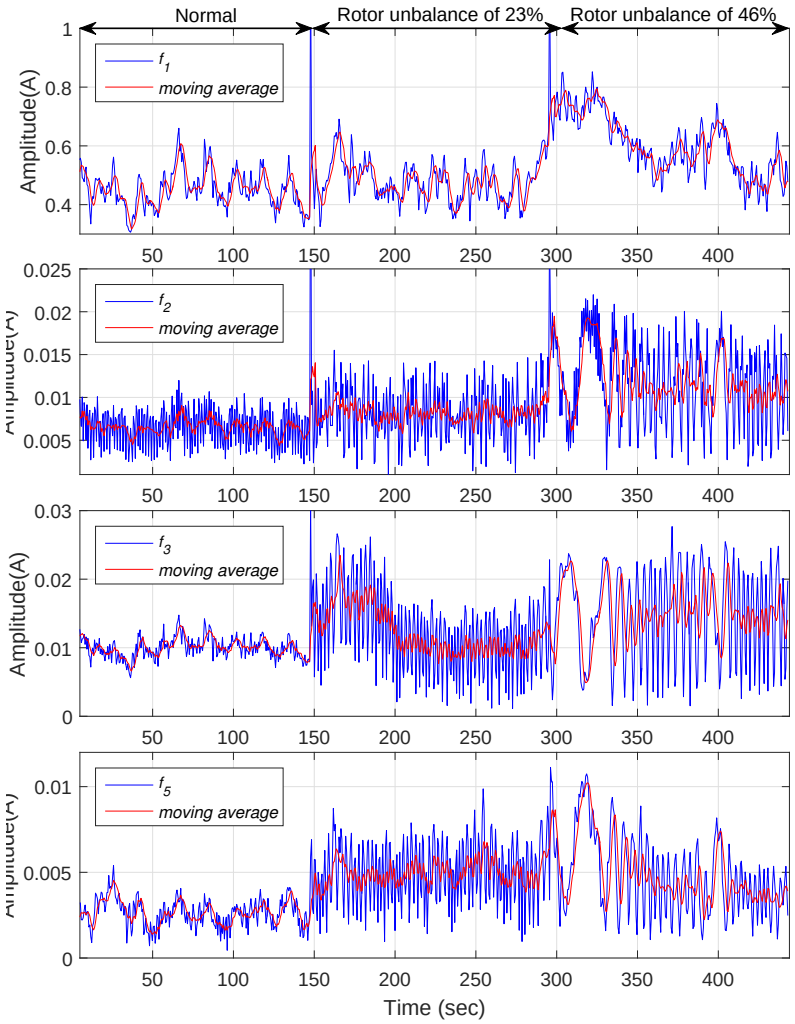

Figure 5.12 Tracking the magnitude of fault signature frequencies of interest using the IDFT for test case 3.

captured the frequencies related to the fault and continued to track them over time despite the fact that the actual frequencies are more affected by the speed variations and follow exactly the same speed variation tendencies as shown in Fig. 5.4. It can also be seen for case 3 that the f_1 and f_5 FSCs are particularly difficult to capture compared to the others cases due to the operation at low load near to synchronous speed, resulting in FSCs manifesting themselves in the vicinity of the supply frequency and its harmonics with extraneous noise as shown in Fig. 5.3. This led to an increase in the variation of the innovation vector r_k for these conditions. However, the magnitude of the tracked f_1 and f_5 FSCs is still useful for fault

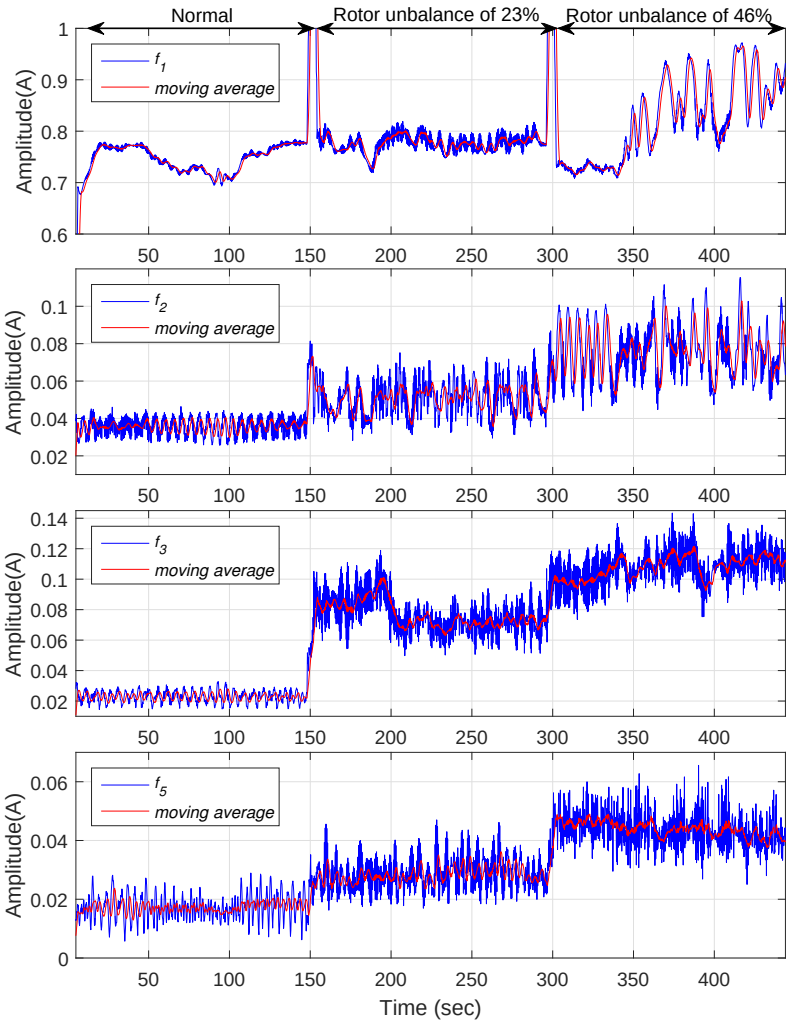

Figure 5.13 Tracking the magnitude of fault signature frequencies of interest using the EKF for test case 3.

detection, and did show a step change in magnitude when the fault condition was present or was changed as discussed above.

In summary, the results for the three cases show that the rotor electrical unbalance fault can be accurately detected by tracking any component using the EKF, but overall the second component f_2 showed the lowest RMSE in revealing the fault degree. Whereas, the results using the IDFT in Table 5.1 and 5.2 show that the fifth component f_5 provides the lowest RMSE (0.404 as an average percentage) while the results obtained from other components are not effective in revealing the degree of rotor unbalance. If one only considers component f_5 for fault diagnosis, the

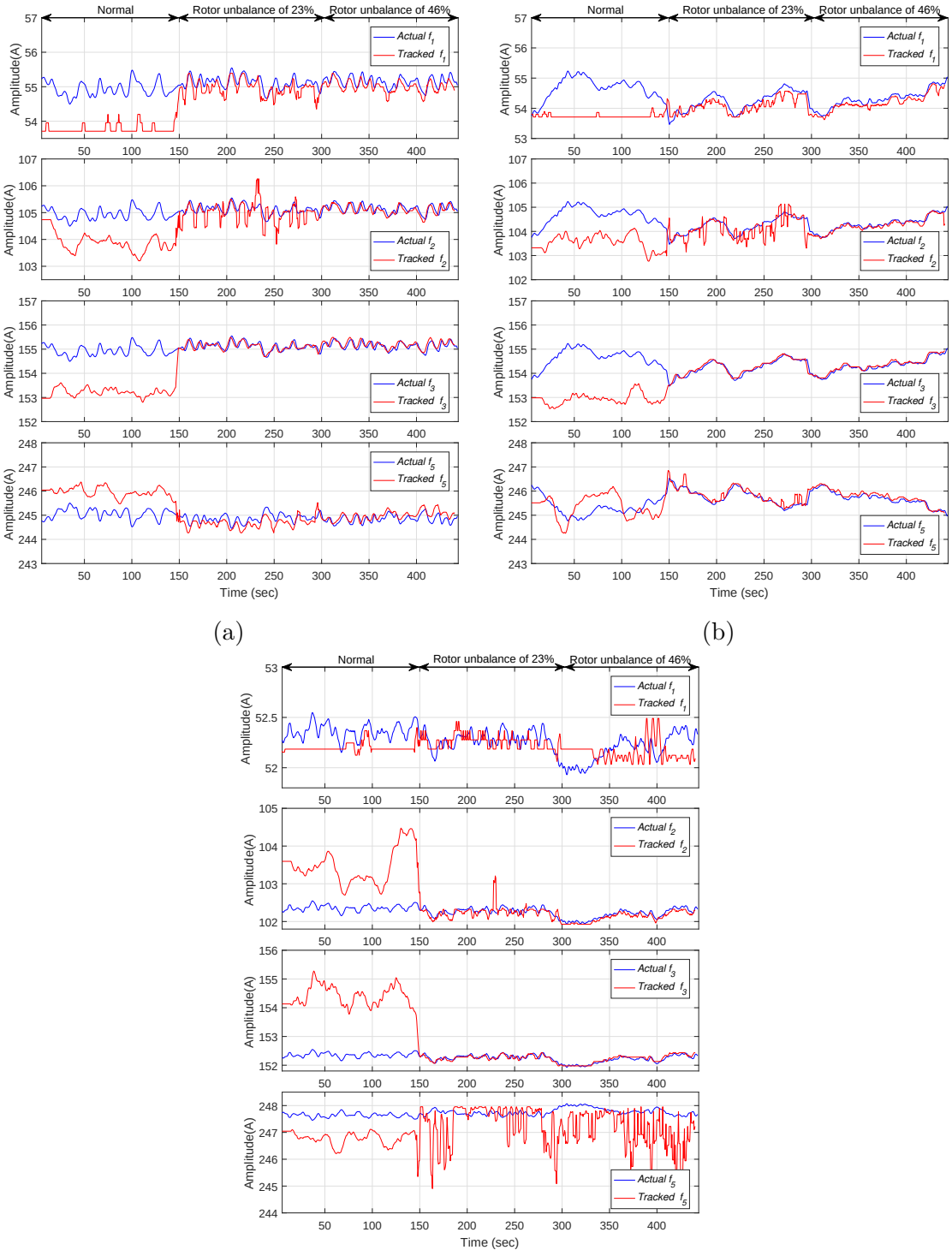

Figure 5.14 Tracking the fault frequencies of interest using EKF for (a) test case 1 (b) test case 2 and (c) test case 3.

proposed approach demonstrates a significant improvement over the IDFT method in imbalance diagnosis accuracy by reducing the percentage RMSE from 0.404 to 0.235. Since the results show that the second component f_2 has the best accuracy in the case of the EKF while the fifth component f_5 provides the best accuracy in the case of the IDFT, this indicates that the volume of data required for analysis and storage has been successfully reduced. To clarify, based on the Nyqist-Shannon sampling theorem, the data requirements to monitor component f_5 for a period of 1 year would enable the monitoring of component f_2 for a period of approximately 2 years and 4 months, due to the fundamental fact that f_5 is greater than f_2 and requires a higher sampling rate to capture. Hence, the approach shows success in tracking the magnitude of the FSCs and revealing the severity of the faults over time with significant gains in both the computational efficiency and the diagnosis accuracy.

5.5 Computational Time

To further highlight the improvement offered by an EKF, a computational time (CT) analysis is performed comparing the EKF method against the CWT and IDFT methods. The calculations were performed on a computer with an Intel i7 core processor and 32.0GB RAM.

Table 5.3 shows the plot of the averaged CT for the results obtained in Figs. 5.5-5.13 for the series of FSCs. It is seen that the CWT method requires a higher CT for the FSCs with lower frequencies because these tend to have much longer wavelengths with a high signal to noise ratio, whereas the higher FSCs have much shorter wavelengths with low signal to noise ratio. Accordingly, this affects the width of the window function in time to capture the frequencies of interest; therefore, it requires more computational resources. In contrast, the IDFT and EKF require far less computational resource compared to the CWT. This is due to the fact that the

IDFT and EKF methods apply a discrete Fourier analysis over a narrow band around the frequency of interest. The IDFT and EKF have very similar CT requirements making them more suitable for online monitoring than the CWT.

Table 5.3 Computational complexity of the tracking methods.

Fault Signature Components	Computational Time (s)		
	CWT	IDFT	EKF
f_1	35.65	0.98	1.2
f_2	20.05	1.01	1.1
f_3	14.79	1.05	1.16
f_5	4.32	1.09	1.1

5.6 Summary

Determining the magnitude of particular fault signature components (FSCs) generated by WT faults from stator current signals has been used as an effective way to detect early abnormalities. However, the current signals from an operational WT are not stationary but are time-varying in nature due to the constantly varying generator speed. Additionally, the WT frequently operates with the generator close to synchronous speed, resulting in FSCs manifested in the vicinity of the supply frequency (50 Hz) and its harmonics, making their detection more challenging. To address this challenge, the detection of rotor electrical asymmetry in WT doubly-fed induction generators (DFIGs), indicative of common winding, brush gear or high resistance connection faults, has been investigated in this chapter using a test rig operated under three different driving conditions, and then an EKF-based method is proposed to iteratively estimate the FSCs and track their magnitude. The FSCs performance has been compared with that of the commonly applied standard CWT and IDFT. The experimental results demonstrate that the CWT and IDFT algorithms fail to track the FSCs at low load operation near synchronous speed. In contrast, the EKF was more successful in tracking the FSC magnitude in all

operating conditions, unambiguously determining the severity of the faults over time and providing significant gains in both computation efficiency and accuracy of fault diagnosis.

The proposed tracker based EKF in this chapter proved capable of dealing with the non-stationary and non-linear characteristics of the WT generator current signals. However, the characteristic of faults in the current signal need to be identified in advance in order to use the EKF to track the fault signatures. This is likely to be a challenge when applying the EKF to the monitoring of operational WT generators where large volumes of high frequency data of a wider range of WT faults are being recorded. In this situation, the fault frequencies cannot easily be tracked via the EKF unless the fault signatures are identified to the tracker. The major restriction on the application of the EKF in the field to be used for detection of a wider range of WT faults such as generator bearing, gearbox-bearing and rotor eccentricity faults is the certainty of obtaining useful data. If the CM system is installed on a single turbine it is likely to record large amounts of data during which no faults are present. In fact, there is a significant risk that no faults will occur and the CM system will simply be overrun with data. Addressing this problem will mean a time-frequency analysis technique is required to identify the fault frequencies in the current signal. To this end, the next chapter will present an improved technique for fault feature extraction and fault diagnosis which at the same time can deal with the non-stationary nature of WT CM signals.

Chapter 6

Improved Continuous Wavelet Transform

6.1 Introduction

In the previous chapter, an effective technique for WT CM was proposed to facilitate the extraction of fault-related features from the non-stationary current signals due to the constantly varying shaft rotating speeds and varying loads of the turbines. This technique is capable of detecting a rotor electrical unbalance fault occurring in a WT. However, the proposed technique cannot be applied directly to detect a wider range of WT faults unless fault-related features are identified in advance. It therefore follows that an effective CM technique needs to be developed to define the fault features first then one can apply the EKF to track these features, which will be the objective of this chapter. This chapter proposes a novel frequency tracking technique to analyse the non-stationary current signals by improving the capability of the continuous wavelet transform (CWT). The novel contribution of this work relates to the use of an adaptable shape for the mother wavelet rather than the fixed shape in the conventional CWT to track only the fault signature frequencies from the non-stationary characteristics of the WT current signal, while other frequencies

unrelated to the fault will be left unprocessed. The shape and oscillatory nature of the proposed mother wavelet is adapted according to the oscillatory behaviour of the fault features in the WT current signal. Simulations and experiments have been performed to verify the proposed method for detecting early faults in a WT generator. The improved CWT is then applied for developing a new real-time CM technique dedicated to detect early anomalies in an operational WT generator current signal. The results show that the improved CWT has overcome conventional CWT limitations, is capable of identifying frequency components of interest and is able to cope with the non-linear and non-stationary fault features in the current signal.

6.2 The Use of Wavelet Transforms for WT CM

The use of wavelet transforms in the analysis of current signals has been successfully established for detecting induction motor faults [129, 94, 130, 124]. These studies have employed the discrete (dyadic) wavelet transform (DWT) to decompose the current signal and extract the fault features in the signal. The DWT is unable to cope with non-stationary WT generator current signals. More recently, the CWT based on the Morlet wavelet has been proposed for WT generator condition monitoring [131, 5]. However, the transform used in this work was mainly used to track only a given variable frequency component (e.g. the twice slip frequency divided by pole pairs ($2ksf_1/p$)) in time and determine its magnitude. The transform was not used to represent the time and frequency content of the monitored CM signal. In addition, it has been reported in [31, 98, 20] that high time resolution and high frequency resolution cannot be achieved simultaneously using the CWT and so cannot provide accurate interpretation of non-stationary WTG signals. In light of this previous work, satisfactory results have not been achieved today using the CWT. Moreover, the computational resource or the computational time required to

produce a suitable result for a signal over a long period of time with wide frequency or scale ranges has not been clearly addressed. It seems that for these reasons the commercial application of the CWT for WT generator monitoring has been held back. This chapter aims to improve the use of the CWT for WT generator condition monitoring. The theory behind conventional wavelet analysis and its improvement will be presented in the next sections.

6.3 Conventional CWT

The fundamental principle behind the application of wavelet and its theory have been discussed in Chapter 4. However, it is worth discussing here the limitation of the conventional CWT and how to address these limitations. The CWT can be represented as:

$$\mathbf{H}_{a,\tau}(\boldsymbol{\omega}) = \frac{\sqrt{a}}{2\pi} \int_{-\infty}^{+\infty} \mathbf{\Psi}^*(s\omega)\mathbf{X}(\omega)\mathbf{e}^{-j\omega\tau}\mathbf{d}\omega \tag{6.1}$$

Equation (6.1) shows in the frequency domain the wavelet is scaled by $1/a$ and multiplied by a phase factor $\mathbf{e}^{-j\omega\tau}$. It is also clear that the amplitude of the scaled wavelet is proportional to $\mathbf{a}^{-1/2}$ in the time domain, whereas it is proportional to $\mathbf{a}^{1/2}$ in the frequency domain. This is a useful characteristic of the CWT where the low frequency (worse time resolution) components are firstly extracted using a larger scale parameter. The scale parameter is subsequently reduced in order to extract out higher frequency components and better time resolution localizations. However, the current signal from an operational variable wind turbine generator has non-stationary characteristics and shows strong oscillations particularly in the peak values as shown in Fig. 6.1. That is the main reason why the conventional CWT failed to analyse the current signals and achieve satisfactory results. Thus, the mother wavelet needs to be modified in such a way that it can continuously change

its shape and the number of oscillations within its envelope to make the detection of the FSCs related to the fault easier to detect with better resolution. The next section will introduce a new transform which is parametrized by its **Q**-factor to control the number of oscillations of the mother wavelet during analysis.

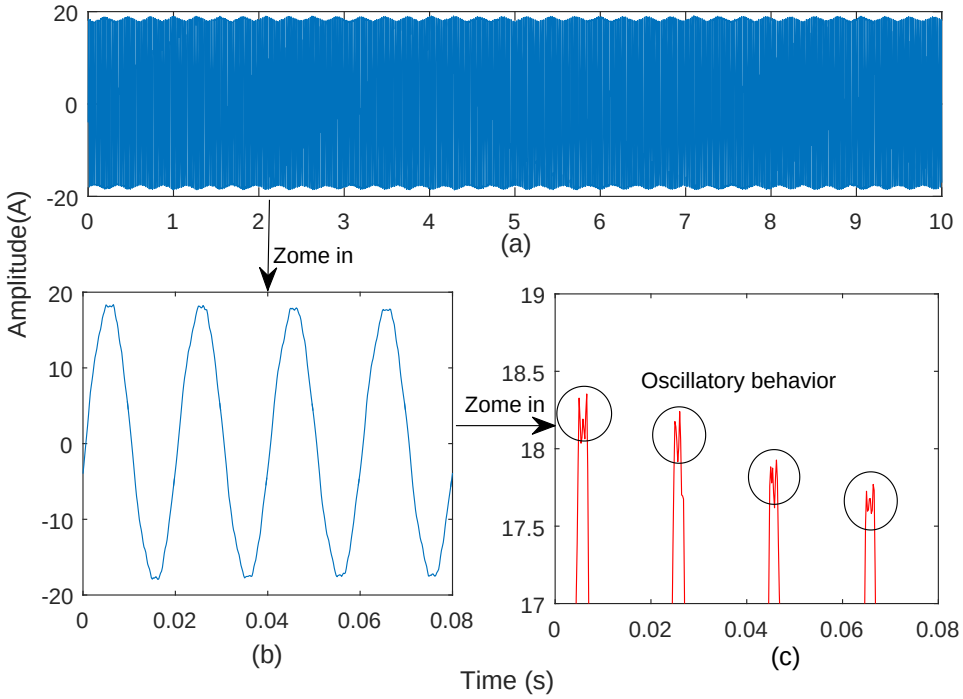

Figure 6.1 The generator current signal (a) during 10sec, (b) zoomed between 0 and 0.08sec and (c) zoomed for the positive peaks.

6.4 Modified CWT-Based Frequency Tracking

The proposed wavelet transform uses a modified mother wavelet to track only the fault signature frequencies from the non-stationary characteristics of the WT current signal, while other frequencies unrelated to the fault will be left unprocessed. By doing this, we can significantly reduce the computational time, and we can reveal the time information of any frequency changes, making the proposed technique suitable for on-line application. The central idea for this modified CWT based frequency tracking is to use an adaptable shape for the mother wavelet rather than the fixed

shape as used in the conventional CWT. The shape with the number of oscillations of the proposed mother wavelet is continuously adapted by a **Q** factor according to the oscillatory behaviour of the fault features in the WT CM signals. The **Q**-factor represents the ratio of the centre-frequency to the frequency bandwidth ($\boldsymbol{\Delta}\omega_\psi$) of the mother wavelet function, which is defined as follows:

$$\mathbf{Q} = \frac{\boldsymbol{\omega}_o}{\boldsymbol{\Delta}\omega_\psi} \tag{6.2}$$

where $\boldsymbol{\omega}_o$ denotes the centre-frequency and $\boldsymbol{\Delta}\omega_\psi$ denotes the frequency bandwidth of the mother wavelet function. The frequency components in the current signal range from 0 Hz to half of the sampling frequency so it is difficult to tune the **Q**-factor to ensure the oscillatory behaviour of the mother wavelet is matched with the oscillation of the current signal. Hence, a mother wavelet whose oscillatory behaviour is continuously tuned with the desired **Q**-factor is designed to capture the oscillation of the current signal. The bandwidth of the proposed mother wavelet is determined by the minimum and maximum cutoff frequencies $\boldsymbol{\omega}_{min}$ and $\boldsymbol{\omega}_{max}$. Using this approximation, the bandwidth is given by

$$\boldsymbol{\Delta}\omega_\psi = \frac{1}{2}(\boldsymbol{\omega}_{max} - \boldsymbol{\omega}_{min}). \tag{6.3}$$

The center frequency of the mother wavelet is the average of $\boldsymbol{\omega}_{min}$ and $\boldsymbol{\omega}_{max}$,

$$\boldsymbol{\omega}_0 = \frac{1}{2}(\boldsymbol{\omega}_{max} + \boldsymbol{\omega}_{min}). \tag{6.4}$$

By substituting (6.3) and (6.4) into (6.2) we can express the **Q**-factor in terms of $\boldsymbol{\omega}_{min}$ and $\boldsymbol{\omega}_{max}$

$$\mathbf{Q} = \frac{\boldsymbol{\omega}_{max} + \boldsymbol{\omega}_{min}}{\boldsymbol{\omega}_{max} - \boldsymbol{\omega}_{min}} \tag{6.5}$$

Hence, the frequency components irrelevant to the fault are left unprocessed, resulting in reducing the calculation time for the new technique compared to the conventional CWT applied to the entire region.

6.4.1 Modifying the mother wavelet

A mother wavelet with a fixed time window was proposed in [131] to extract the energy in the power signal and reduce calculation time. The width of the window in the frequency domain was adapted to the fluctuation of the generator rotational speed. However, this approach is not effective for the online monitoring of the WT health condition as the current signals in modern WTs are usually nonlinear and non-stationary in nature because of the constantly varying generator speeds and nonlinear loads. Moreover, the resolution in [131] depends on the accurate measurement of the generator rotational speed. To address these limitations, an adaptable shape for the mother wavelet rather than the fixed shape is designed in this work to better match the oscillation of the current signal. In this way, there is no need to measure the generator rotational speed because the shape and the number of oscillations of the mother wavelet in the time domain is continuously adapted by the $\mathbf{Q}$ factor according to the oscillatory behaviour of the fault features.

The mother wavelet used, in this work, is based on the Gabor wavelet described as a modulated Gaussian function by a complex exponential [179]:

$$\boldsymbol{\psi}(t) = \mathbf{e}^{\frac{-t^2}{2\boldsymbol{\sigma}^2}} \mathbf{e}^{i\omega_o t} \tag{6.6}$$

where the parameter $\boldsymbol{\sigma}$ is controlling the size of the envelope of the wavelet. It is evident from Eq. (6.6) that the Gabor wavelet function is basically the Morlet wavelet function with $\boldsymbol{\sigma} > 1$. The goal now is to express the parameter $\boldsymbol{\sigma}$ in terms of the **Q** factor:

$$\boldsymbol{\sigma} = 2Q/k\sqrt{2\ln 2} \tag{6.7}$$

By substituting (6.7) and (6.6), we can express the mother wavelet in terms of the **Q** factor:

$$\boldsymbol{\psi}(t) = \mathbf{e}^{\frac{-t^2k^2}{16Q^2\ln 2}}\mathbf{e}^{i\omega_o t} \tag{6.8}$$

Note, from equation (6.8) the **Q**-factor affects the oscillatory behaviour of the mother wavelet, where higher values of **Q** result in more oscillations in the mother wavelet. As a result, the number of oscillations of the mother wavelet in the time domain is continuously adapted by the **Q** factor according to the oscillatory behaviour of the fault features. It is, therefore, better suited to capture the fault signature frequencies over time.

6.4.2 Selecting a

The foregoing discussion shows the local resolution of the CWT in the time and in frequency domain also depends on the scaling parameter **a** so that we define **a** in terms of any frequency between the specified frequencies $\boldsymbol{\omega}_{min}$ and $\boldsymbol{\omega}_{max}$:

$$\mathbf{a} = \frac{\boldsymbol{\omega}_o}{\boldsymbol{\omega}} \tag{6.9}$$

Hence, the range of the wavelet scales during the analysis can be expressed as:

$$\mathbf{a}_{min} = \frac{\boldsymbol{\omega}_o}{\boldsymbol{\omega}_{min}}, \qquad \mathbf{a}_{max} = \frac{\boldsymbol{\omega}_o}{\boldsymbol{\omega}_{max}}. \tag{6.10}$$

The scaling parameter $\mathbf{a}$ satisfies $\mathbf{a} \in [\mathbf{a}_{min}\ \mathbf{a}_{max}]$, leading to only the frequency information of interest being analysed rather than analysing wide frequency bands. In this way, the frequency components irrelevant to the fault are left unprocessed, resulting in reduced calculation time compared to the conventional CWT applied to a broad bandwidth signal. Hence, the proposed CWT-based frequency tracking method should be more efficient for online fault feature extraction from WT generator signals than conventional CWT.

6.5 Application of The Modified CWT to WT CM

To demonstrate the potential of the modified CWT in WT CM, the modified CWT has been applied to the stator current signals produced in a simulation, collected from a WT drive train test rig and from an operational WT.

6.5.1 WT Simulation Model

To demonstrate the effectiveness of the proposed method for WT condition monitoring and fault diagnosis, the modified CWT was applied to a simulated generator current signal obtained from the same model described in chapter 3 in order to reveal the FSCs related to an inherent eccentricity under variable speed conditions.

Based on the results shown in Fig. 6.2, it is shown that the modified CWT can successfully provide explicit time frequency information of the FSCs related to the inherent eccentricity even when the machine operates at actual variable

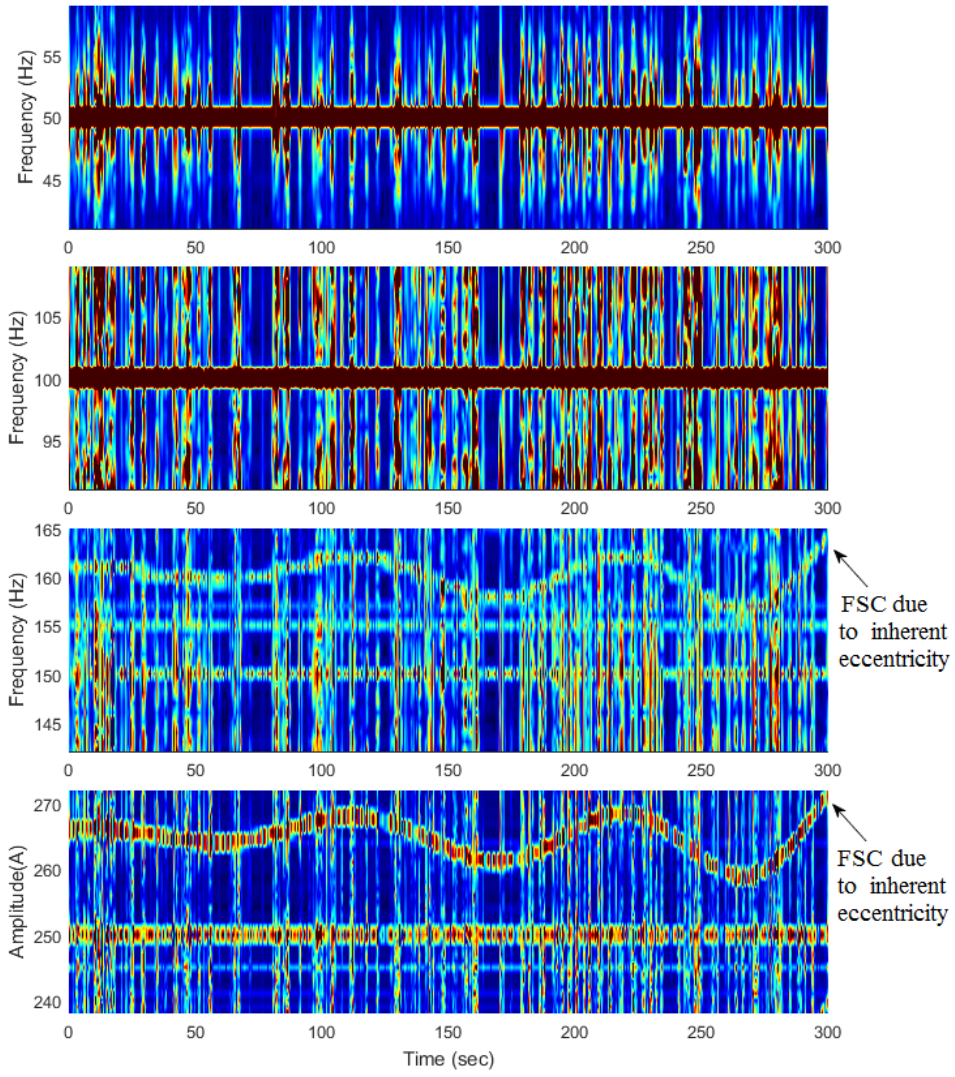

Figure 6.2 Modified CWT results when tracking the current signal with an inherent eccentricity simulated at variable rotational speed.

speed conditions. Following the successful detection of the inherent eccentricity, the modified CWT was applied to the current signal to identify the FSCs related to the rotor electrical unbalance under actual variable speed conditions, and the result is shown in Fig. 6.3.

In Fig. 6.3, both the inherent eccentricity and the rotor electrical unbalance faults have been successfully detected by the modified CWT despite the significantly varying generator speed. Moreover, the modified CWT is capable of capturing the FSCs related to the fault which are combined and hidden in other dominant

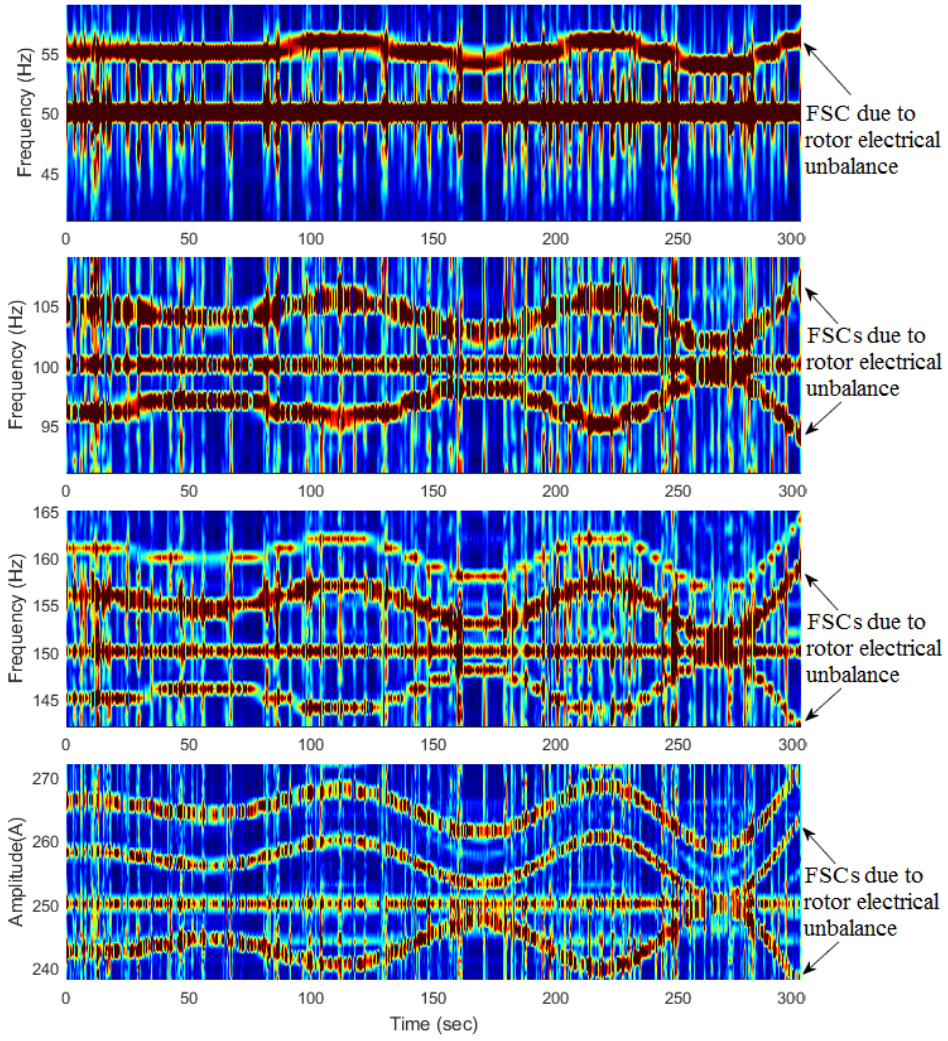

Figure 6.3 Modified CWT result for the current signal when the rotor electrical unbalance was simulated at variable rotational speed.

frequency components of the current signal that are irrelevant to the fault due to the constantly varying shaft rotating speeds and varying loads on the generator. Thus, it can be concluded that the modified CWT is effective in dealing with the non-stationary characteristics of the current signal under more than one fault condition.

6.5.2 Test Rig

The experimental data obtained from the purpose-built WT drive train test rig are used in this section to show the improvement offered by the proposed modified CWT. As has been briefly mentioned in Chapter 4, a generator rotor winding fault was implemented on the test rig by changing the phase resistances in the load bank externally connected to the rotor. To observe the effect of the fault, two levels of rotor asymmetry were applied to investigate the effect of an incipient fault. The first fault level corresponds to 23% rotor unbalance from 150 s to 300 s, then the fault level was increased to 46% from 300 s to 450 s. The test rig enables the generator to be driven at a desired pre-programmed wind speed profile that emulates realistic WT transient behaviour and is achieved by providing a pre-defined speed reference profile to the controller. Data were sampled at 5 kHz.

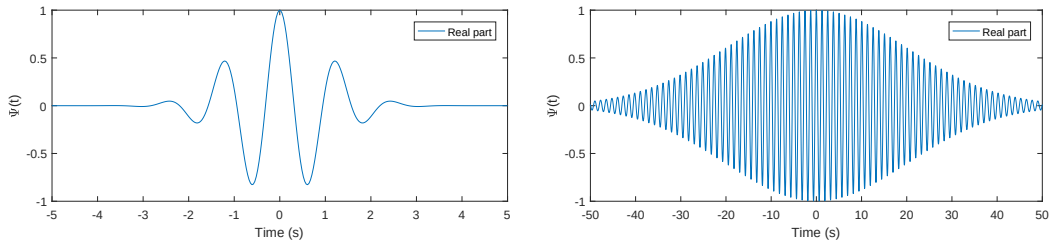

(a) (b)

Figure 6.4 Mother wavelets with different values of the parameter $\boldsymbol{\sigma}$ (a) $\boldsymbol{\sigma}$ =1 and (b) $\boldsymbol{\sigma} > 1$.

In order to show the effectiveness of the modified CWT, a mother wavelet with different values of the parameter $\boldsymbol{\sigma}$ that controls the size of the envelope of the wavelet, as shown in Fig.6.4, has been designed to analyse the time series of the stator current signal. The stator current signal was measured during the experiments at three conditions normal, 23% and 46% unbalance, to allow a relative comparison between frequency components in the current signal under these three operating conditions. The rotor electrical asymmetry condition in the DFIG is manifested through a range of additional sideband components at the twice slip frequency $2sf$. Herein, s refers to induction machine slip and f indicates the electrical supply

frequency. Fig.6.5 compares the results when the data are analysed using the conventional wavelet and the modified wavelet for the test rig run at a low mean wind speed (7.5m/s) with low turbulence intensity (6%). The CWTs have been applied to the stator current signal to capture the fault-induced characteristics around the supply frequency (50 Hz) at $(1 + 2s)f$.

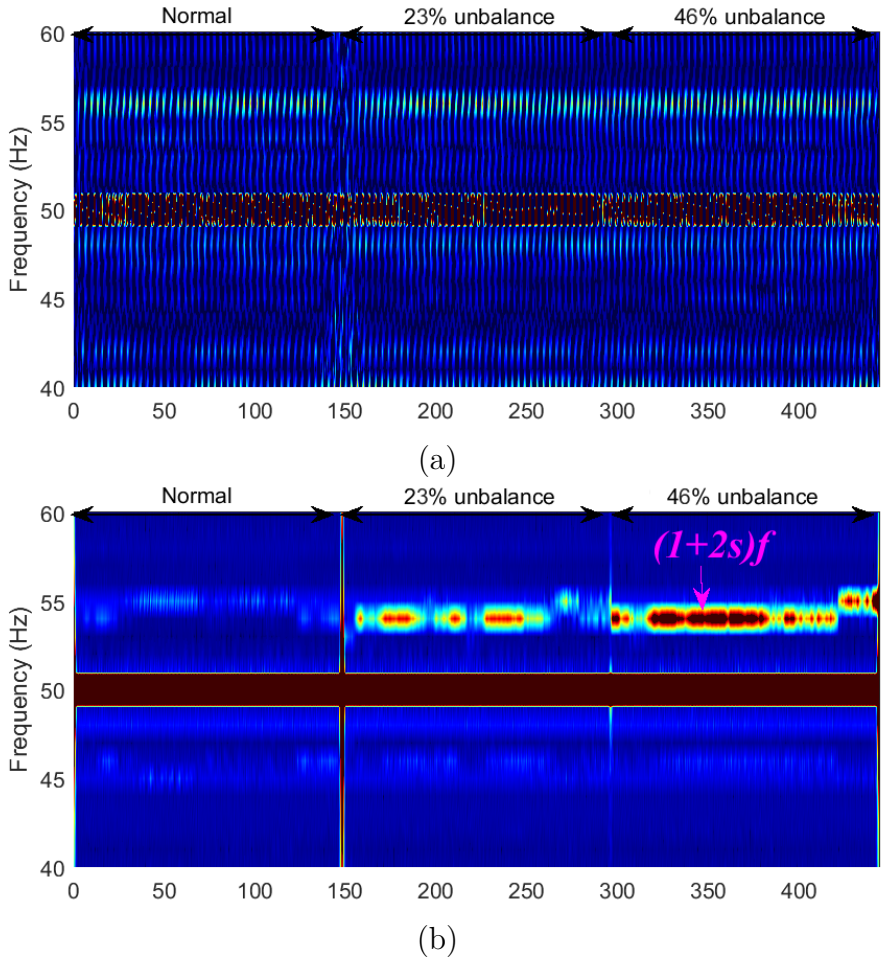

Figure 6.5 Time frequency representation of the current signal using the (a) conventional CWT and (b)modified CWT with the test rig driven by 7.5m/s, 6% turbulence conditions.

In Fig.6.5(a) the conventional CWT has difficulty extracting explicit time-frequency features of the current signal. One explanation for the poor performance of the conventional CWT method can be the fixed shape for the mother wavelet which can not deal with the non-stationary characteristics and strong oscillations in the current signal. By contrast, the modified CWT overcomes this problem and is better

able to characterize the time-frequency content of the non-stationary signal. The information available from the modified CWT shows that the supply frequency is present throughout the entire length of the signal with strong evidence of additional sideband component at $(1 + 2s)f$ and the time-frequency representation obtained is well concentrated.

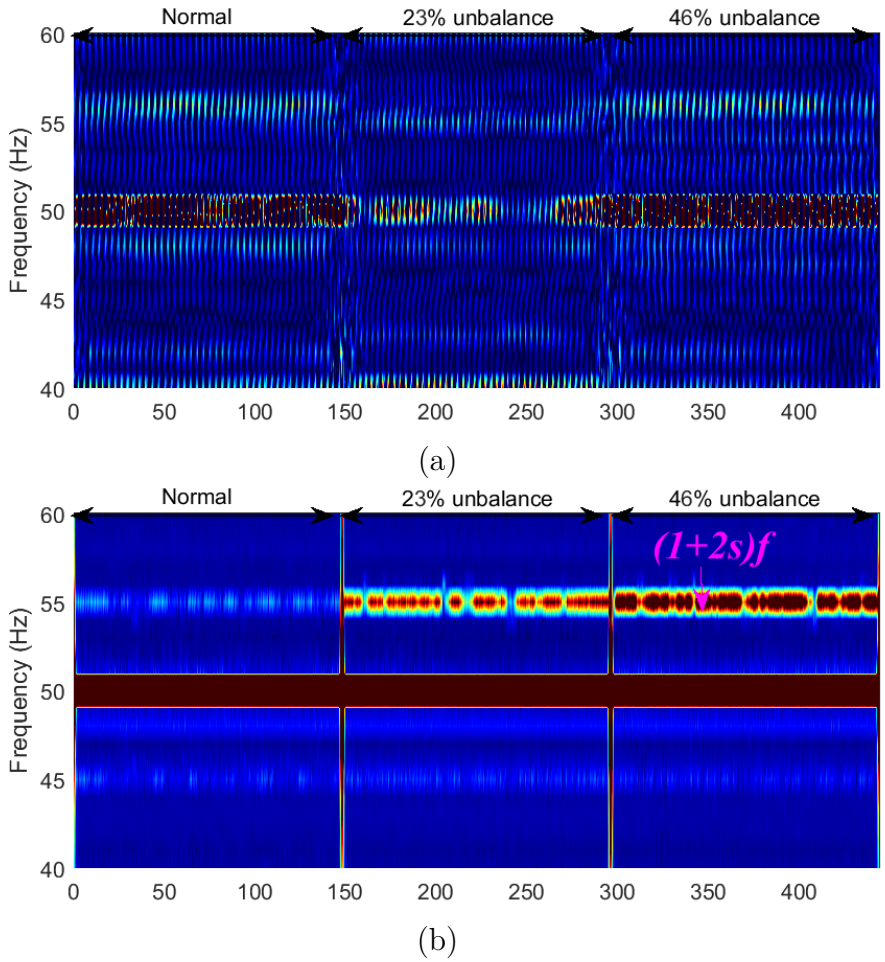

Figure 6.6 Time frequency representation of the current signal using the (a) conventional CWT and (b)modified CWT with the test rig driven by 15m/s, 20% turbulence conditions.

Fig.6.6 shows a similar comparison between the conventional and modified CWT for the case where the test rig is run at a high mean wind speed (15m/s) with high turbulence intensity (20%). The time-frequency representation obtained by the conventional CWT is still not well concentrated. On the other hand, the modified CWT shows much better resolution of the frequency component related to the fault.

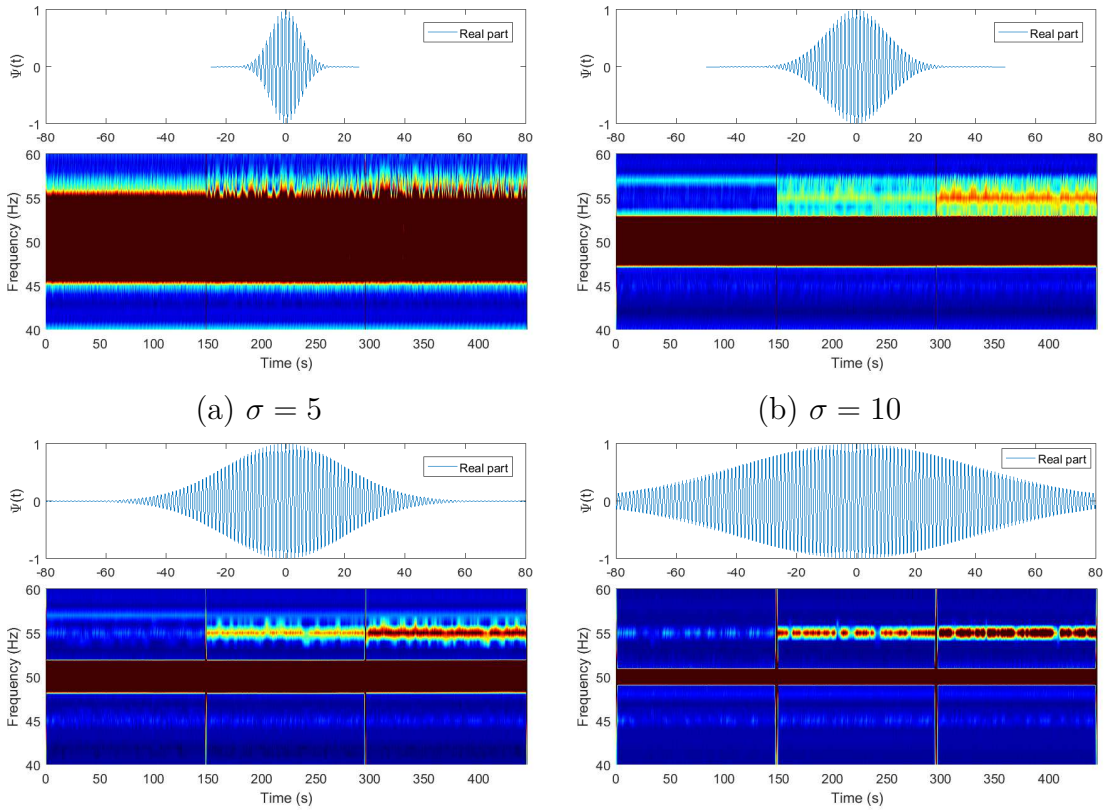

(a) $\sigma = 5$ (b) $\sigma = 10$

(c) $\sigma = 20$ (d) $\sigma = 40$

Figure 6.7 modified CWT results for the current signal using various Gabor wavelets

To provide a sensitivity analysis of the impact of the mother wavelet shape on the results of the CWT, various mother wavelets with different values of the parameter $\boldsymbol{\sigma}$ that control the size of the envelope of the wavelet, as shown in Fig.6.7, have been designed to analyse the time series of the stator current signal. It can be seen that higher values of $\boldsymbol{\sigma}$ result in more oscillations in the mother wavelet, and provide more explicit time-frequency features of the current signal. By extracting the magnitude of the fault-induced frequency, we can clearly see using mother wavelets with $\boldsymbol{\sigma} >= 10$ that there is a step change in magnitude when the fault condition was present or was changed as shown in Fig.6.8. However, the magnitude follows different variation tendencies due to the fact that the current signals from an operational WT are not stationary but are time-varying in nature because of the constantly varying generator speed, making the detection of the frequency component related to the fault more challenging. In order to demonstrate the best achieved mother wavelet

design for detecting the fault signatures with better resolution, the performance of mother wavelets with different values of the parameter $\boldsymbol{\sigma}$ during the fault event is evaluated using root mean squared error (RMSE) values. The increase in the degree of rotor unbalance can be evaluated from the instantaneous amplitude variations from the tracking results by calculating the difference between the instantaneous amplitude of the fault-induced frequency under healthy and faulty conditions divided by the instantaneous amplitude under healthy conditions.

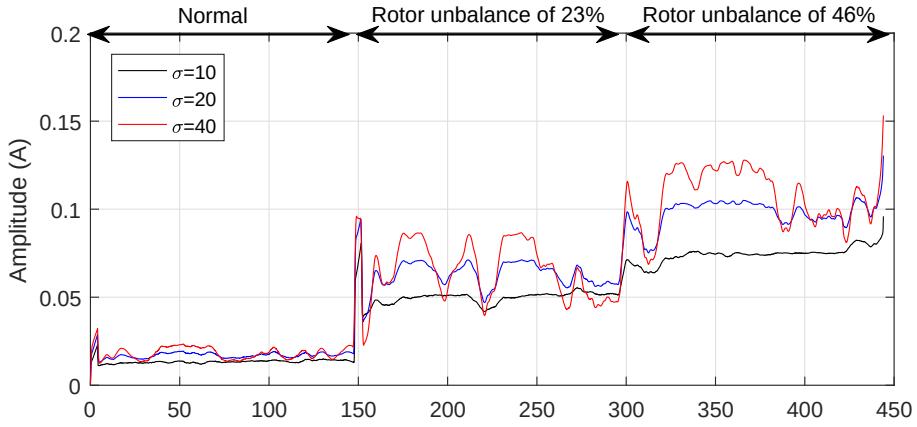

(a) 7.5m/s, 6% turbulence conditions

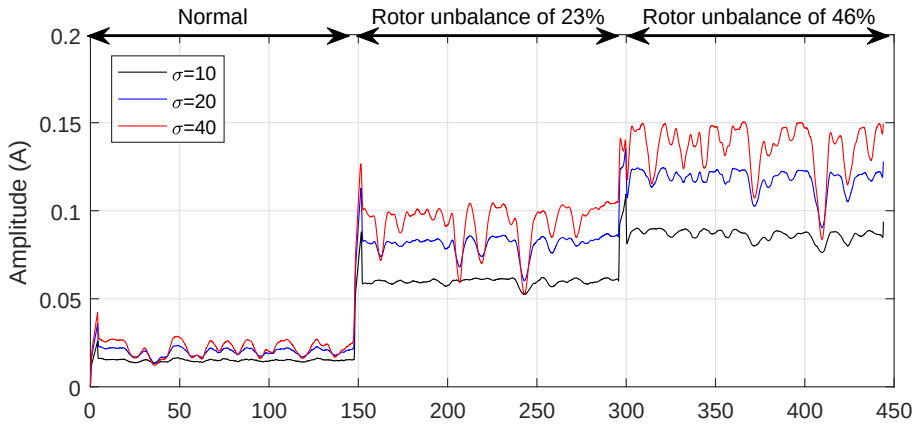

(b) 15m/s, 20% turbulence conditions

Figure 6.8 Tracking the magnitude of fault signature frequencies of interest for the detection of rotor unbalance.

Table6.1 summarizes the results of the performance evaluation. It can be seen that higher values of $\boldsymbol{\sigma}$ result in lower RMSE value which means better fault detection. This is due to the fact that the current signal has non-stationary characteristics and strong oscillations due to the variable speed operation but changing the shape

Table 6.1 RMSE of the modified CWT using various Gabor wavelets

Speed test condition	RMSE Values (%)			
	$\sigma = 10$	$\sigma = 20$	$\sigma = 30$	$\sigma = 40$
7.5m/s	1.857	0.922	0.727	0.921
15m/s	2.038	1.053	0.846	1.052

and the number of oscillations of the mother wavelet within its envelope has led to improved detection of the fault signatures with better resolution. However, the results show that the optimal value of $\boldsymbol{\sigma}$ is 30; higher values of $\boldsymbol{\sigma}$ lead to an increase in the percentage RMSE. This is because there is a trade off in the choice of window size where a longer time window improves frequency resolution while resulting in poorer time resolution because the Fourier transform loses all time resolution over the duration of the window. Whereas, a shorter time window improves time localization while resulting in poorer frequency resolution.

Table 6.2 Computational efficiency comparison between the modified and conventional CWTs

Speed test	Standard CWT	Modified CWT			
		$\sigma = 10$	$\sigma = 20$	$\sigma = 30$	$\sigma = 40$
7.5m/s	3.13 s	0.76 s	0.78 s	0.81 s	0.84 s
15m/s	3.15 s	0.77 s	0.79 s	0.83 s	0.89 s

A computational time analysis was performed on a computer with an Intel i7 core processor and 32.0GB RAM to demonstrate the excellent computational efficiency of the modified CWT in comparison with the conventional CWT. Table6.2 shows the time taken by the modified CWT to analyse 10 minutes of data from the current signal is less than half of that taken by the conventional CWT. Hence, it can be concluded that the modified CWT is much more computationally efficient than the conventional CWT and therefore more suitable for real operating WTs.

6.5.3 Operational Wind Turbine

To further highlight the effectiveness of the proposed technique for WT CM, the modified CWT is applied to an operational commercial WT current signal. A Vestas V42 600-kW wind turbine with an asynchronous generator was instrumented to provide high frequency WT CM data sampled at 10.24 kHz for a number of operational parameters including wind speed, vibration and three-phase voltage and current. The data were recorded from June 2015 to April 2016. Since the sampling frequency for the data is quite high, this potentially presents a significant challenge for data storage and analysis on common personal computers.

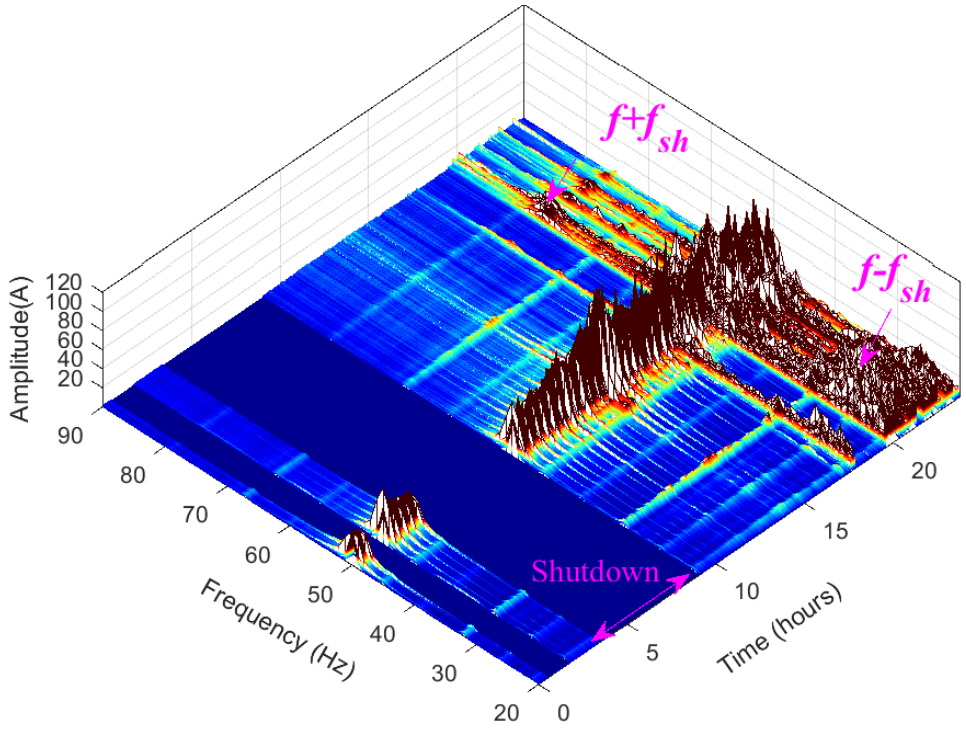

Figure 6.9 modified CWT result for the stator current after an emergency stop on 4^{th} April 2016.

Although no fault occurred or component replaced during the period of recording of the data, the modified CWT detected an abnormal feature from the stator current after an emergency stop on 4th April 2016 as shown in Fig.6.9. The results suggest that after the WT was shutdown, two spectral components at $f - f_{sh}$ and $f + f_{sh}$ appeared in the spectrogram. These component frequencies correspond to $f_{sh} =$

25.56 Hz and $f = 50$ Hz. Both these components that occurred on the 4^{th} of April were still present on the following day as shown in Fig.6.10 until the WT went into another shutdown. It is also clear that the variation tendencies of the IAs at $f - f_{sh}$ and $f + f_{sh}$ appeared in the spectrogram have been correctly extracted despite the time-varying features due to the variable speed operation. Hence, determining the magnitude of these component frequencies generated by WT faults from stator current signals can be used as an effective way to detect early abnormalities.

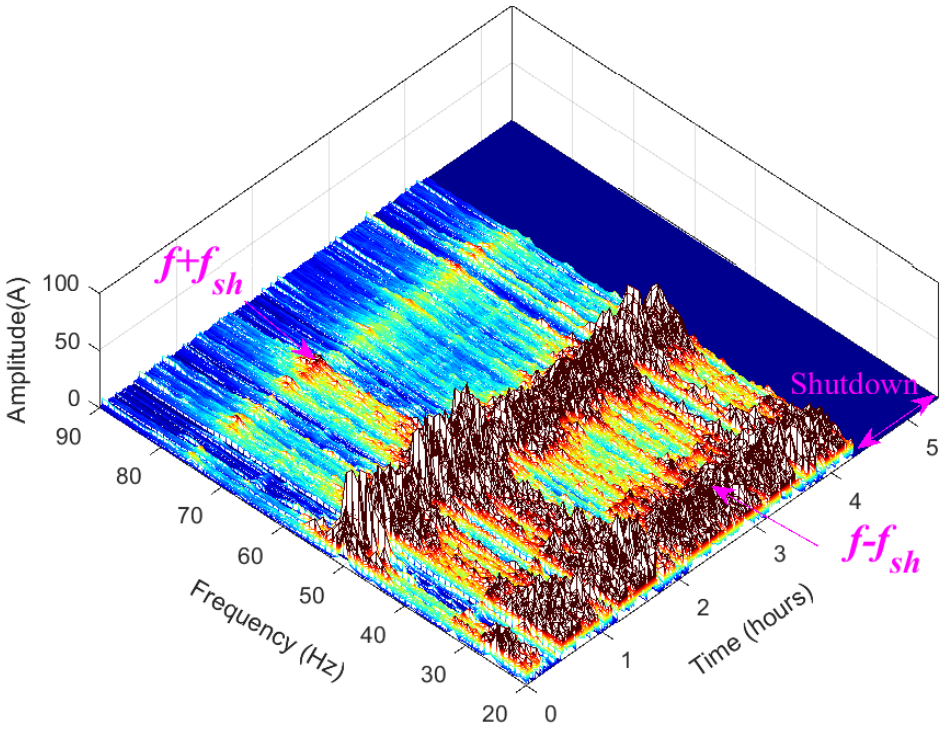

Figure 6.10 modified CWT result for the stator current before an emergency stop on 5^{th} April 2016.

As the modified CWT algorithm has successfully revealed the time information of two spectral components at $f - f_{sh}$ and $f + f_{sh}$ that can be used for fault occurrence and progression monitoring. As an evidence, the modified CWT results show that the magnitude of both components did show a marked change as shown in Fig.6.11 when the fault condition occurred. Thus, the modified CWT can be proposed to detect faults by monitoring the magnitudes of these additional components over time, by taking into account variable operating conditions. It has commonly been assumed

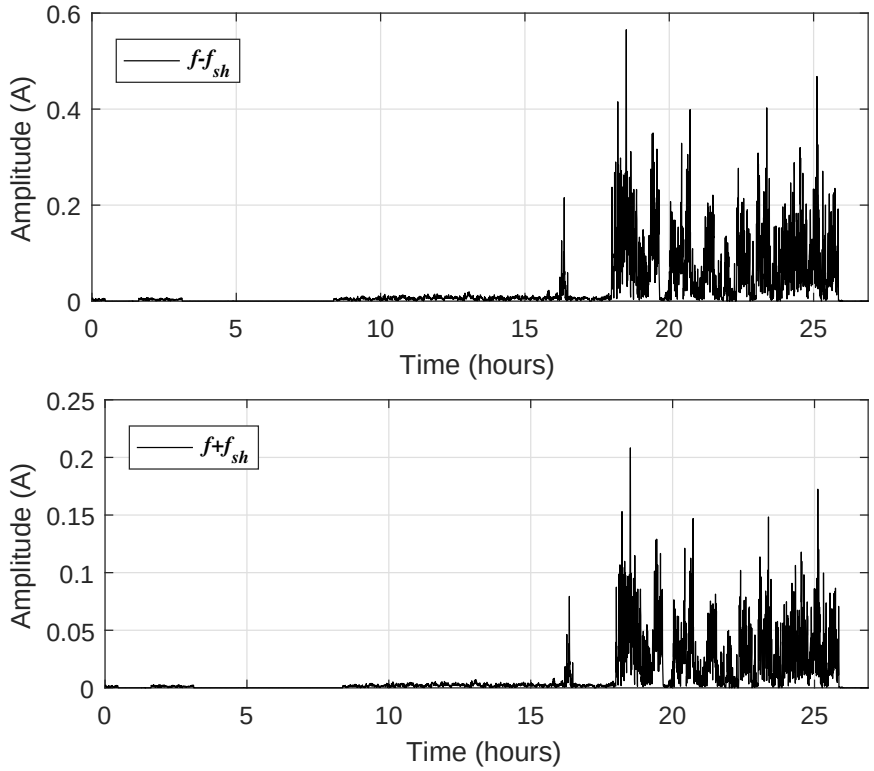

Figure 6.11 The amplitude of spectral components at $f \pm f_{sh}$ for the period between 4^{th} and 5^{th} April 2016.

that these additional components manifest themselves due to eccentricity-related faults [93, 132] that exist between the stator and rotor. The eccentricity creates a disturbance in the air-gap flux density. The action of eccentricity-related faults is such that it will induce new air-gap flux density frequency components, and their magnitude is directly proportional to the magnitude of a fault condition [92]. The resulting unbalanced radial forces can cause stator to rotor rub, and this can result in damage of the stator and rotor [132].

6.6 Summary

This chapter featured the development of an improved WT CM technique, based on modifying the CWT. The technique was shown capable of providing explicit time- frequency features from the current signal. The adaptable shape for the mother wavelet used in this method instead of the fixed shape in the conventional

CWT enables the improved CWT to track only the fault signature frequencies from the non- stationary characteristics of the WT current signal, and avoid problems associated with the conventional CWT. The proposed technique was evaluated using simulated,experimental and real data. For the simulated data, the improved CWT showed success in detecting a wider range of WT faults e.g. static eccentricity and rotor electrical unbalance faults occurring in a WT, despite the constantly varying shaft rotating speeds and varying loads. Secondly, the performance of the proposed technique is compared to the conventional CWT for interpreting non-stationary WT CM signals. The proposed method showed better performance in terms of accuracy and computation complexity. Due to the efficient computational algorithm of the modified CWT, accurate analysis of lengthy WT CM signals does not require more costly WT CM computational requirements. The effectiveness of the modified CWT was further demonstrated on real field measurements collected from a commercial WT (Vestas V42 600-kW machine) to detect early abnormalities. Results showed that it detected a problem from the stator current after an emergency stop on 4th April 2016 approximately 19 hours before the WT went to another shutdown on the following day.

Chapter 7

Conclusion and Future Work

7.1 Conclusions

The main goal of this thesis was to develop new and improved techniques for WT generator CM and fault detection using advanced signal processing methods, that can overcome existing CM limitations due to the constantly varying shaft rotating speeds caused by turbine variable loads. The proposed techniques use the measurement of stator current, already available for control purposes which means no additional sensors or data acquisition devices are needed, so that the detection is more beneficial, comprehensive, simpler, and cheaper than other techniques. The successful development and application of the proposed techniques and performance metrics in this thesis through simulations, experiments and real field measurements prove that the proposed techniques are viable and effective approaches for on-line WT CM. The proposed techniques provide accurate interpretation of the WT generator electrical output with sufficient sensitivity and reasonable computational efficiency to extract the instantaneous amplitude of fault signature components from the WT current signals. A critique of the key contributions of this thesis is given as follows.

Simulation studies have been carried in the MATLAB/Simulink environment to describe how fault signatures may occur in current signals, and potentially how they

may deviate from a healthy state under variable speed conditions. The performance of the model was validated by experimental measurements made on a physical test rig under healthy and faulty conditions. The WT model was then run at actual variable speed conditions collected from an operational WT to produce signals of similar noise, variability and information content as those encountered on operational turbines. The results of this investigation showed that the fault signatures in the WT current signals are non-stationary with low signal to noise ratio due to the constantly varying shaft rotating speeds and varying loads.

Two commonly encountered signal processing techniques: the short-time Fourier transform and the wavelet transform are discussed and conclusions drawn about their applicability and suitability for analysis of non-stationary signals. Having examined these techniques, it is shown that the time-frequency representations obtained by STFTs and CWTs appear to be unsuitable for WT CM. However, the CWT was more successful in producing better information in the time domain at different frequency bands from the data analysed. The concept of a frequency tracking algorithm was introduced and the previously published IDFT method was used as an example. This method proved successful on a simulation case study for a WT running under variable speed conditions. The IDFT has good computing efficiency by applying a discrete Fourier analysis over a narrow band around the frequency of interest to extract peak amplitudes which are assumed to be the amplitudes of the fault frequency of interest within the predefined window. However, the problem with this assumption is that the fault frequencies do not always have maximum amplitude especially when the fault frequencies are corrupted by other components irrelevant to the fault or hidden in other components like the supply frequency and its harmonics due to the variable operating conditions, making the use of the IDFT impractical for continuous application on large WT populations. Another technique to detect faults in variable speed WTs based on ANNs has been also introduced. A framework is discussed for training of fault detection with simulated signals from

faults for later online detection in real WTs. For each set of limited rotational speed variation a separate ANN will detect the fault. In a simulation study of a rotor imbalance under varying rotational speed as expected in 5 minutes operation the feasibility of the fault detection approach is demonstrated. Simple classification of healthy or faulty condition is achieved with a high accuracy. In a further step towards fault prognosis, the severity of the fault is successfully detected.

Despite the improvement in computational efficiency offered by the IDFT method, the FSC can be difficult to isolate accurately due to the fact that the WT frequently operates with the generator close to synchronous speed, resulting in FSCs manifesting themselves in the vicinity of the supply frequency and its harmonics, making their detection more challenging using the IDFT. To address this challenge, Chapter 5 has proposed an effective EKF based method that is better capable of dealing with the non-stationary and non-linear characteristics of the WT generator current signals. The proposed approach is used to iteratively track the strength of particular frequency components, characteristic of faults in the current signal. The proposed technique has been validated experimentally on a WT drive train test rig with two fault levels of rotor electrical asymmetries at three different driving conditions whose variability is representative of WT generator field operation. The EKF performance was compared with that of a CWT and an IDFT in terms of its ability to provide significant gains in both computational efficiency and accuracy of fault diagnosis. The EKF demonstrated better overall resolution of fault frequencies particularly where those frequencies are close to the synchronous frequencies and their harmonics; a condition that can occur frequently when a turbine is operating with the generator close to synchronous speed. Due to the parsimonious nature of the EKF and the fact that it does not employ windowing, it is able to accurately detect fault frequencies with minimal computational requirements when compared with a CWT. The EKF was shown to be capable of detecting the degree of rotor unbalance with greater accuracy than an IDFT or CWT. The results presented show that the EKF algorithm

shows promise as a low cost, efficient method for condition monitoring the output of a WT generator particular with regard to the detection of electrical faults such as rotor unbalance.

However, the proposed technique based on an EKF cannot be applied directly to detect a wide range of WT faults until fault-related features are identified in advance. To address this issue, Chapter 6 has proposed a new WT CM technique, based on modifying the CWT. The new technique is capable of providing explicit time-frequency features of the current signal. The adaptable shape for the mother wavelet used in this method instead of the fixed shape in the conventional CWT enables the improved CWT to track only the fault signature frequencies from the non-stationary characteristics of the WT current signal, and avoid issues associated with the conventional CWT. The proposed technique was evaluated using simulated, experimental and real data. For the simulated data, the improved CWT showed success in detecting a wide range of WT faults e.g. static eccentricity and rotor electrical unbalance faults occurring in a WT, despite the constantly varying shaft rotating speeds and varying loads. Secondly, the performance of the proposed technique is compared to the conventional CWT for interpreting non-stationary WT CM signals. The proposed method showed better performance in terms of accuracy and computational complexity. Due to the efficient computational algorithm of the improved CWT, accurate analysis of lengthy WT CM signals does not require more costly WT CM hardware. Finally, the effectiveness of the improved CWT was further demonstrated on real field measurements collected from a commercial WT (Vestas V42 600-kW machine) to detect early abnormalities. An abnormality was detected by the modified CWT in the stator current after an emergency stop on 4th April 2016 approximately 19 hours before the WT went to another shut-down on the following day.

7.2 Future Work

From the work presented in this thesis, the following areas for further work arise:

- The proposed signal processing techniques need to be implemented on real WTs, which may be suffering from rotor electrical asymmetries, and to use the detection of the fault degree to potentially predict the fault progression some time in advance.

- Work is necessary to assess the potential of the reported techniques to be used for detection of a wider range of WT faults like generator bearing, gearbox-bearing and rotor eccentricity faults as it will establish the detectability of the proposed techniques and to make them ready for commercial implementations.

- Combination of the proposed EKF developed in this work with the modified CWT in order to improve the detection performance and to identify and track fault signatures in WTs.

- Work is also necessary to employ the proposed signal processing techniques with intelligent systems for fault classification such as support vector machines, genetic algorithms and fuzzy logic to automate and provide reliable alarms with a high degree of confidence system.

- Work could be done to determine the minimum required sampling frequency to capture fault frequency components in the measured current signal in order to keep the amount of data as low as possible. This will require the analysis of the frequency components in the spectra at various sampling rate for both healthy and faulty conditions if this were done this would substantially reduce memory requirement and computational complexity.

- Further work could be done to include the analysis of the continuously measured voltage and power signals to identify their fault frequency components

manifestation. This may improve the performance of WT CM and fault detection.

- It is highly recommended to move forward towards fault prognosis by using the extracted fault features. Fault prognosis for WTs is important to lead to better remaining useful life prediction which will results in a much optimized maintenance schedule and less unscheduled maintenance events. Further analysis of the extracted fault features may provide the capabilities of new prognostic solutions for addressing the uncertainty challenges in predicting the remaining useful life of abatement systems, subject to uncertain future operating loads and conditions.

References

[1] Global Wind Energy Council, "Global wind report 2017," [Online]: http://files.gwec.net/files/GWR2017.pdf?ref=Website, Brussel, Belgium, 2017.

[2] C. Crabtree, Y. Feng, and P. Tavner, "Detecting incipient wind turbine gearbox failure: a signal analysis method for on-line condition monitoring," in *Proceedings of European Wind Energy Conference (EWEC 2010), Warsaw, Poland*, vol. 2023, 2010, p. 154156.

[3] K. Alewine and W. Chen, "Wind turbine generator failure modes analysis and occurrence," in *Wind Power 2010 Conference, Dallas*, 2010.

[4] P. Tavner, "Review of condition monitoring of rotating electrical machines," *Electric Power Applications, IET*, vol. 2, no. 4, pp. 215–247, 2008.

[5] S. J. Watson, B. J. Xiang, W. Yang, P. J. Tavner, and C. J. Crabtree, "Condition monitoring of the power output of wind turbine generators using wavelets," *Energy Conversion, IEEE Transactions on*, vol. 25, no. 3, pp. 715–721, 2010.

[6] Global Wind Energy Council, "Global Cumulative Installed Capacity 1997-2014," [Online]: http://www.gwec.net/global-figures/graphs/, 2014.

[7] F. Lauha, S. Steve, S. Sgruti, and Q. Limig, "Global wind report annual market update 2013," *Global Wind Energy Council*, 2012.

[8] "Wind energy scenarios for 2020," The European Wind Energy Association. [Online]. Available: http://www.ewea.org/fileadmin/files/library/publications/scenarios/EWEA-Wind-energy-scenarios-2020.pdf

[9] "China wind energy development roadmap 2050," International Energy Agency (IEA), Energy Research Institute (ERI) and National Development and Reform Commission (NDRC) of P. R. China, 2011. [Online]. Available: http://www.ewea.org/fileadmin/files/library/publications/scenarios/EWEA-Wind-energy-scenarios-2020.pdf

[10] E. Artigao, A. Honrubia-Escribano, and E. Gomez, "In-service wind turbine dfig diagnosis using current signature analysis," *IEEE Transactions on Industrial Electronics*, 2019.

[11] C. Q. Gómez Muñoz, F. P. García Marquez, B. Hernandez Crespo, and K. Makaya, "Structural health monitoring for delamination detection and location in wind turbine blades employing guided waves," *Wind Energy*, vol. 22, no. 5, pp. 698–711, 2019.

[12] J. Wang, X. Zhao, and X. Guo, "Optimizing wind turbine's maintenance policies under performance-based contract," *Renewable energy*, vol. 135, pp. 626–634, 2019.

[13] R. Hyers, J. McGowan, K. Sullivan, J. Manwell, and B. Syrett, "Condition monitoring and prognosis of utility scale wind turbines," *Energy Materials*, vol. 1, no. 3, pp. 187–203, 2006.

[14] U. Bhardwaj, A. Teixeira, and C. G. Soares, "Reliability prediction of an offshore wind turbine gearbox," *Renewable Energy*, vol. 141, pp. 693–706, 2019.

[15] P. Tamilselvan, Y. Wang, and P. Wang, "Optimization of wind turbines operation and maintenance using failure prognosis," *2012 IEEE Conference on Prognostics and Health Management*, pp. 1–9, Jun. 2012. [Online]. Available: http://ieeexplore.ieee.org/lpdocs/epic03/wrapper.htm?arnumber=6299538

[16] Z. Daneshi-Far, G. Capolino, and H. Henao, "Review of failures and condition monitoring in wind turbine generators," in *Electrical Machines (ICEM), 2010 XIX International Conference on*. IEEE, 2010, pp. 1–6.

[17] J. Nilsson and L. Bertling, "Maintenance management of wind power systems using condition monitoring systems mdash;life cycle cost analysis for two case studies," *IEEE Transactions on Energy Conversion*, vol. 22, no. 1, pp. 223–229, March 2007.

[18] Z. Hameed, Y. Hong, Y. Cho, S. Ahn, and C. Song, "Condition monitoring and fault detection of wind turbines and related algorithms: A review," *Renewable and Sustainable energy reviews*, vol. 13, no. 1, pp. 1–39, 2009.

[19] M. R. Shahriar, "Electrical signature analysis-based condition monitoring of wind turbine drivetrain," Ph.D. dissertation, Queensland University of Technology, 2017.

[20] W. Qiao and D. Lu, "A survey on wind turbine condition monitoring and fault diagnosis; part ii: Signals and signal processing methods," *IEEE Transactions on Industrial Electronics*, vol. 62, no. 10, pp. 6546–6557, Oct 2015.

[21] C. J. Crabtree, S. Djurović, P. J. Tavner, and A. C. Smith, "Fault frequency tracking during transient operation of wind turbine generators," in *The XIX International Conference on Electrical Machines - ICEM 2010*, Sept 2010, pp. 1–5.

[22] X. Chen, W. Xu, Y. Liu, and M. R. Islam, "Bearing corrosion failure diagnosis of doubly-fed induction generator in wind turbines based on stator current analysis," *IEEE Transactions on Industrial Electronics*, pp. 1–1, 2019.

[23] D. Zappalá, N. Sarma, S. Djurović, C. Crabtree, A. Mohammad, and P. Tavner, "Electrical & mechanical diagnostic indicators of wind turbine induction generator rotor faults," *Renewable energy*, vol. 131, pp. 14–24, 2019.

[24] Y. Gritli, C. Rossi, D. Casadei, F. Filippetti, and G. A. Capolino, "A diagnostic space vector-based index for rotor electrical fault detection in wound-rotor

induction machines under speed transient," *IEEE Transactions on Industrial Electronics*, vol. 64, no. 5, pp. 3892–3902, May 2017.

[25] S. Williamson and S. Djurovic, "Origins of stator current spectra in dfigs with winding faults and excitation asymmetries," in *2009 IEEE International Electric Machines and Drives Conference*, May 2009, pp. 563–570.

[26] E. Artigao, A. Honrubia-Escribano, and E. Gomez-Lazaro, "Current signature analysis to monitor dfig wind turbine generators: A case study," *Renewable Energy*, 2017.

[27] Y. Qiu, Y. Feng, P. Tavner, P. Richardson, G. Erdos, and B. Chen, "Wind turbine scada alarm analysis for improving reliability," *Wind Energy*, vol. 15, no. 8, pp. 951–966, 2012.

[28] S. Djurovic, S. Williamson, and A. Renfrew, "Dynamic model for doubly-fed induction generators with unbalanced excitation, both with and without winding faults," *IET Electric Power Applications*, vol. 3, no. 3, pp. 171–177, 2009.

[29] S. Djurovic, C. J. Crabtree, P. J. Tavner, and A. Smith, "Condition monitoring of wind turbine induction generators with rotor electrical asymmetry," *Renewable Power Generation, IET*, vol. 6, no. 4, pp. 207–216, 2012.

[30] C. Crabtree, S. Djurovic, P. Tavner, and A. Smith, "Condition monitoring of a wind turbine dfig by current or power analysis," in *Power Electronics, Machines and Drives (PEMD 2010), 5th IET International Conference on*, April 2010, pp. 1–6.

[31] W. Yang, C. Little, P. J. Tavner, and R. Court, "Data-driven technique for interpreting wind turbine condition monitoring signals," *IET Renewable Power Generation*, vol. 8, no. 2, pp. 151–159, March 2014.

[32] Y. Amirat, M. Benbouzid, B. Bensaker, and R. Wamkeue, "Condition monitoring and ault diagnosis in wind energy conversion systems: a review," in

Electric Machines & Drives Conference, 2007. IEMDC'07. IEEE International, vol. 2. IEEE, 2007, pp. 1434–1439.

[33] W. Qiao and D. Lu, "A survey on wind turbine condition monitoring and fault diagnosis; part i: Components and subsystems," *IEEE Transactions on Industrial Electronics*, vol. 62, no. 10, pp. 6536–6545, Oct 2015.

[34] P. Tavner, G. Van Bussel, and F. Spinato, "Machine and converter reliabilities in wind turbines," 2006.

[35] H. Li and Z. Chen, "Overview of different wind generator systems and their comparisons," *Renewable Power Generation, IET*, vol. 2, no. 2, pp. 123–138, June 2008.

[36] J. Machowski, J. Bialek, and J. Bumby, *Power system dynamics: stability and control*. John Wiley & Sons, 2011.

[37] Y. Zhou, P. Bauer, J. A. Ferreira, and J. Pierik, "Operation of grid-connected dfig under unbalanced grid voltage condition," *Energy Conversion, IEEE Transactions on*, vol. 24, no. 1, pp. 240–246, 2009.

[38] J. Carroll, A. McDonald, I. Dinwoodie, D. McMillan, M. Revie, and I. Lazakis, "Availability, operation and maintenance costs of offshore wind turbines with different drive train configurations," *Wind Energy*, vol. 20, no. 2, pp. 361–378, 2017, wE-15-0246.R1. [Online]. Available: http://dx.doi.org/10.1002/we.2011

[39] Y. Gritli, L. Zarri, C. Rossi, F. Filippetti, G. A. Capolino, and D. Casadei, "Advanced diagnosis of electrical faults in wound-rotor induction machines," *IEEE Transactions on Industrial Electronics*, vol. 60, no. 9, pp. 4012–4024, Sept 2013.

[40] M. Zaggout, P. Tavner, C. Crabtree, and L. Ran, "Detection of rotor electrical asymmetry in wind turbine doubly-fed induction generators," *IET Renewable Power Generation*, vol. 8, no. 8, pp. 878–886, 2014.

[41] M. Mengoni, L. Zarri, A. Tani, Y. Gritli, G. Serra, F. Filippetti, and D. Casadei, "Online detection of high-resistance connections in multiphase induction machines," *IEEE Transactions on Power Electronics*, vol. 30, no. 8, pp. 4505–4513, Aug 2015.

[42] Y. Gritli, A. Stefani, A. Chatti, C. Rossi, and F. Filippetti, "The combined use of the instantaneous fault frequency evolution and frequency sliding for advanced rotor fault diagnosis in dfim under time-varying condition," in *2009 35th Annual Conference of IEEE Industrial Electronics*, Nov 2009, pp. 3471–3476.

[43] G. A. Skrimpas, C. W. Sweeney, B. B. Jensen, N. Mijatovic, J. Holb *et al.*, "Analysis of generator bearing vibration data for diagnosing rotor circuit malfunction in dfigs," in *Electrical Machines (ICEM), 2014 International Conference on*. IEEE, 2014, pp. 1746–1751.

[44] S. Nandi, S. Choi, and H. Meshgin-kelk, *Electric Machines: Modeling, Condition Monitoring, and Fault Diagnosis*. CRC Press, 2012.

[45] Y. Zhu, C. Zhu, C. Song, Y. Li, X. Chen, and B. Yong, "Improvement of reliability and wind power generation based on wind turbine real-time condition assessment," *International Journal of Electrical Power & Energy Systems*, vol. 113, pp. 344–354, 2019.

[46] P. Zhou and P. Yin, "An opportunistic condition-based maintenance strategy for offshore wind farm based on predictive analytics," *Renewable and Sustainable Energy Reviews*, vol. 109, pp. 1–9, 2019.

[47] I. Ejaz, M. Alvarado, N. Gautam, N. Gebraeel, and M. Lawley, "Condition-based maintenance for queues with degrading servers," *IEEE Transactions on Automation Science and Engineering*, 2019.

[48] T. Wang, Q. Han, F. Chu, and Z. Feng, "Vibration based condition monitoring and fault diagnosis of wind turbine planetary gearbox: A review," *Mechanical Systems and Signal Processing*, vol. 126, pp. 662–685, 2019.

[49] I. Vamsi, G. Sabareesh, and P. Penumakala, "Comparison of condition monitoring techniques in assessing fault severity for a wind turbine gearbox under non-stationary loading," *Mechanical Systems and Signal Processing*, vol. 124, pp. 1–20, 2019.

[50] F. P. G. Márquez, A. M. Tobias, J. M. P. Pérez, and M. Papaelias, "Condition monitoring of wind turbines: Techniques and methods," *Renewable Energy*, vol. 46, pp. 169 – 178, 2012. [Online]. Available: http://www.sciencedirect.com/science/article/pii/S0960148112001899

[51] B. Wang, Y. Wang, and X. Chen, "Research on Wind Turbine Generator Dynamic Reliability Test System Based on Feature Recognition," *Research Journal of Applied Sciences, Engineering and Technology*, vol. 6, pp. 3065–3071, 2013.

[52] J. Ribrant and L. M. Bertling, "Survey of failures in wind power systems with focus on swedish wind power plants during 1997 ndash;2005," *IEEE Transactions on Energy Conversion*, vol. 22, no. 1, pp. 167–173, March 2007.

[53] P. Tchakoua, R. Wamkeue, M. Ouhrouche, F. Slaoui-Hasnaoui, T. A. Tameghe, and G. Ekemb, "Wind turbine condition monitoring: State-of-the-art review, new trends, and future challenges," *Energies*, vol. 7, no. 4, pp. 2595–2630, 2014.

[54] Z. Bo, H. Ming, Z. Zhicheng, S. Zhu, Z. Jiwei, W. Dong, and Z. Lin, "A novel type of online oil monitoring method in gearbox of wind turbine," in *Instrumentation, Measurement, Computer, Communication and Control (IMCCC), 2013 Third International Conference on.* IEEE, 2013, pp. 1712–1715.

[55] J. Zhu, J. M. Yoon, D. He, and E. Bechhoefer, "Online particle-contaminated lubrication oil condition monitoring and remaining useful life prediction for wind turbines," *Wind Energy*, vol. 18, no. 6, pp. 1131–1149, 2015.

[56] J. Zhu, J. M. Yoon, D. He, Y. Qu, and E. Bechhoefer, "Lubrication oil condition monitoring and remaining useful life prediction with particle filtering," *International Journal of Prognostics and Health Management*, vol. 4, pp. 124–138, 2013.

[57] J. Zhu, D. He, and E. Bechhoefer, "Survey of lubrication oil condition monitoring, diagnostics, and prognostics techniques and systems," *Journal of chemical science and technology*, vol. 2, no. 3, pp. 100–115, 2013.

[58] M. Schlechtingen and I. Ferreira Santos, "Comparative analysis of neural network and regression based condition monitoring approaches for wind turbine fault detection," *Mechanical Systems and Signal Processing*, vol. 25, no. 5, pp. 1849–1875, jul 2011. [Online]. Available: http://linkinghub.elsevier.com/retrieve/pii/S0888327010004310

[59] M. Wilkinson, B. Darnell, T. van Delft, and K. Harman, "Comparison of methods for wind turbine condition monitoring with scada data," *IET Renewable Power Generation*, vol. 8, no. 4, pp. 390–397, 2014.

[60] M. Schlechtingen, I. F. Santos, and S. Achiche, "Wind turbine condition monitoring based on SCADA data using normal behavior models. Part 1: System description," *Applied Soft Computing*, vol. 13, no. 1, pp. 447–460, jan 2013. [Online]. Available: http://linkinghub.elsevier.com/retrieve/pii/S1568494613003104http://dx.doi.org/10.1016/j.asoc.2012.08.033

[61] P. Sun, J. Li, C. Wang, and X. Lei, "A generalized model for wind turbine anomaly identification based on SCADA data," *Applied Energy*, vol. 168, pp. 550–567, 2016. [Online]. Available: http://linkinghub.elsevier.com/retrieve/pii/S0306261916301210

[62] P. Bangalore, S. Letzgus, D. Karlsson, and M. Patriksson, "An artificial neural network-based condition monitoring method for wind turbines, with application to the monitoring of the gearbox," *Wind Energy*, 2017. [Online]. Available: http://doi.wiley.com/10.1002/we.2102

[63] Y. Feng, Y. Qiu, C. J. Crabtree, H. Long, and P. J. Tavner, "Monitoring wind turbine gearboxes," *Wind Energy*, vol. 16, no. 5, pp. 728–740, jul 2013. [Online]. Available: http://onlinelibrary.wiley.com/doi/10.1002/we.1521/fullhttp://doi.wiley.com/10.1002/we.1521

[64] C. S. Gray and S. J. Watson, "Physics of failure approach to wind turbine condition based maintenance," *Wind Energy*, vol. 13, no. 5, pp. 395–405, 2010.

[65] Y. Qiu, Y. Feng, J. Sun, W. Zhang, and D. Infield, "Applying thermophysics for wind turbine drivetrain fault diagnosis using SCADA data," *IET Renewable Power Generation*, vol. 10, no. 5, pp. 661–668, may 2016. [Online]. Available: http://digital-library.theiet.org/content/journals/10.1049/iet-rpg.2015.0160

[66] Y. Feng, Y. Qiu, C. J. Crabtree, H. Long, and P. J. Tavner, "Monitoring wind turbine gearboxes," *Wind Energy*, vol. 16, no. 5, pp. 728–740, 2013.

[67] B. Maru and P. A. Zotos, "Anti-friction bearing temperature rise for nema frame motors," *IEEE Transactions on Industry Applications*, vol. 25, no. 5, pp. 883–888, Sep 1989.

[68] M. R. Wilkinson, F. Spinato, and P. J. Tavner, "Condition monitoring of generators & other subassemblies in wind turbine drive trains," in *Diagnostics for Electric Machines, Power Electronics and Drives, 2007. SDEMPED 2007. IEEE International Symposium on.* IEEE, 2007, pp. 388–392.

[69] M. Wilkinson and P. Tavner, "Extracting condition monitoring information from a wind turbine drive train," in *Universities Power Engineering Conference, 2004. UPEC 2004. 39th International*, vol. 2. IEEE, 2004, pp. 591–594.

[70] M. Wilkinson, F. Spianto, and M. Knowles, "Towards the zero maintenance wind turbine," in *Universities Power Engineering Conference, 2006. UPEC'06. Proceedings of the 41st International*, vol. 1. IEEE, 2006, pp. 74–78.

[71] D. J. Gardels, W. Qiao, and X. Gong, "Simulation studies on imbalance faults of wind turbines," in *Power and Energy Society General Meeting, 2010 IEEE.* IEEE, 2010, pp. 1–5.

[72] M. R. Castelli, A. Dal Monte, M. Quaresimin, and E. Benini, "Numerical evaluation of aerodynamic and inertial contributions to darrieus wind turbine blade deformation," *Renewable Energy*, vol. 51, pp. 101–112, 2013.

[73] W. Yang, P. Tavner, and M. Wilkinson, "Wind turbine condition monitoring and fault diagnosis using both mechanical and electrical signatures," in *Advanced Intelligent Mechatronics, 2008. AIM 2008. IEEE/ASME International Conference on.* IEEE, 2008, pp. 1296–1301.

[74] D. Zurita, M. Delgado, J. A. Ortega, and L. Romeral, "Intelligent sensor based on acoustic emission analysis applied to gear fault diagnosis," in *Diagnostics for Electric Machines, Power Electronics and Drives (SDEMPED), 2013 9th IEEE International Symposium on.* IEEE, 2013, pp. 169–176.

[75] C. Niezrecki, P. Avitabile, J. Chen, J. Sherwood, T. Lundstrom, B. LeBlanc, S. Hughes, M. Desmond, A. Beattie, M. Rumsey *et al.*, "Inspection and monitoring of wind turbine blade-embedded wave defects during fatigue testing," *Structural Health Monitoring*, p. 1475921714532995, 2014.

[76] S. Kim, D. E. Adams, H. Sohn, G. Rodriguez-Rivera, N. Myrent, R. Bond, J. Vitek, S. Carr, A. Grama, and J. J. Meyer, "Crack detection technique for operating wind turbine blades using vibro-acoustic modulation," *Structural Health Monitoring*, vol. 13, no. 6, pp. 660–670, 2014.

[77] S. Soua, P. Van Lieshout, A. Perera, T.-H. Gan, and B. Bridge, "Determination of the combined vibrational and acoustic emission signature of a wind turbine gearbox and generator shaft in service as a pre-requisite for effective condition monitoring," *Renewable Energy*, vol. 51, pp. 175–181, 2013.

[78] S. H. Kia, H. Henao, and G.-A. Capolino, "A comparative study of acoustic, vibration and stator current signatures for gear tooth fault diagnosis," in *Electrical Machines (ICEM), 2012 XXth International Conference on.* IEEE, 2012, pp. 1514–1519.

[79] A. Zaher, S. McArthur, D. Infield, and Y. Patel, "Online wind turbine fault detection through automated scada data analysis," *Wind Energy*, vol. 12, no. 6, pp. 574–593, 2009.

[80] J. Dai, D. Liu, L. Wen, and X. Long, "Research on power coefficient of wind turbines based on scada data," *Renewable Energy*, vol. 86, pp. 206–215, 2016.

[81] J. Tautz-Weinert and S. J. Watson, "Using scada data for wind turbine condition monitoring – a review," *IET Renewable Power Generation*, vol. 11, pp. 382–394(12), March 2017. [Online]. Available: http://digital-library.theiet.org/content/journals/10.1049/iet-rpg.2016.0248

[82] P. Tchakoua, R. Wamkeue, T. A. Tameghe, and G. Ekemb, "A review of concepts and methods for wind turbines condition monitoring," in *Computer and Information Technology (WCCIT), 2013 World Congress on.* IEEE, 2013, pp. 1–9.

[83] E. Gonzalez and J. J. Melero, "Wind turbine fault detection by monitoring its performance using high frequency SCADA data," *30th International Congress & Exhibition on Condition Monitoring and Diagnostic Engineering, COMADEM*, pp. 85–93, 2017.

[84] A. Rettenmeier, D. Schlipf, I. Würth, and P. W. Cheng, "Power Performance Measurements of the NREL CART-2 Wind Turbine Using a Nacelle-Based Lidar Scanner," *Journal of Atmospheric and Oceanic Technology*, vol. 31, no. 10, pp. 2029–2034, oct 2014. [Online]. Available: http://journals.ametsoc.org/doi/abs/10.1175/JTECH-D-13-00154.1

[85] Z. Zhang and A. Kusiak, "Monitoring Wind Turbine Vibration Based on SCADA Data," *Journal of Solar Energy Engineering*, vol. 134, no. 2, pp. 021 004–1–021 004–12, 2012. [Online]. Available: http://solarenergyengineering.asmedigitalcollection.asme.org/article.aspx?articleid=1458828

[86] T. Burton, N. Jenkins, D. Sharpe, and E. Bossanyi, *Wind energy handbook.* John Wiley & Sons, 2001.

[87] A. Siddique, G. S. Yadava, and B. Singh, "A review of stator fault monitoring techniques of induction motors," *IEEE Transactions on Energy Conversion*, vol. 20, no. 1, pp. 106–114, March 2005.

[88] S. Nandi, H. Toliyat, and X. Li, "Condition monitoring and fault diagnosis of electrical motors-a review," *Energy Conversion, IEEE Transactions on*, vol. 20, no. 4, pp. 719–729, Dec 2005.

[89] M. E. H. Benbouzid, "A review of induction motors signature analysis as a medium for faults detection," *IEEE transactions on industrial electronics*, vol. 47, no. 5, pp. 984–993, 2000.

[90] M. Seera, C. P. Lim, D. Ishak, and H. Singh, "Fault detection and diagnosis of induction motors using motor current signature analysis and a hybrid fmm–cart model," *Neural Networks and Learning Systems, IEEE Transactions on*, vol. 23, no. 1, pp. 97–108, 2012.

[91] B. M. Ebrahimi, M. Javan Roshtkhari, J. Faiz, and S. V. Khatami, "Advanced eccentricity fault recognition in permanent magnet synchronous motors using stator current signature analysis," *Industrial Electronics, IEEE Transactions on*, vol. 61, no. 4, pp. 2041–2052, 2014.

[92] N. Arthur and J. Penman, "Induction machine condition monitoring with higher order spectra," *IEEE Transactions on Industrial Electronics*, vol. 47, no. 5, pp. 1031–1041, Oct 2000.

[93] D. G. Dorrell, W. T. Thomson, and S. Roach, "Analysis of airgap flux, current, and vibration signals as a function of the combination of static and dynamic airgap eccentricity in 3-phase induction motors," *IEEE Transactions on Industry Applications*, vol. 33, no. 1, pp. 24–34, Jan 1997.

[94] J. A. Corral-Hernandez, J. Antonino-Daviu, J. Pons-Llinares, V. Climente-Alarcon, and V. Frances-Galiana, "Transient-based rotor cage assessment in induction motors operating with soft starters," *IEEE Transactions on Industry Applications*, vol. 51, no. 5, pp. 3734–3742, 2015.

[95] A. Ibrahim, M. E. Badaoui, F. Guillet, and F. Bonnardot, "A new bearing fault detection method in induction machines based on instantaneous power factor," *IEEE Transactions on Industrial Electronics*, vol. 55, no. 12, pp. 4252–4259, Dec 2008.

[96] A. J. M. Cardoso *et al.*, "Discriminating the simultaneous occurrence of three-phase induction motor rotor faults and mechanical load oscillations by the instantaneous active and reactive power media signature analyses," *Industrial Electronics, IEEE Transactions on*, vol. 59, no. 3, pp. 1630–1639, 2012.

[97] S. F. Legowski, A. H. M. S. Ula, and A. M. Trzynadlowski, "Instantaneous stator power as a medium for the signature analysis of induction motors," in *IAS '95. Conference Record of the 1995 IEEE Industry Applications Conference Thirtieth IAS Annual Meeting*, vol. 1, Oct 1995, pp. 619–624 vol.1.

[98] X. Gong and W. Qiao, "Current-based mechanical fault detection for direct-drive wind turbines via synchronous sampling and impulse detection," *Industrial Electronics, IEEE Transactions on*, vol. 62, no. 3, pp. 1693–1702, 2015.

[99] J. Wang, Y. Peng, W. Qiao, and J. L. Hudgins, "Bearing fault diagnosis of direct-drive wind turbines using multiscale filtering spectrum," *IEEE Transactions on Industry Applications*, vol. 53, no. 3, pp. 3029–3038, May 2017.

[100] M. R. Shahriar, P. Borghesani, and A. C. C. Tan, "Electrical signature analysis-based detection of external bearing faults in electromechanical drivetrains," *IEEE Transactions on Industrial Electronics*, vol. 65, no. 7, pp. 5941–5950, July 2018.

[101] F. Cheng, L. Qu, and W. Qiao, "Fault prognosis and remaining useful life prediction of wind turbine gearboxes using current signal analysis," *IEEE Transactions on Sustainable Energy*, vol. 9, no. 1, pp. 157–167, Jan 2018.

[102] X. Gong and W. Qiao, "Imbalance fault detection of direct-drive wind turbines using generator current signals," *IEEE Transactions on Energy Conversion*, vol. 27, no. 2, pp. 468–476, June 2012.

[103] W. Q. Jeffries, J. A. Chambers, and D. G. Infield, "Experience with bicoherence of electrical power for condition monitoring of wind turbine blades," *IEE Proceedings - Vision, Image and Signal Processing*, vol. 145, no. 3, pp. 141–148, June 1998.

[104] P. Zhang and P. Neti, "Detection of gearbox bearing defects using electrical signature analysis for Doubly-fed wind generators," *2013 IEEE Energy Conversion Congress and Exposition*, pp. 4438–4444, Sep. 2013. [Online]. Available: http://ieeexplore.ieee.org/lpdocs/epic03/wrapper.htm?arnumber=6647294

[105] J. P. Barton and S. J. Watson, "Analysis of electrical power data for condition monitoring of a small wind turbine," *Renewable Power Generation, IET*, vol. 7, no. 4, pp. 341–349, 2013.

[106] E. Artigao, A. Honrubia-Escribano, and E. Gomez-Lazaro, "Current signature analysis to monitor dfig wind turbine generators: A case study," *Renewable Energy*, vol. 116, pp. 5–14, 2018.

[107] X. Gong and W. Qiao, "Bearing fault diagnosis for direct-drive wind turbines via current-demodulated signals," *IEEE Transactions on Industrial Electronics*, vol. 60, no. 8, pp. 3419–3428, 2013.

[108] Z. Xiaoxia and X. Haosong, "Fault diagnosis of wind turbine rolling bearing based on wavelet and hilbert transforms," in *Control Conference (CCC), 2012 31st Chinese*. IEEE, 2012, pp. 5290–5293.

[109] K. Bassett, "Vibration based structural health monitoring for utility scale wind turbines," *Master's Thesis, University of Windsor, Ontario, Canada*, 2010.

[110] E. Sainz, A. Llombart, and J. Guerrero, "Robust filtering for the characterization of wind turbines: Improving its operation and maintenance," *Energy Conversion and Management*, vol. 50, no. 9, pp. 2136–2147, 2009.

[111] X. Jia, C. Jin, M. Buzza, W. Wang, and J. Lee, "Wind turbine performance degradation assessment based on a novel similarity metric for machine performance curves," *Renewable Energy*, vol. 99, pp. 1191 – 1201, 2016. [Online]. Available: http://www.sciencedirect.com/science/article/pii/S0960148116307194

[112] D. Villanueva and A. Feijóo, "Normal-based model for true power curves of wind turbines," *IEEE Transactions on Sustainable Energy*, vol. 7, no. 3, pp. 1005–1011, July 2016.

[113] M. Schlechtingen, I. F. Santos, and S. Achiche, "Using data-mining approaches for wind turbine power curve monitoring: A comparative study," *IEEE Transactions on Sustainable Energy*, vol. 4, no. 3, pp. 671–679, July 2013.

[114] M. Lydia, S. S. Kumar, A. I. Selvakumar, and G. E. Prem Kumar, "A comprehensive review on wind turbine power curve modeling techniques," *Renewable and Sustainable Energy Reviews*, vol. 30, pp. 452–460, 2014. [Online]. Available: http://dx.doi.org/10.1016/j.rser.2013.10.030

[115] R. M. Jones, "Enveloping for bearing analysis," *Sound and vibration*, vol. 30, no. 2, pp. 10–15, 1996.

[116] P. Caselitz, J. Giebhardt, M. Mevenkamp, and M. Reichardt, "Application of condition monitoring systems in wind energy converters," in *EWEC-CONFERENCE-*. BOOKSHOP FOR SCIENTIFIC PUBLICATIONS, 1997, pp. 579–582.

[117] J. Antoni and R. Randall, "The spectral kurtosis: application to the vibratory surveillance and diagnostics of rotating machines," *Mechanical systems and signal processing*, vol. 20, no. 2, pp. 308–331, 2006.

[118] R. R. Schoen, B. K. Lin, T. G. Habetler, J. H. Schlag, and S. Farag, "An unsupervised, on-line system for induction motor fault detection using stator current monitoring," *IEEE Transactions on Industry Applications*, vol. 31, no. 6, pp. 1280–1286, Nov 1995.

[119] R. K. Ibrahim, S. J. Watson, S. Djurović, and C. J. Crabtree, "An effective approach for rotor electrical asymmetry detection in wind turbine dfigs," *IEEE Transactions on Industrial Electronics*, vol. 65, no. 11, pp. 8872–8881, Nov 2018.

[120] D. Zappalá, N. Sarma, S. Djurović, C. Crabtree, A. Mohammad, and P. Tavner, "Electrical mechanical diagnostic indicators of wind turbine induction generator rotor faults," *Renewable Energy*, vol. 131, pp. 14 – 24, 2019. [Online]. Available: http://www.sciencedirect.com/science/article/pii/S096014811830750X

[121] J. P. Barton and S. J. Watson, "Analysis of electrical power data for condition monitoring of a small wind turbine," *IET Renewable Power Generation*, vol. 7, no. 4, pp. 341–349, 2013.

[122] M. E. H. Benbouzid and G. B. Kliman, "What stator current processing-based technique to use for induction motor rotor faults diagnosis?" *IEEE Transactions on Energy Conversion*, vol. 18, no. 2, pp. 238–244, June 2003.

[123] M. Lopez-Ramirez, R. J. Romero-Troncoso, D. Morinigo-Sotelo, O. Duque-Perez, L. M. Ledesma-Carrillo, D. Camarena-Martinez, and A. Garcia-Perez, "Detection and diagnosis of lubrication and faults in bearing on induction motors through stft," in *2016 International Conference on Electronics, Communications and Computers (CONIELECOMP)*, Feb 2016, pp. 13–18.

[124] J. A. Antonino-Daviu, J. Pons-Llinares, and S. B. Lee, "Advanced rotor fault diagnosis for medium-voltage induction motors via continuous transforms," *IEEE Transactions on Industry Applications*, vol. 52, no. 5, pp. 4503–4509, 2016.

[125] R. K. Ibrahim and S. J. Watson, "Advanced algorithms for wind turbine condition monitoring and fault diagnosis," in *Proc. the WindEurope Summit Conference, Hamburg*, 2016.

[126] C. Crabtree, S. Djurovic, P. Tavner, and A. Smith, "Fault frequency tracking during transient operation of wind turbine generators," in *Electrical Machines (ICEM), 2010 XIX International Conference on*. IEEE, 2010, pp. 1–5.

[127] W. Yang, P. Tavner, and M. Wilkinson, "Condition monitoring and fault diagnosis of a wind turbine synchronous generator drive train," *IET Renewable Power Generation*, vol. 3, no. 1, pp. 1–11, 2009.

[128] W. Yang, P. J. Tavner, C. J. Crabtree, and M. Wilkinson, "Cost-effective condition monitoring for wind turbines," *Industrial Electronics, IEEE Transactions on*, vol. 57, no. 1, pp. 263–271, 2010.

[129] Y. Gritli, S. B. Lee, F. Filippetti, and L. Zarri, "Advanced diagnosis of outer cage damage in double-squirrel-cage induction motors under time-varying conditions based on wavelet analysis," *IEEE Transactions on Industry Applications*, vol. 50, no. 3, pp. 1791–1800, 2014.

[130] J. Pons-Llinares, J. A. Antonino-Daviu, M. Riera-Guasp, S. B. Lee, T.-j. Kang, and C. Yang, "Advanced induction motor rotor fault diagnosis via continuous and discrete time-frequency tools," *IEEE Transactions on Industrial Electronics*, vol. 62, no. 3, pp. 1791–1802, 2015.

[131] W. Yang, P. J. Tavner, C. J. Crabtree, and M. Wilkinson, "Cost-effective condition monitoring for wind turbines," *IEEE Transactions on industrial electronics*, vol. 57, no. 1, pp. 263–271, 2010.

[132] S. Nandi, H. A. Toliyat, and X. Li, "Condition monitoring and fault diagnosis of electrical motors-a review," *IEEE transactions on energy conversion*, vol. 20, no. 4, pp. 719–729, 2005.

[133] Y. Yang, Z. K. Peng, G. Meng, and W. M. Zhang, "Spline-kernelled chirplet transform for the analysis of signals with time-varying frequency and its

application," *IEEE Transactions on Industrial Electronics*, vol. 59, no. 3, pp. 1612–1621, March 2012.

[134] W. Yang, P. J. Tavner, and W. Tian, "Wind turbine condition monitoring based on an improved spline-kernelled chirplet transform," *IEEE Transactions on Industrial Electronics*, vol. 62, no. 10, pp. 6565–6574, Oct 2015.

[135] H. Malik, Y. Pandya, A. Parashar, and R. Sharma, "Feature extraction using emd and classifier through artificial neural networks for gearbox fault diagnosis," in *Applications of Artificial Intelligence Techniques in Engineering*. Springer, 2019, pp. 309–317.

[136] M. He, D. He, J. Yoon, T. J. Nostrand, J. Zhu, and E. Bechhoefer, "Wind turbine planetary gearbox feature extraction and fault diagnosis using a deep-learning-based approach," *Proceedings of the Institution of Mechanical Engineers, Part O: Journal of Risk and Reliability*, vol. 233, no. 3, pp. 303–316, 2019.

[137] F. Elasha, S. Shanbr, X. Li, and D. Mba, "Prognosis of a wind turbine gearbox bearing using supervised machine learning," *Sensors*, vol. 19, no. 14, p. 3092, 2019.

[138] J. Herp, N. L. Pedersen, and E. S. Nadimi, "Assessment of early stopping through statistical health prognostic models for empirical rul estimation in wind turbine main bearing failure monitoring," *Energies*, vol. 13, no. 1, p. 83, 2020.

[139] A. P. Marugán, F. P. G. Márquez, J. M. P. Perez, and D. Ruiz-Hernández, "A survey of artificial neural network in wind energy systems," *Applied energy*, vol. 228, pp. 1822–1836, 2018.

[140] R. K. Ibrahim, J. Tautz-Weinert, and S. J. Watson, "Neural networks for wind turbine fault detection via current signature analysis," 2016.

[141] R. Ata *et al.*, "Artificial neural networks applications in wind energy systems: a review," *Renewable and Sustainable Energy Reviews*, vol. 49, no. 534-562, 2015.

[142] J. Liu, F. Qu, X. Hong, and H. Zhang, "A small-sample wind turbine fault detection method with synthetic fault data using generative adversarial nets," *IEEE Transactions on Industrial Informatics*, 2018.

[143] S. Simani, S. Farsoni, and P. Castaldi, "Fault diagnosis of a wind turbine benchmark via identified fuzzy models," *IEEE Transactions on Industrial Electronics*, vol. 62, no. 6, pp. 3775–3782, 2014.

[144] H. Li, Y. Hu, C. Yang, Z. Chen, H. Ji, and B. Zhao, "An improved fuzzy synthetic condition assessment of a wind turbine generator system," *International Journal of Electrical Power & Energy Systems*, vol. 45, no. 1, pp. 468–476, 2013.

[145] P. Sun, J. Li, C. Wang, and X. Lei, "A generalized model for wind turbine anomaly identification based on scada data," *Applied Energy*, vol. 168, pp. 550–567, 2016.

[146] F. Cheng, L. Qu, and W. Qiao, "Fault prognosis and remaining useful life prediction of wind turbine gearboxes using current signal analysis," *IEEE Transactions on Sustainable Energy*, vol. 9, no. 1, pp. 157–167, 2017.

[147] M. Schlechtingen, I. F. Santos, and S. Achiche, "Wind turbine condition monitoring based on scada data using normal behavior models. part 1: System description," *Applied Soft Computing*, vol. 13, no. 1, pp. 259–270, 2013.

[148] A. Agasthian, R. Pamula, and L. Kumaraswamidhas, "Fault classification and detection in wind turbine using cuckoo-optimized support vector machine," *Neural Computing and Applications*, vol. 31, no. 5, pp. 1503–1511, 2019.

[149] A. Turnbull, J. Carroll, S. Koukoura, and A. McDonald, "Prediction of wind turbine generator bearing failure through analysis of high-frequency vibration

data and the application of support vector machine algorithms," *The Journal of Engineering*, vol. 2019, no. 18, pp. 4965–4969, 2019.

[150] Y. Wu and X. Ma, "Alarms-related wind turbine fault detection based on kernel support vector machines," *The Journal of Engineering*, vol. 2019, no. 18, pp. 4980–4985, 2019.

[151] J. Penman, H. Sedding, B. Lloyd, and W. Fink, "Detection and location of interturn short circuits in the stator windings of operating motors," *Energy conversion, ieee transactions on*, vol. 9, no. 4, pp. 652–658, 1994.

[152] G. Acosta, C. Verucchi, and E. Gelso, "A current monitoring system for diagnosing electrical failures in induction motors," *Mechanical Systems and Signal Processing*, vol. 20, no. 4, pp. 953–965, 2006.

[153] J. Faiz, B. M. Ebrahimi, B. Akin, and H. A. Toliyat, "Comprehensive eccentricity fault diagnosis in induction motors using finite element method," *IEEE Transactions on Magnetics*, vol. 45, no. 3, pp. 1764–1767, 2009.

[154] J. Faiz and S. Moosavi, "Eccentricity fault detection–from induction machines to dfig—a review," *Renewable and Sustainable Energy Reviews*, vol. 55, pp. 169–179, 2016.

[155] S. Nandi, T. C. Ilamparithi, S. B. Lee, and D. Hyun, "Detection of eccentricity faults in induction machines based on nameplate parameters," *IEEE Transactions on Industrial Electronics*, vol. 58, no. 5, pp. 1673–1683, May 2011.

[156] J. R. Cameron, W. T. Thomson, and A. B. Dow, "Vibration and current monitoring for detecting airgap eccentricity in large induction motors," *IEE Proceedings B - Electric Power Applications*, vol. 133, no. 3, pp. 155–163, May 1986.

[157] S. Nandi, R. M. Bharadwaj, and H. A. Toliyat, "Performance analysis of a three-phase induction motor under mixed eccentricity condition," *IEEE Transactions on Energy Conversion*, vol. 17, no. 3, pp. 392–399, 2002.

[158] M. Haji and H. A. Toliyat, "Pattern recognition-a technique for induction machines rotor broken bar detection," *IEEE Transactions on Energy Conversion*, vol. 16, no. 4, pp. 312–317, Dec 2001.

[159] M. Seera, C. P. Lim, D. Ishak, and H. Singh, "Fault detection and diagnosis of induction motors using motor current signature analysis and a hybrid fmm–cart model," *IEEE Transactions on Neural Networks and Learning Systems*, vol. 23, no. 1, pp. 97–108, Jan 2012.

[160] K. Alewine and W. Chen, "A review of electrical winding failures in wind turbine generators," *IEEE Electrical Insulation Magazine*, vol. 28, no. 4, pp. 8–13, July 2012.

[161] Y. Lei, A. Mullane, G. Lightbody, and R. Yacamini, "Modeling of the wind turbine with a doubly fed induction generator for grid integration studies," *IEEE Transactions on Energy Conversion*, vol. 21, no. 1, pp. 257–264, March 2006.

[162] C. Eisenhut, F. Krug, C. Schram, and B. Klockl, "Wind-turbine model for system simulations near cut-in wind speed," *IEEE Transactions on Energy Conversion*, vol. 22, no. 2, pp. 414–420, June 2007.

[163] M. Asmine, J. Brochu, J. Fortmann, R. Gagnon, Y. Kazachkov, C. E. Langlois, C. Larose, E. Muljadi, J. MacDowell, P. Pourbeik, S. A. Seman, and K. Wiens, "Model validation for wind turbine generator models," *IEEE Transactions on Power Systems*, vol. 26, no. 3, pp. 1769–1782, Aug 2011.

[164] R. K. Ibrahim and S. J. Watson, "Condition monitoring of permanent magnet synchronous generator for wind turbine applications," in *2016 3rd Conference on Control and Fault-Tolerant Systems (SysTol)*, 2016, pp. 648–653.

[165] ——, "Wind turbine simulation model for the study of combined mechanical and electrical faults," in *Scientific Track Proceedings of European Wind Energy Association. EWEA*, 2015.

[166] S. Heier, *Grid integration of wind energy conversion systems.* 2nd edition, John Wiley Sons, Inc, 2006.

[167] J. Morren and S. W. De Haan, "Short-circuit current of wind turbines with doubly fed induction generator," *Energy Conversion, IEEE Transactions on*, vol. 22, no. 1, pp. 174–180, 2007.

[168] F. Gu, Y. Shao, N. Hu, A. Naid, and A. Ball, "Electrical motor current signal analysis using a modified bispectrum for fault diagnosis of downstream mechanical equipment," *Mechanical Systems and Signal Processing*, vol. 25, no. 1, pp. 360–372, 2011.

[169] W. Yang, P. Tavner, C. Crabtree, and M. Wilkinson, "Cost-effective condition monitoring for wind turbines," *Industrial Electronics, IEEE Transactions on*, vol. 57, no. 1, pp. 263–271, Jan 2010.

[170] S. F. Johnston, "Absorbing new subjects: holography as an analog of photography," *Physics in Perspective*, vol. 8, no. 2, pp. 164–188, 2006.

[171] G. Y. Kulikov and M. V. Kulikova, "The accurate continuous-discrete extended kalman filter for radar tracking," *IEEE Transactions on Signal Processing*, vol. 64, no. 4, pp. 948–958, Feb 2016.

[172] F. Auger, M. Hilairet, J. M. Guerrero, E. Monmasson, T. Orlowska-Kowalska, and S. Katsura, "Industrial applications of the kalman filter: A review," *IEEE Transactions on Industrial Electronics*, vol. 60, no. 12, pp. 5458–5471, Dec 2013.

[173] E. Zerdali and M. Barut, "The comparisons of optimized extended kalman filters for speed-sensorless control of induction motors," *IEEE Transactions on Industrial Electronics*, vol. 64, no. 6, pp. 4340–4351, June 2017.

[174] S. Yu, K. Emami, T. Fernando, H. H. C. Iu, and K. P. Wong, "State estimation of doubly fed induction generator wind turbine in complex power systems," *IEEE Transactions on Power Systems*, vol. 31, no. 6, pp. 4935–4944, Nov 2016.

[175] B. F. La Scala, R. R. Bitmead, and M. R. James, "Conditions for stability of the extended kalman filter and their application to the frequency tracking problem," *Mathematics of Control, Signals, and Systems (MCSS)*, vol. 8, no. 1, pp. 1–26, 1995.

[176] B. F. La Scala and R. R. Bitmead, "Design of an extended kalman filter frequency tracker," *IEEE Transactions on Signal Processing*, vol. 44, no. 3, pp. 739–742, 1996.

[177] S. Bittanti and S. M. Savaresi, "On the parametrization and design of an extended kalman filter frequency tracker," *IEEE transactions on automatic control*, vol. 45, no. 9, pp. 1718–1724, 2000.

[178] M. Saha, R. Ghosh, and B. Goswami, "Robustness and sensitivity metrics for tuning the extended kalman filter," *IEEE Transactions on Instrumentation and Measurement*, vol. 63, no. 4, pp. 964–971, April 2014.

[179] I. Simonovski and M. Boltezar, "The norms and variances of the gabor, morlet and general harmonic wavelet functions," *Journal of Sound and Vibration*, vol. 264, no. 3, pp. 545–557, 2003.